LAPPEENRANTA UNIVERSITY OF TECHNOLOGY
LUT School of Energy Systems
LUT Mechanical Engineering

Henri Pirinen

FATIGUE STRENGTH OF WELDED JOINTS MADE OF S1100 STRUCTURAL STEEL

Examiners: Prof. Timo Björk
M.Sc. (Tech.) Antti Ahola

ABSTRACT

Lappeenranta University of Technology
LUT School of Energy Systems
LUT Mechanical Engineering

Henri Pirinen

Fatigue strength of welded joints made of S1100 structural steel

Master's thesis

2019

91 pages, 69 figures, 19 tables and 5 appendices

Examiners: Professor Timo Björk
M.Sc. (Tech.) Antti Ahola

Keywords: fatigue, UHSS, S1100, FE-analysis, 4R method, post-weld treatment

Fatigue strength of butt welded joints, non-load carrying T-joints, load carrying X-joints and longitudinal gusset joints made of SSAB's Strenx® 1100 Plus structural steel is investigated in this study. There is no design code or standard for ultra-high strength steels at the moment so the target is to get necessary information for design recommendation. All the test specimens are welded with robotized GMAW except of two butt joints that are welded by fiber laser. In addition, the effect of post-weld treatments on the fatigue strength is investigated. Some of the joints are post-weld treated by high frequency impact treatment (HiFIT) or tungsten inert gas (TIG) treatment. Fatigue tests are performed with constant amplitude tensile loading with applied stress ratios $R = 0.1$ and $R = 0.5$. The total number of test specimens is 33. Experimental fatigue test results are compared with the results of fatigue strength assessment by the nominal stress, structural stress, effective notch stress (ENS) and 4R methods. FE-analysis is performed by Femap/NxNastran to obtain stress concentration factors for fatigue strength assessment by the ENS and 4R methods. In addition, 2D measurements, residual stress measurements and hardness measurements are carried out. Experimental results indicates that the applied stress ratio has substantial effect on the fatigue strength of test specimens. Post-weld treatments improves significantly fatigue strength of the joints with both applied stress ratios. Generally, nominal and structural stress methods provides conservative results with applied stress ratio $R = 0.1$ but even unsafe results with $R = 0.5$ in some cases. The ENS method provides accurate results for GMAW butt welded and non-load carrying T-joints in as-welded condition at low stress ratio but results are unsafe in other cases in as-welded condition. The 4R method takes in to account stress ratio and residual stresses which results in more accurate results especially at high stress ratios compared to other fatigue strength assessment methods.

TIIVISTELMÄ

Lappeenrannan teknillinen yliopisto
LUT Energiajärjestelmät
LUT Kone

Henri Pirinen

S1100 rakenneteräksestä valmistettujen hitsausliitosten väsymislujuus

Diplomityö

2019

91 sivua, 69 kuvaa, 19 taulukkoa ja 5 liitettä

Tarkastajat: Professori Timo Björk
DI Antti Ahola

Hakusanat: väsyminen, ultraluja teräs, S1100, FE-analyysi, 4R-menetelmä, hitsin jälkikäsittely

Tässä työssä tutkitaan SSAB:n Strenx® 1100 Plus rakenneteräksestä valmistettujen päittäisliitosten, kuormaa kantamattomien T-liitosten, kuormaa kantavien X-liitosten ja pitkittäinen ripa -liitosten väsymislujuutta. Tällä hetkellä ei ole olemassa ohjeistusta tai standardia ultralujille teräksille, joten tavoite on saada tarvittavaa tietoa suunnitteluohjeita varten. Koekappaleet hitsattiin robotisoidulla GMAW-hitsauksella, lukuun ottamatta kahta päittäisliitosta, jotka hitsattiin kuitulaserilla. Osa liitoksista jälkikäsiteltiin high frequency impact treatment (HiFIT) tai tungsten inert gas (TIG) -käsittelyllä. Väsytyskokeet suoritettiin vakioamplitudisella vetokuormituksella jännityssuhteilla R = 0.1 ja R = 0.5. Koekappaleiden kokonaismäärä on 33. Kokeellisia väsytyskoetuloksia verrataan nimellisen jännityksen, rakenteellisen jännityksen, tehollisen lovijännityksen (ENS) ja 4R -menetelmien tuloksiin. FE-analyysi suoritettiin Femap/NxNastran-ohjelmalla, jotta saatiin jännityskonsentraatiokertoimet väsymislujuuden arviointia varten ENS ja 4R -menetelmillä. Lisäksi 2D-, jäännösjännitys- ja kovuusmittauksia suoritettiin koekappaleille. Kokeet osoittavat, että jännityssuhteella on merkittävä vaikutus liitosten väsymislujuuteen. Jälkikäsittelymenetelmät parantavat huomattavasti liitosten väsymislujuutta molemmilla jännityssuhteilla. Yleensä nimellisen ja rakenteellisen jännityksen menetelmät antavat konservatiivisia tuloksia jännityssuhteella R = 0.1, mutta jopa epäturvallisia tuloksia jännityssuhteella R = 0.5. ENS-menetelmä antaa tarkkoja tuloksia GMAW-hitsatuille päittäisliitoksille ja kuormaa kantamattomille T-liitoksille hitsatussa tilassa pienellä jännityssuhteella mutta tulokset ovat epäturvallisia muissa tapauksissa hitsatussa tilassa. 4R -menetelmä ottaa huomioon jännityssuhteen ja jäännösjännitykset, joka johtaa tarkempiin tuloksiin varsinkin suurella jännityssuhteella muihin väsymislujuuden arviointimenetelmiin verrattuna.

ACKNOWLEDGEMENTS

I would like to thank the examiners of this work Professor Timo Björk and M.Sc. (Tech.) Antti Ahola for valuable guidance and feedback during this work. It has been comfortable to work with laboratory staff and without them this work would not have been successful so thank you Matti Koskimäki, Olli-Pekka Pynnönen, Mika Kärmeniemi and Jari Koskinen for your effort to this work. Thanks to the employees of other laboratories who have contributed to the progress of the work.

Finally, I would like to thank my family and friends for their support and encouragement during my studies.

Henri Pirinen
Lappeenranta 7.3.2019

TABLE OF CONTENTS

LIST OF SYMBOLS AND ABBREVIATIONS

A	Area [mm^2]
A_5	Elongation at break [%]
C	Fatigue capacity [MPa^m]
E	Modulus of elasticity [MPa]
F	Force [N]
H	Strength coefficient [MPa]
$k_{t,m}$	Stress concentration factor for membrane stress [-]
$k_{t,b}$	Stress concentration factor for bending stress [-]
m	Slope of the S-N curve [-]
n	Strain hardening exponent [-]
N_f	Fatigue life [cycles]
R	Applied stress ratio [-]
r	Weld toe radius [mm]
R_{local}	Local stress ratio [-]
R_m	Ultimate tensile strength [MPa]
$R_{p0.2}$	Yield strength [MPa]
$Stdv$	Standard deviation [-]
t	Thickness [mm]
$t_{8/5}$	Cooling time from 800 °C to 500 °C [s]
α_k	Stress concentration factor [-]
σ	Stress [MPa]
$\Delta\sigma$	Stress range [MPa]
ε	Strain [-]
v	Poisson's ratio [-]

Indices

avg	Average
b	Bending
char	Characteristic value
ens,k	Effective notch stress

m	Membrane
max	Maximum value
mean	Mean value
min	Minimum value
nom	Nominal value
ref	Reference
res	Residual stress
str,hs	Structural, hot spot

4R	Novel notch stress approach: R, R_m, σ_{res}, r
ASW	As-welded condition
BM	Base material
BW	Butt welded joint
CAL	Constant amplitude loading
CEV	Equivalent carbon content
EC3	Eurocode 3
ENS	Effective notch stress
FAT	Fatigue class
FEA	Finite element analysis
GMAW	Gas metal arc welding
HAZ	Heat-affected zone
HCF	High cycle fatigue
HFHP	High frequency hammer peening
HFMI	High frequency mechanical impact
HiFIT	High frequency impact treatment
HSS	High strength steel
IIW	International Institute of Welding
LCF	Low cycle fatigue
LCX	Load-carrying X-joint
LEFM	Linear elastic fracture mechanics
LG	Longitudinal gusset joint
LW	Laser welded joint

MSSPD	Minimization of sum of squared perpendicular distances
NLCT	Non-load carrying T-joint
S-N	Stress-Fatigue life
SG	Strain gage
SWT	Smith-Watson-Topper approach
TIG	Tungsten inert gas
UHSS	Ultra-high strength steel
UTS	Ultimate tensile strength
VAL	Variable amplitude loading

1 INTRODUCTION

Nowadays the use of natural resources must be sensible since they are used faster than they can regenerate. Development of technology and product design plays an important role reducing the consumption of natural resources. In Finland, one of the largest natural resource user is metal industry and steel mill's carbon dioxide emissions are about 1800 kg CO_2 per produced steel ton so there is great possibility for reducing carbon dioxide emissions and the use of natural resources by increasing material efficiency. (Climate guide 2018.)

By using of ultra-high strength steel (UHSS) rather than conventional structural steel carbon dioxide emissions can be reduced. According to Ruoppa et al. (2016 p. 32), UHSS is an informal title for steel with yield strength over 550 MPa and ultimate tensile strength (UTS) over 700 MPa. However, steel with yield strength over 355 MPa until 700 MPa is high strength steel (HSS) and yield strength over 700 MPa is UHSS at Lappeenranta University of Technology. Because of the greater strength of the material, less steel is needed to maintain simultaneously similar performance to the structures made of conventional steels so the structures can become lighter, more cost-effective and longer lasting. Hence, the most typical applications for UHSSs are booms, lifters and vehicles of all kind. Lower demand for the steel leads to the less production of the steel which lowers production phase CO_2 emissions and traffic emissions will decrease when vehicles become lighter and fuel consumption decreases. (Ruoppa et al. 2016, p. 32-34.) Figure 1 shows potential weight saving as a percentage when using UHSS compared with conventional structural steel.

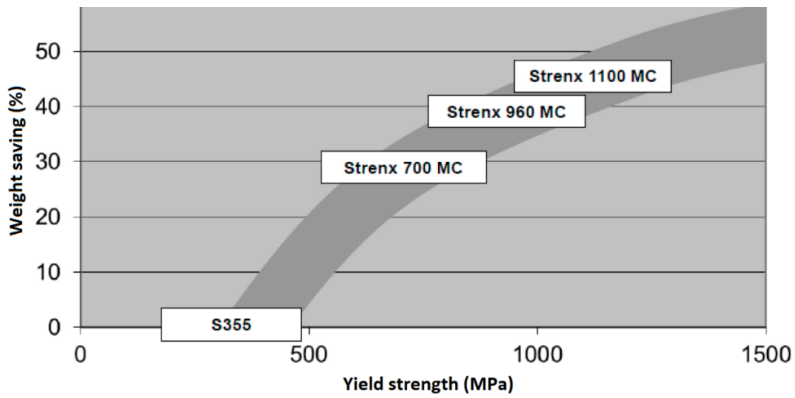

Figure 1. Potential weight saving as a percentage when using Strenx structural steels compared to regular structural steel (Mod. Mikkonen et al. 2017, p. 27).

However, there are some difficulties in the use of UHSSs. Eurocode 3 (EC3) does not include information about designing structures using over 700 MPa yield strength steels (SFS-EN 1993-1-12 2007, p. 4). Other inconveniences with the use of the UHSSs are that cold forming and welding becomes more challenging when yield strength becomes higher. The cold forming point of view higher strength of the steel leads to higher spring-back effect, larger possible bending radius and the need of more powerful bending machines (Ruoppa et al. 2016, p. 34-38.) In turn, welded joints represent critical part in durability of welded steel structures. After welding, quenched and tempered UHSSs have vulnerability to cold- and hydrogen cracking and welding itself also causes softening phenomenon in heat-affected zone (HAZ) which means lower strength area is formed to HAZ due to welding and it may have effect on the overall strength of the welded joint. However, there are also steels that do not suffer from softening of the HAZ as transformation induced plasticity and complex phase steels. (Kah et al. 2014, p. 358.) Thus, it is obvious that more research and information is needed so that UHSS structures can be designed and used better in practical terms. Typical applications for UHSSs are shown in figure 2.

Figure 2. Typical applications for UHSS (Mod. SSAB 2018).

1.1 Research problem and questions

The fatigue strength of typical welded joints made of SSAB's Strenx® 1100 Plus structural steel is investigated in this thesis. Results from fatigue tests are needed for basic design information. The research problem is that there is no design code or standard for UHSS at the moment. This research attempts to answer the following research questions:

- What is the fatigue strength of the test specimens and how it differ from fatigue strength of lower strength steels such as S960?
- Can accurate fatigue strength results be obtained by finite element analysis (FEA) and analytic calculations for welded joints made of S1100?
- How post-weld treatments, such as HiFIT-treatment and TIG-dressing, affect the fatigue strength capacity?
- How test results differ from fatigue strength estimations obtained by the 4R method?

1.2 Objective and research methods

The objective of this study is to investigate strength properties and conduct fatigue tests for welded joints made of S1100 structural steel. Literature review, experimental tests and numerical calculations are used as research methods. Literature review is used to find out information and fatigue test results about earlier research related to same strength level UHSSs. Experimental tests are performed to find out the fatigue strength of test specimens. FE-analyses and analytic calculations are carried out to support the test results. In addition, obtained results are compared with each other. Femap/NxNastran is used to perform FE-analysis, SolidWorks is used to make manufacturing drawings, AutoCAD is used to analyze 2D measurement data and MathCAD is used for fatigue strength calculations. The target is to get necessary information about UHSS for design recommendation.

1.3 Research boundary

The types of welded joints studied in this work are butt welded joints (BW), non-load carrying T-joints (NLCT), load carrying X-joints (LCX) and longitudinal gusset joints (LG). Most of the joints are welded with robotized gas metal arc welding (GMAW) and two of the butt welds are welded with the fiber laser. Some of the NLCT- and LG-joints are post-weld treated by high frequency impact treatment (HiFIT) or tungsten inert gas (TIG) dressing. Fatigue tests for the test specimens are carried out at Laboratory of Steel Structures and tests are performed with constant amplitude (CAL) tensile loading with applied stress ratios R = 0.1 and R = 0.5. The total number of the test specimens is 33. Test results are compared with values obtained by FE-analyses and analytic calculations which are made by nominal stress, structural stress, effective notch stress (ENS) and 4R methods. Various measurements, such as 2D measurements, residual stress measurements and hardness measurements are carried out.

2 LITERATURE REVIEW

This chapter discusses both the literature review and the fatigue strength assessment methods. First, a literature review is presented that discusses about recent research from the fatigue of UHSS welded joints and standards related to this study. Subsequently fatigue strength assessment methods that are used are briefly presented.

2.1 Existing studies on UHSS

The literature review was made to obtain information about the research development of UHSSs, recent studies related to the fatigue of welded joints made of UHSSs and possible post-weld treatments for them. The main focus was to search comparative results for fatigue tests and analyses for this work. Standards and guidelines related to this study were briefly presented.

Document search was made in the Scopus-database to find out how the research of UHSSs has developed. The search was limited to articles and conference papers with the subject area of engineering, materials science and exact keyword "Ultra High Strength Steel" was chosen. The total number of documents received was 722 between the years 2001 and 2017. Figure 3 introduces a diagram about published documents annually.

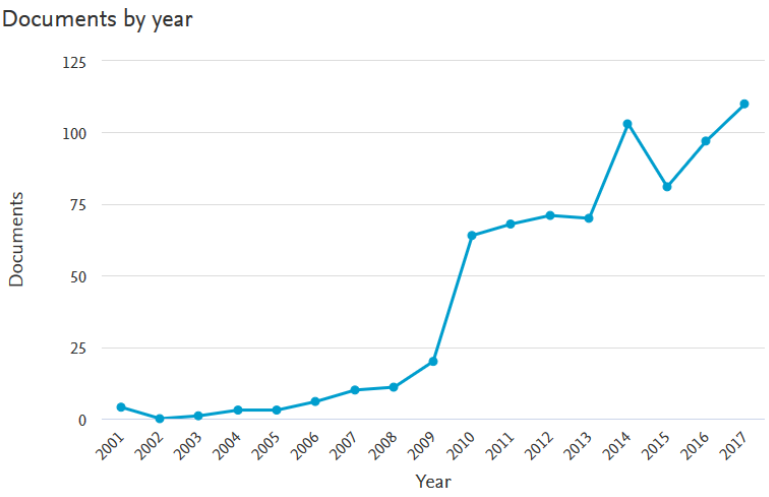

Figure 3. Diagram of published documents related to UHSS this millennium (Scopus 2018). Keyword in the search was "Ultra AND High AND Strength AND Steel".

The diagram shows that in 2010 the number of research outputs related to UHSSs has increased clearly compared to the beginning of the 2000s. After 2010 research outputs have stayed almost same level for a few years after which growth has been increasing so far. Reason for the increased research might be that manufacturing technology has developed and at that time in the early 2000s yield strength limit of structural steel 1000 MPa was exceeded. However, the search results from Scopus-database does not necessarily correspond to reality because there is no standardized terminology for high strength steels of different kind so term UHSS may mean different strength properties of steel between different users and manufacturers. (Lukkari, Kyröläinen, Kauppi 2016, p. 65.) Anyway, it is obvious that research is increasing constantly because of the benefits of the UHSS.

2.1.1 Recent research related to the fatigue of welded joints made of UHSS

Comparative results for fatigue tests were searched from the literature. Particularly information about the fatigue test results of UHSS welded joints was collected. In addition, test results were also searched about high frequency mechanical impact (HFMI) and tungsten inert gas (TIG) post-weld treatment methods.

Pijpers et al. (2009) studied the tensile and fatigue strength of base material and transverse butt welds made from Thyssen Krupp's Naxtra M 70 S690 and SSAB's Weldox S1100 E steels. Base material tensile test specimens were tested in plasma cut (S690, S1100) and water cut (S1100) conditions and all fatigue test specimens were milled and ground at the edges. In tensile tests, two displacement meters and two strain gages were used. Measurement indicated that yield strength of the cut edge S1100 was 12% lower and ultimate tensile strength was 25% lower than manufacturer material specifications. In fatigue tests, axial constant amplitude loading (CAL) was used with applied stress ratio R = 0.1 and frequency of 5.3 Hz. Fatigue strength of S690 exceeded standard EN 1993-1-9 values. In those base material tests, S690 specimens had better fatigue strength than S1100 specimens which may be due to coarser surface roughness at the plate surface in the S1100 specimens. Base material test specimens had 10% tapered area in the middle of the specimen which edge most of the cracks initiated in case of S690 and in case of S1100 cracks initiated outside that area at the surface of the plate material. The fatigue strength of butt-welded joints made of S1100 steel was better than S690 and S1100 specimens had a longer crack initiation period that was monitored using strain gages but shorter crack propagation period than S690

specimens. Cracks initiated at near of the weld toe from the edges of the plate in all tests except one where cracks initiated also in other places. The characteristic fatigue strength of transverse butt joints made from S690 was nearby FAT 90 from the EC3. High fabrication quality with the S1100 is essential because it is sensitive to surface condition and thermal influence. (Pijpers et al. 2009, p. 14-32.) Figures 4 and 5 fatigue test results in an S-N curve.

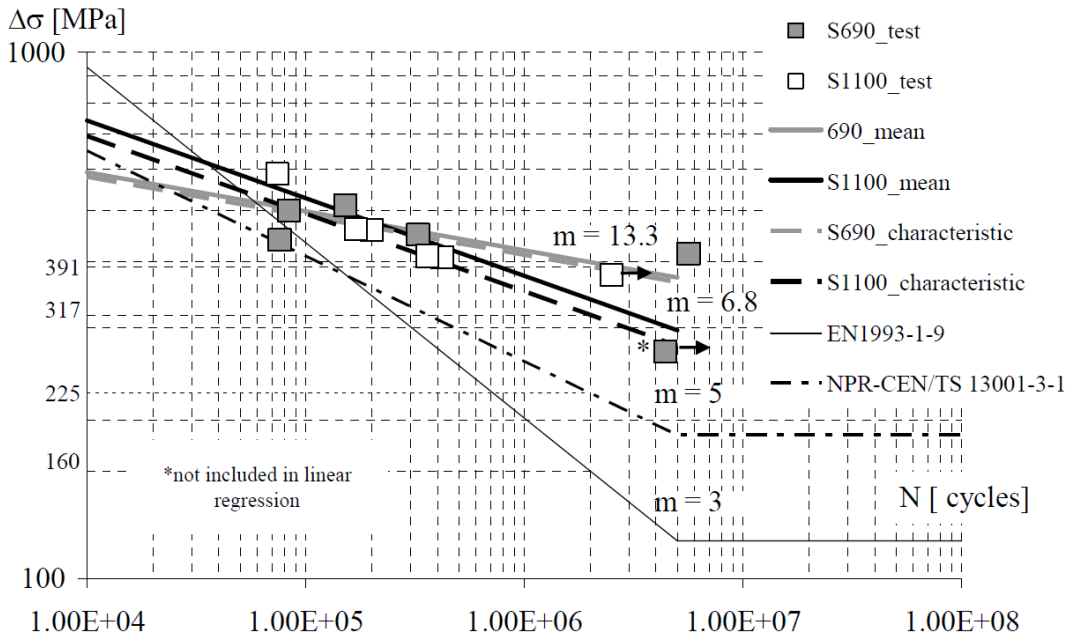

Figure 4. The S-N curve of the base material specimens (Pijpers et al. 2009, p. 28).

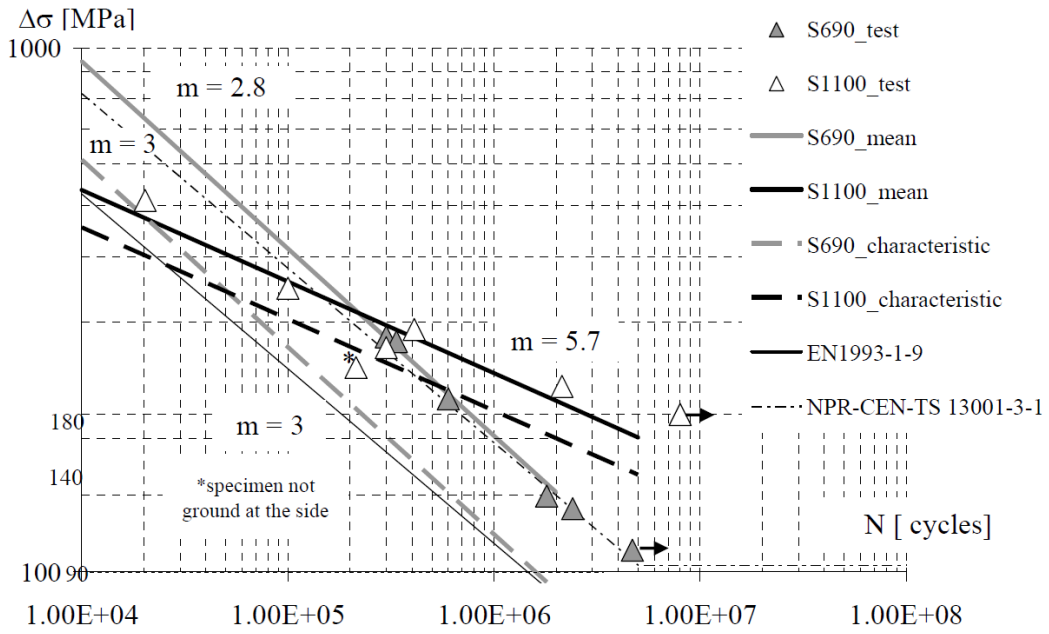

Figure 5. The S-N curve of the transverse butt weld specimens (Pijpers et al. 2009, p. 30).

Möller et al. (2015) studied the fatigue strength of butt welds at low cycle fatigue regime (LCF) under variable amplitude loading (VAL) and constant amplitude loading (CAL). Stress-time history of the truck crane data logging system was used in VAL experiments. Three steel grades S960QL, S960M and S1100QL were tested. Manual and automated MAG welding processed were used and filler material has minimum yield strength of 890 MPa. Uniaxial stress-controlled loading was used with applied stress ratio R = 0.1. Based on the test results notch radius of the weld toe and welding quality played a significant role in the fatigue strength of MAG welded joints at the high cycle fatigue (HCF) regime under CAL and the thing is the same under LCF regime under VAL. No improvement in fatigue strength was found in the case of S1100QL compared to other steel grades in this study because of the undermatching filler material but overall automatic welding showed improved fatigue strength compared with a manual process under both loading cases. Improvement can be explained with a continuous welding process with less welding defects and misalignment versus the manual process. In both loading cases, crack initiation started at the weld toe as assumed and consequently the fatigue strength could be increased by post-weld treatments. (Möller et al. 2015, p. 293-301.) Fatigue test results from butt joint tests under both loading cases are shown in figure 6.

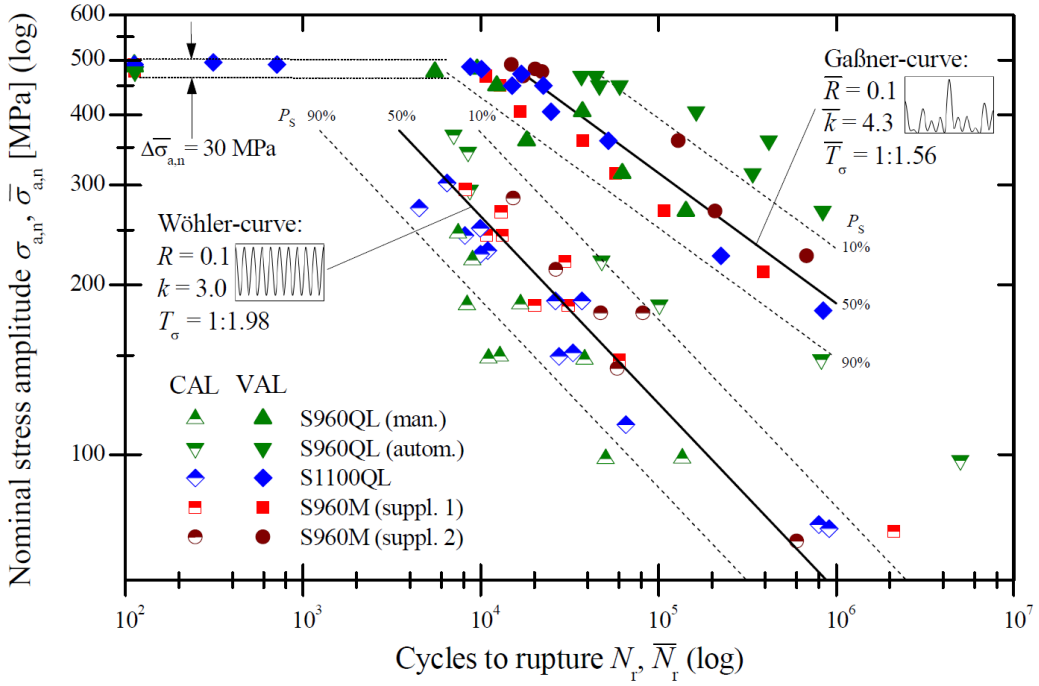

Figure 6. The S-N curves of the butt welded joints (Möller et al. 2015, p. 297).

Goss & Marecki (2012) conducted LCF tests for butt welded joints made of S960QL steel. TIG welding with X96-IG filler material was used in the specimen preparation. Tensile tests for base material were done to determine material properties. Residual stresses were measured with X-ray diffraction and specimens were tested under CAL. The fatigue life of the butt welded joints was up to 90% lower than base material and trend is the same at the HCF regime. Stress concentration factors α_k were also determined via Lawrence's method, Jawdokimov's method and FEA. Obtained α_k values with a Lawrence method for the weld top side reinforcement was 1.202 – 1.255 and for weld root 1.339 – 1.399. Values with the Jawdokimov method were 1.39 for weld top side reinforcement and 1.53 for weld root, respectively. FEA gave the lowest values for stress concentrations 1.20 for the weld root and 1.08 for the weld top side reinforcement. Residual stresses and external forces during tension had high influence on the test results. According to the test results welding has large effect on the fatigue strength of the S960QL. (Goss & Marecki 2012, p. 93-99.) S-N curves for the test results are shown in figure 7.

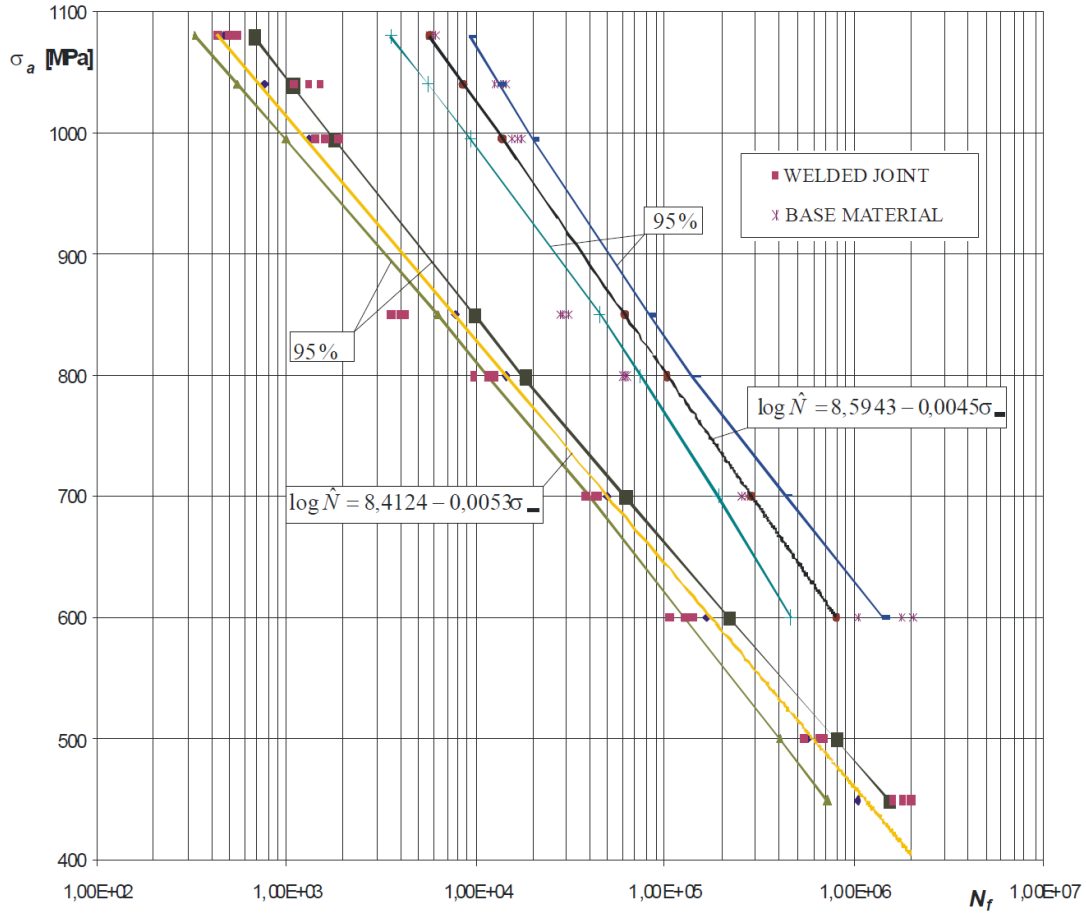

Figure 7. The S-N curves of the butt welded joints (Mod. Goss & Marecki 2012, p. 94).

Yildirim and Marquis (2012) evaluated published experimental results about high frequency mechanical impact (HFMI) -treated welds. Experimental tests related on longitudinal attachments, cruciform joints and butt joints subjected to axial loading with applied stress ratio $R = 0.1$ were examined and the yield strength of the materials within the collected data points vary between 260 MPa and 960 MPa. The study confirmed that when the yield strength of the material increases the fatigue strength of HFMI-treated joints also increases as many of previous studies had discovered and the increase in fatigue strength is around 12.5% towards each 200 MPa increase in the yield strength of the material compared to yield strength of 355 MPa. However, the improvement of fatigue strength by the HFMI-treatment method is sensitive to applied stress ratio and major benefit is obtained when $R \leq 0.15$. (Yildirim & Marquis 2012, p. 1-9.) The S-N curve from the existing data of HFMI treated longitudinal attachments is shown in figure 8.

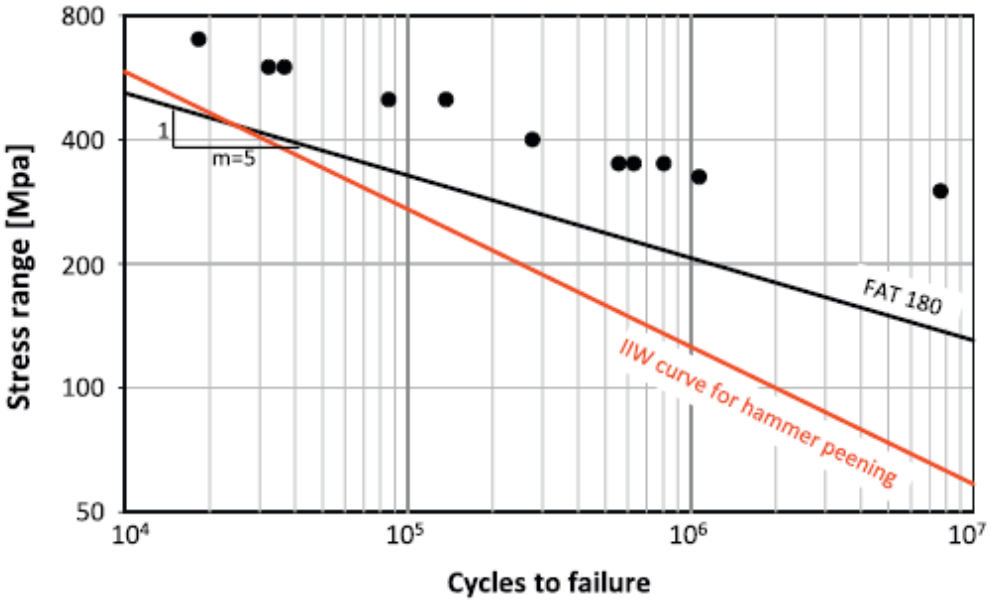

Figure 8. The S-N curve of HFMI treated longitudinal attachments when the yield strength of the steel is over 950 MPa (Mod. Yildirim & Marquis 2012, p. 7).

Berg and Stranghoener (2014) conducted fatigue tests for UHSS welded joints made of S960, S1100 and S1300 steels some of which were treated with high frequency hammer peening (HFHP) to find out its effect on the fatigue strength capacity. Longitudinal stiffeners, transversal stiffeners, cover plates and butt welds were investigated in the study with CAL with applied stress ratio R = 0.1. The fatigue strength of treated specimens was more than double compared with the untreated specimens and fatigue strength of the treated specimen increased about 15% in case of the longitudinal stiffener between steels S1100 and S1300 and 10% in case of butt weld between steels S960 and S1100. Available design recommendations for this treatment method is for material yield strength under 960 MPa and produces conservative results compared with the test results of this study. (Berg & Stranghoener 2014, p. 71-76.) Comparison of fatigue lives in different conditions is shown in figure 9.

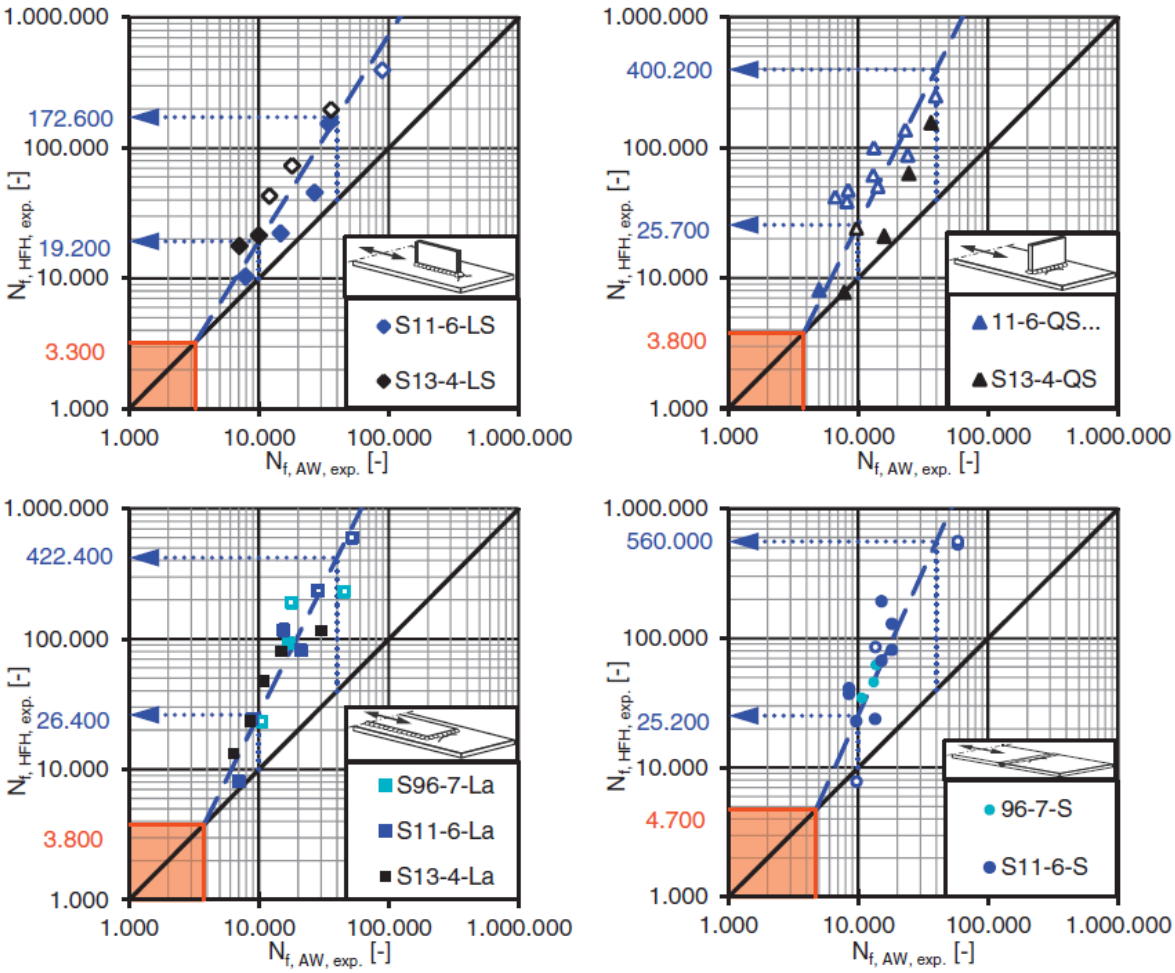

Figure 9. Comparison of fatigue lives in as-welded and HFHP-treated conditions (Berg & Stranghoener 2014, p. 75).

Leitner et al. (2015) studied HFMI-treated and as-welded (ASW) T-joints some of which are additionally stress-relief annealed. Tested materials were S690 and S960 steels and the applied stress ratio was R = 0.1. HFMI-treatment increased the fatigue strength of T-joints up to 60% as expected by other studies. Post-weld stress relieving conducted for HFMI-treated specimens decreased the fatigue strength of specimens about 10-25% with respect to the HFMI-treated specimens with no stress relieving but the fatigue strength is still about 20% better than with untreated specimens. Welding distortion and its effect on clamping was also examined in this study and as a result, it has substantial influence on local effective stress on the weld toe. (Leitner et al. 2015, p. 477-484.) Figure 10 shows test results for S960 in S-N curves.

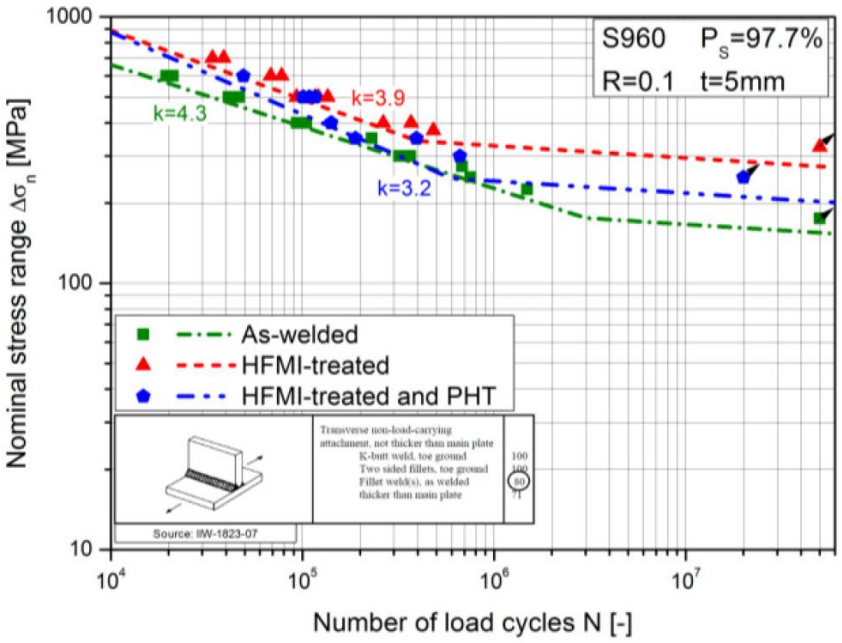

Figure 10. S-N curves for T-joints made from S960 (Leitner et al. 2015, p. 481).

Leitner (2017) studied more HFMI-treatment for butt joints with grinded root surface, T-joints and longitudinal stiffeners made from S960 with filler material G89 and the applied stress ratio of R = 0.1. Within this study the optimization of welding parameters can increase fatigue strength 7% in case of butt joints and 30% in case of T-joints and HFMI-treatment increases the fatigue strength of all studied joints that is even 2.46 times higher than as-welded condition in case of longitudinal stiffeners. Figure 11 shows S-N curves for butt welds, T-joints and longitudinal stiffeners made of S960 in ASW and HFMI -conditions. (Leitner 2017, p. 158-160, 169.)

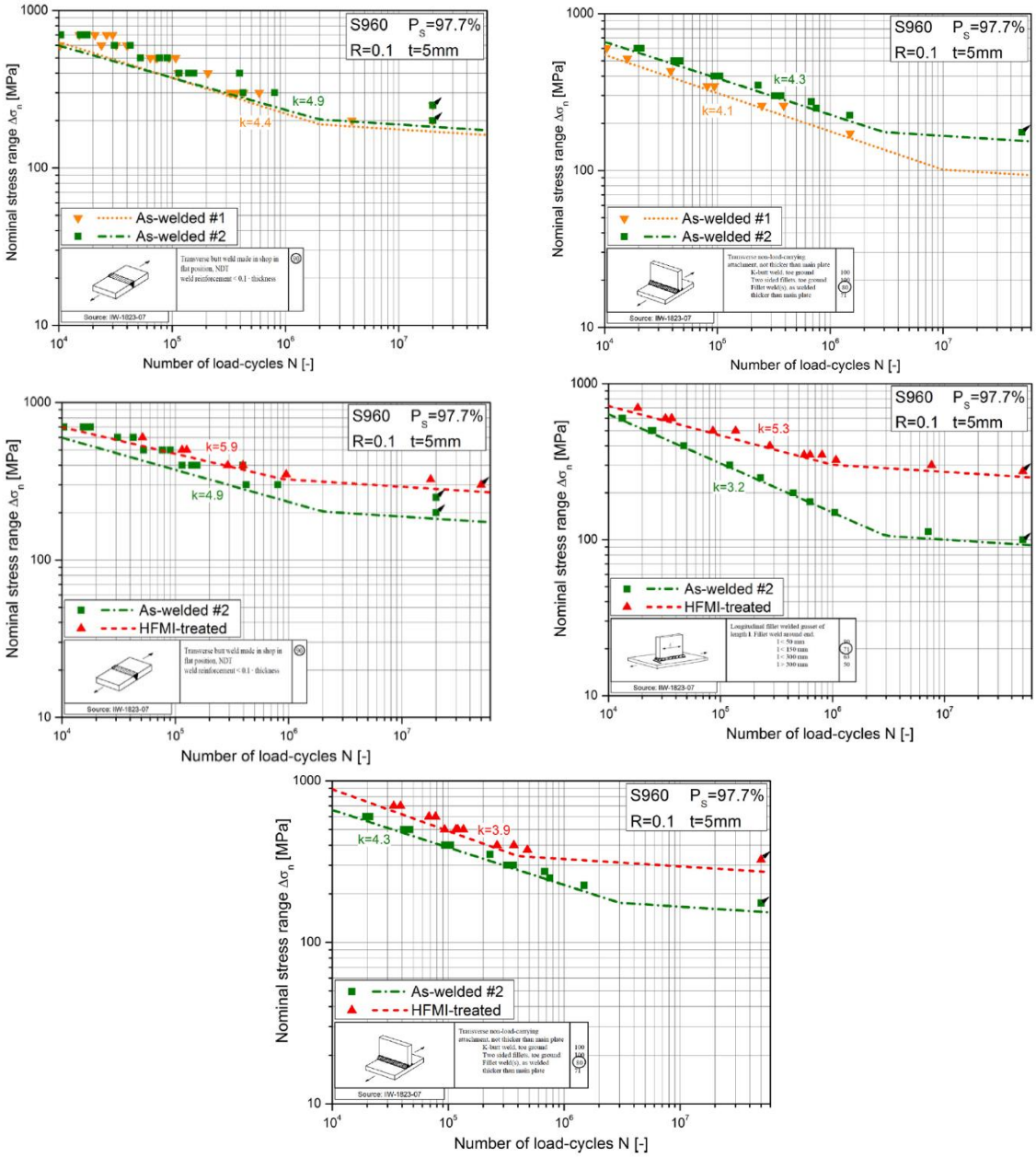

Figure 11. S-N curves for butt welds, T-joints and longitudinal stiffeners made from S960. As-welded #2 means optimized welding parameters. (Mod. Leitner 2017, p. 166-167.)

In the study, residual stresses and effect of clamping were taken into consideration. Local residual stresses on the weld toe were measured with an X-ray diffraction method. A decrease of the residual stresses at the weld toe or achievement of compressive residual stresses are beneficial in terms of having higher fatigue strength for the welded joints. According to the results, welding optimization reduced significantly residual stresses on the weld toe and with the HFMI-treatment, remarkable high compressive residual stresses were

achieved. (Leitner 2017, p. 161.) Measured surface residual stresses on different joint types and conditions are shown in table 1.

Table 1. Surface residual stresses at the weld toe in the loading direction. As-welded #2 means optimized welding parameters. (Mod. Leitner 2017, p. 162.)

Condition	As-welded #1	As-welded #2	HFMI-treated
Butt joint	+300 MPa	+75 MPa	-400 MPa
T-joint	+550 MPa	+320 MPa	-330 MPa
Longitudinal stiffener	N/A	-50 MPa	-600 MPa

The clamping of the specimen to the testing machine can increase stress at the weld toe because of the distortion of the specimen due to welding (Leitner 2017, p. 161). Effect of the angular distortion and the radius of the weld toe on the notch stress is illustrated as diagrams in figure 12.

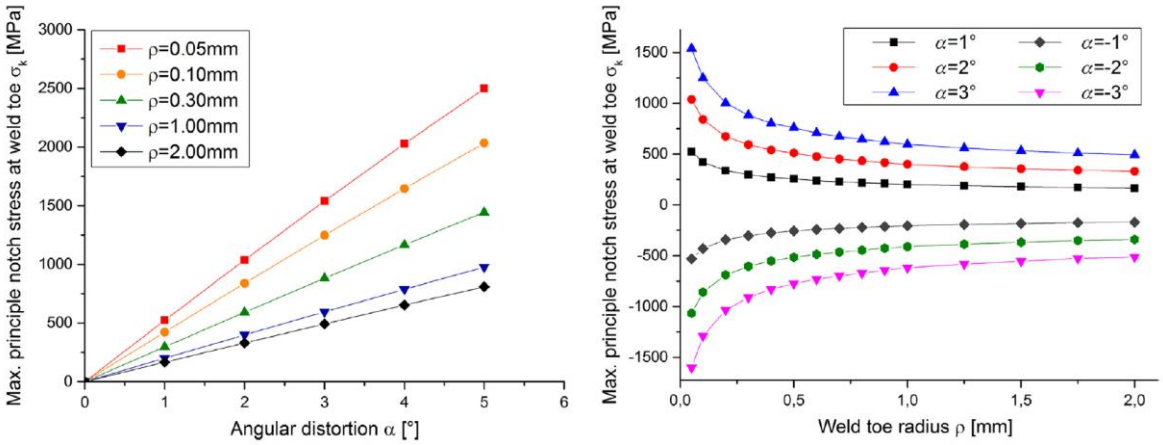

Figure 12. Notch stress at weld toe as a functions of angular distortion and weld toe radius (Leitner 2017, p. 163).

Yildirim (2015) examined existing fatigue data about tungsten inert gas (TIG) dressing. The study includes 311 data points from published test results for butt joints, T-joints, transverse non-load carrying joints and longitudinal attachments with yield strength between 272 MPa and 1100 MPa. Thickness of specimens was between 5 and 15 mm. The majority of the tests was conducted under CAL and applied stress ratio was between -1 to 0.2. Fatigue data from CAL is proven to be in a good relation with the recommended design curves even though

they are conservative in comparison with available data. For instance, when using best-fit slope fatigue life improved 57% and using slope m = 4 the increase was 89% compared with as-welded condition in the case of longitudinal attachment. The S-N slope of m = 4 seems to be better for the TIG dressed joint under CAL but more research is needed to get more data about TIG dressed butt welds, transverse non-load carrying welds and longitudinal attachments made from high or ultra-high strength steels to confirm design proposals. (Yildirim 2015, p. 36-45.) Figure 13 shows the analysis of existing fatigue data for CAL tests.

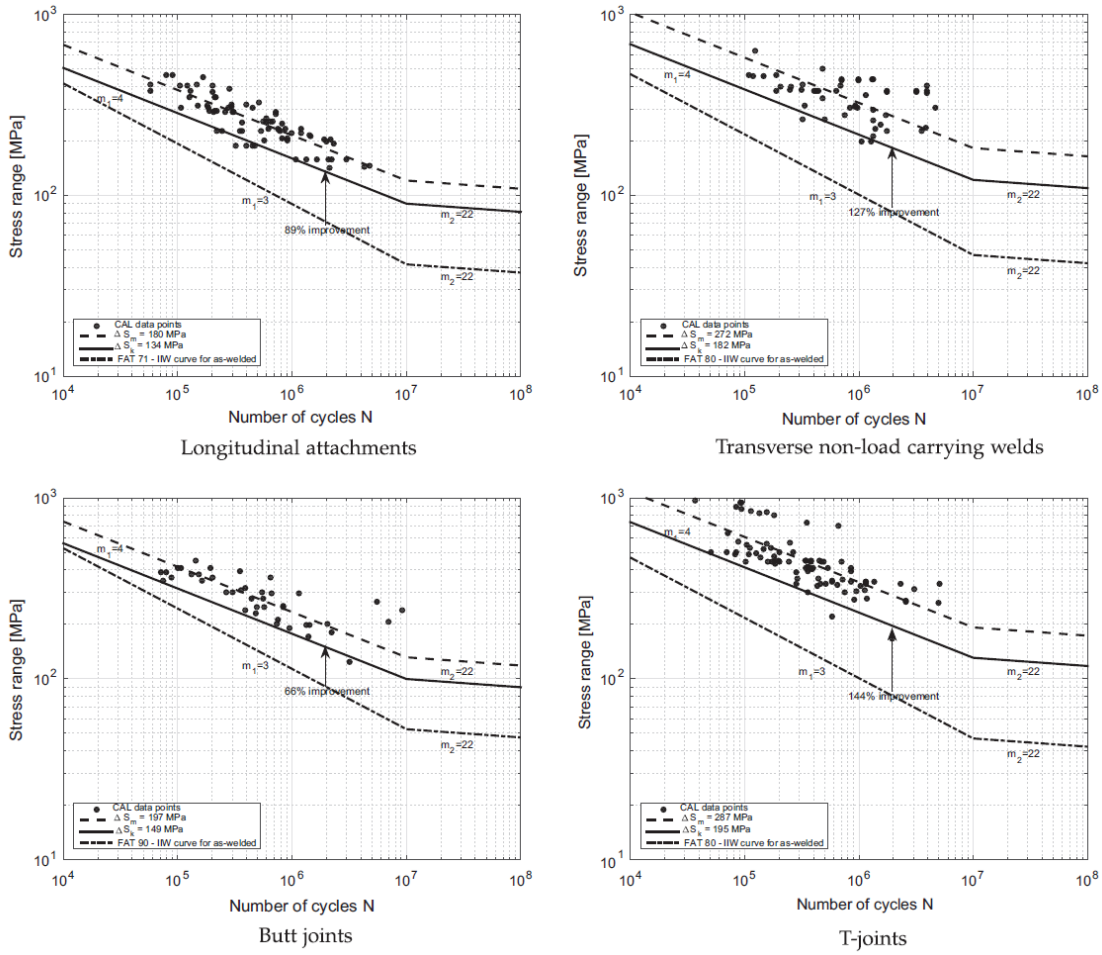

Figure 13. S-N curves based on existing fatigue data for different joint types under CAL (Yildirim 2015, p. 41).

Van Es et al. (2013) studied TIG-dressing for butt welds between two rolled plates (rolled-rolled) and between cast and rolled plates (rolled-cast). Four steel grades were used in the study: S460, S690, S890 and S1100. Thickness of the test specimens was 25 mm except the

case of S1100 that thickness was 20 mm. Part of the S890 and S100 specimens failed at the base material in ASW-condition, so the test results indicates that TIG-dressing improves fatigue strength, if base material failure does not happen. However, base material failure means that TIG-dressing has eliminated the cracking at the weld toe. The number of test specimens was relatively small, so more fatigue test results are needed to make better conclusions. Comparison of the test results of S1100 is shown in figure 14 in which the rolled-rolled joint is marked with V and rolled-cast joint is marked with C. Results were adjusted for mean stress, certain residual stress, reference thickness, pure tension loading and damaged specimens were excluded from results. (van Es et al. 2013, p. 126-128, 133-136.)

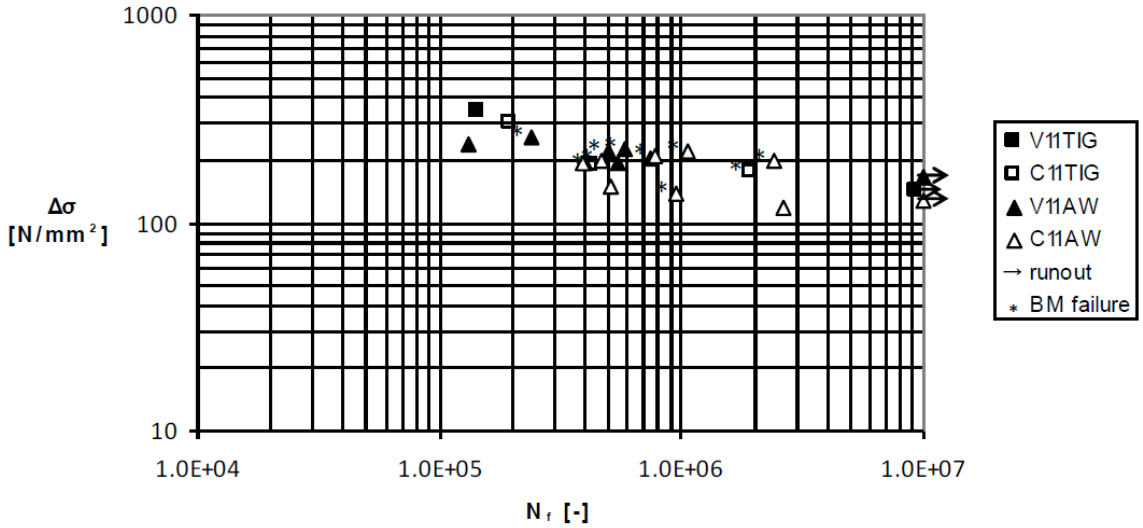

Figure 14. Comparison of the S1100 test results in both conditions. Adjusted data. (van Es et al. 2013, p.134.)

The test results, in which the joint failed from weld toe, were compared with a critical distance theory FE-model. Modelled fatigue life results were non-conservative and did not correspond exactly the test results that might be due to data adjustment or that the model does not describe weld toe failure process in the right way. (van Es et al. 2013, p. 135.) Comparison of the S1100 results is shown in figure 15.

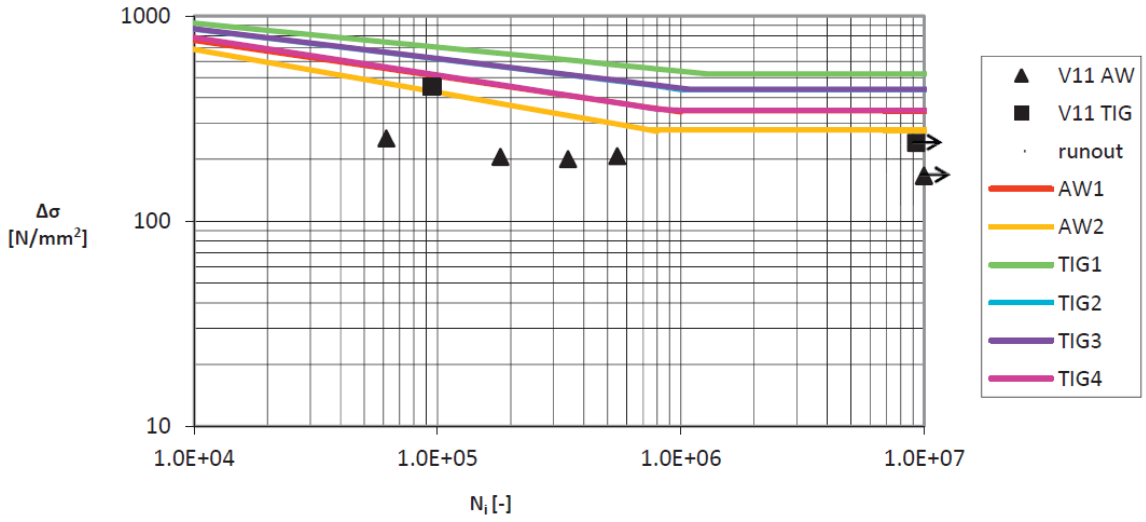

Figure 15. Comparison of the S1100 results (van Es et al. 2013, p. 135).

Skriko et al. (2017) studied fatigue strength of TIG-treated non-load carrying X-joints at high stress ratio under CAL and applied stress ratio varied between $R = 0.1$ and $R = 0.6$. Test specimens were made of Strenx® 960 MC using robotized GMAW with Union X96 fillermaterial. In addition, FE-analyses were conducted to study the effect of TIG-treatment to the stress concentration factor. Residual stress measurements, 2D measurements and hardness measurements were also carried out. The test results showed that IIW recommendations for TIG-treatment are conservative and higher stress ratio decreased fatigue strength of test specimens 30% with slope $m = 4$ between stress ratios $R = 0.1$ and $R \geq 0.5$. The test specimens failed from fusion line of TIG-treated area towards either weld metal or base material. Weld toe radius and possible undercut affected most to the stress concentration factor based on the FE-analyses. According to the measurements TIG-treatment caused both HAZ softening and high compressive residual stresses compared with base material. (Skriko et al. 2017, p. 110-119.) Fatigue test results are shown in figure 16.

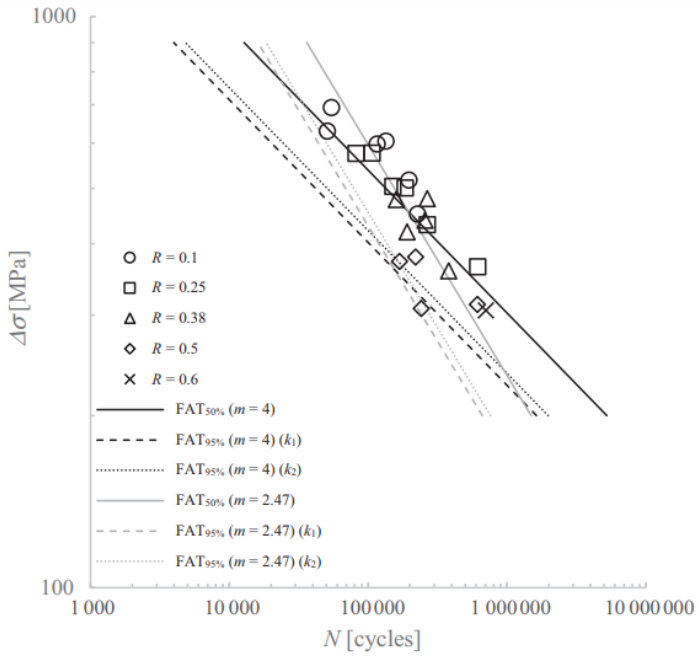

Figure 16. Fatigue test results of TIG-treated specimens (Skriko et al. 2017, p. 115).

The previously introduced articles and conference papers can be summarized. Fatigue life calculation results are conservative because there are no standards or design codes for UHSSs. Weld toe crack is common failure mode and high fabrication quality is very important with UHSSs. Undermatching filler material can lead to that all potential of the S1100 cannot be fully obtained. The automatic welding process and optimization of welding parameters improves fatigue life. In addition, fatigue life can be improved with post-weld treatments and its benefits increases as the yield strength of material increases. Residual stresses, weld toe radius and distortion play an important role in the fatigue strength of structures and clamping of the specimen is important to take into account in testing. HFMI-treatment is used to get beneficial compressive residual stresses at the weld toe from the fatigue strength point of view. TIG-dressing is used to get a smoother weld toe boundary which can eliminate weld toe cracking and improves fatigue strength.

2.1.2 Standards and guidelines related to this study

Standards and guidelines are used for designing of structures and material testing. Eurocode 3 is used in Europe to guide design of load-bearing structures and EC3 covers issues related to the design of steel structures. Eurocode 3: Design of steel structures. Part 1-9: Fatigue covers fatigue life assessment of structures (SFS-EN 1993-1-9 2005, p. 6). The International institute of Welding (IIW) have guidelines for fatigue design, for example, FAT classes and

post-weld treatments like burr grinding, TIG-dressing and HFMI-treatment. However, as mentioned in the introduction the EC3 is justified for steels having yield strength less than 700 MPa and IIW guidelines are for yield strength up to 960 MPa. (SFS-EN 1993-1-12 2007, p. 4; Hobbacher 2016, p. 1-2; Marquis & Barsoum 2016, p. 1; Haagensen & Maddox 2006, p. 1.) Standards related to material testing are usually international ISO-standards so that testing is always done in the same way worldwide. Testing standards are based on general standard SFS-EN 10021 on which basis testing standards covers in more detail testing methods and guidelines so that the similarity and repeatability of the tests are possible. (Finnish Standards Association SFS.) However, standards do not give instructions for all details in testing such as stress ratio values, role of imperfections, clamping and measuring of different parameters. Standards covers tensile and fatigue testing of metallic materials and welded joints and determine dimensions for test specimens (SFS 3099 1974, p. 1; SFS-EN ISO 4136 2012, p. 1; SFS-EN ISO 9018 2015, p. 17). Fatigue tests can be performed by controlling force or strain (SFS-ISO 1099 2017, p. 5; ISO 12106 2017, p. 1).

2.2 Fatigue strength assessment methods for welded joints

Fatigue is a failure mode that fluctuating or cyclic loading leads to the fracture in the structure and it is very important to take account at the design stage (Dowling 2013, p. 25-26). Fatigue is phenomena that consist of crack initiation, crack propagation and the final fracture. Fatigue is a localized process and it is vitally influenced by geometry of structure, type of loading, material properties and operating environment so these things must be properly take into consideration when calculating the fatigue strength of the structure. Welding potentially produces cracks, pores and cavities so there are already initiated cracks in the structure. In addition, undercuts, lack of penetration and overlap of the weld can be considered as initial cracks. Cyclic or fluctuating loading causes stress variation in the potential crack tip that leads to the propagation of the initiated crack. (Radaj, Sonsino & Fricke 2006, p. 1-9.) Figure 17 presents the progress of fatigue failure.

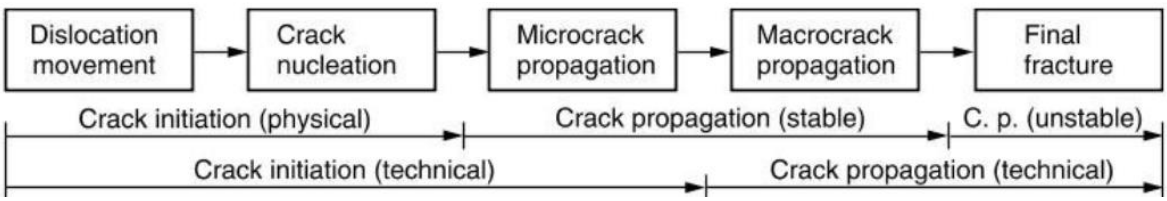

Figure 17. The progress of fatigue failure (Radaj et al. 2006, p. 3).

There are several fatigue strength assessment methods that can be used to estimate fatigue life before final fracture. Typical methods are the nominal stress method, structural stress method (Hot Spot-method), effective notch stress method (ENS) and linear elastic fracture mechanics (LEFM). Methods are based on that the amount of stress ranges are calculated together which are caused by the variable loading within the expected lifetime of the structure. Usually for welded joints so called rainflow method is used to convert variable amplitude stress ranges to equivalent amplitude stress range to be able to calculate fatigue strength. (Hobbacher 2016, p. 8-9, 12, 35-36.) A brief description of the stress-based fatigue strength assessment methods above and novel 4R method is described in the following paragraphs because these methods are used in this study.

2.2.1 Nominal stress method

In the fatigue strength assessment by the nominal stress approach, the nominal stress σ_{nom} is only taken into account including macro-geometric effects which are due to holes or openings in the structure, for example. There is fatigue class value (FAT) for different kind of structural details in the IIW Recommendations to take into account macro-geometric effects of structures in the calculation. Local stress concentrations due to structural details are ignored in this method. (Hobbacher 2016, p. 15-17.) Figure 18 shows nominal stress distribution in beam structure and how the effect of weld is ignored in this method.

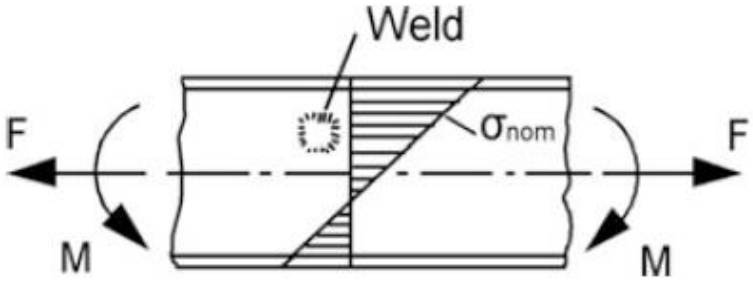

Figure 18. Nominal stress in beam structure loaded by moment and tension (Hobbacher 2016, p. 15).

The nominal stress method gives results with a small amount of work compared with other methods, but the results might not be so accurate depending of the structure. This method is recommended for simple and not so critical structures (Radaj et al. 2006, p. 15).

2.2.2 Structural stress method

The structural stress method is also known as Hot Spot-method and it takes account those structural stress concentrations that nominal stress method ignored but does not take into account the local stress peaks due to profile of the weld. Hot Spot stresses are defined on the surface of the structure that is under consideration. If there is no clear way to define nominal stress or there is no fatigue resistance value for detail that is under consideration, the structural stress method can be used, for example. Hot Spot stress σ_{hs} for the calculation of fatigue life can be determined by FEA or linear extrapolation from stresses measured by strain gages. (Hobbacher 2016, p. 18-21.) Structural stresses due to discontinuities in the structure are shown in figure 19.

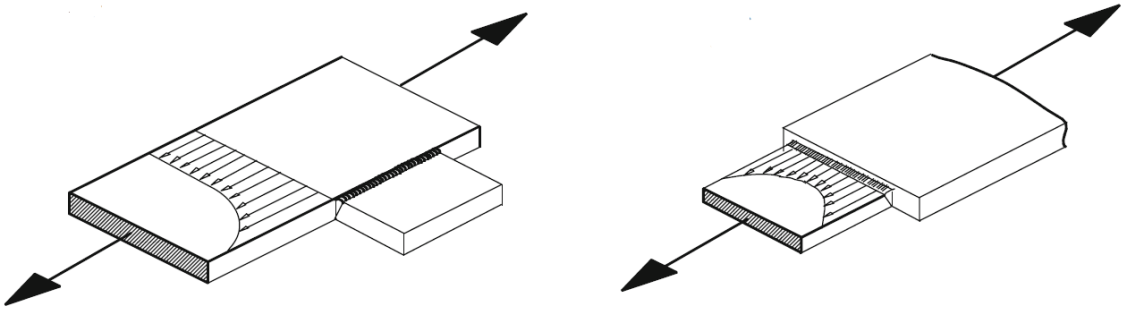

Figure 19. Structural stress distributions for two example cases (Mod. Hobbacher 2016, p. 18).

The structural stress method should give more accurate results than the nominal stress method but in the process it takes more time. This method is applicable especially for the fatigue assessment of weld toe failures, but it can be extended to root side analysis (Hobbacher 2016, p. 19).

2.2.3 Effective notch stress method

In the fatigue strength assessment by the ENS approach, local profile of the weld is taken into account that structural stress method ignored. In this method actual shape of the weld is replaced by the effective notch root radius (1 mm for structural steels with plate thickness 5 mm or more) to obtain the effective notch stress σ_{ens} for fatigue strength calculation. Stress values can be obtained by FEA or parametric formulas. (Hobbacher 2016, p. 27-28.) Figure 20 clarifies how the actual shape of the weld is replaced by fictitious rounding.

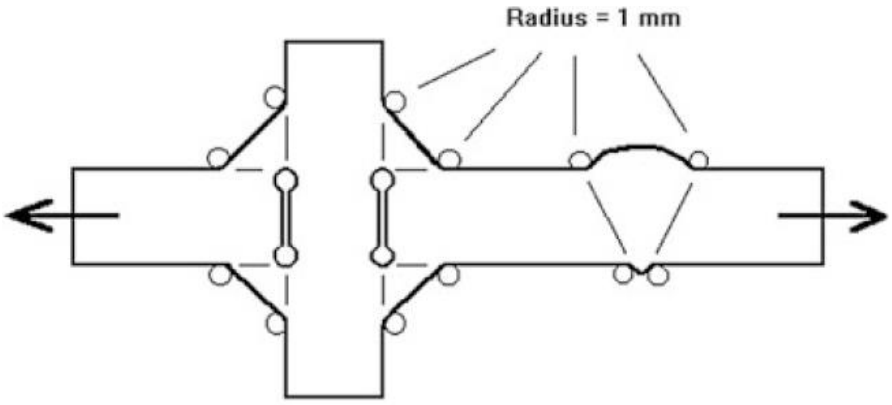

Figure 20. Weld toes and roots are replaced by fictitious rounding (Hobbacher 2016, p. 27).

The ENS method should give even more accurate results than the first two methods but still it also increases the workload. This method is applicable for both weld toe and root side fatigue strength assessment (Hobbacher 2016, p. 27).

2.2.4 4R method

The 4R method is a fatigue strength assessment method for welded joints which is suitable for both variable and constant amplitude loading and it has been developed by Laboratory of Steel Structures at Lappeenranta University of Technology. Material strength R_m, weld toe radius r, local residual stresses σ_{res} and applied stress ratio R in addition to stress range $\Delta\sigma$ are taken into account. (Björk et al. 2018, p. 1-2.) Figure 21 introduces calculation procedure using 4R method.

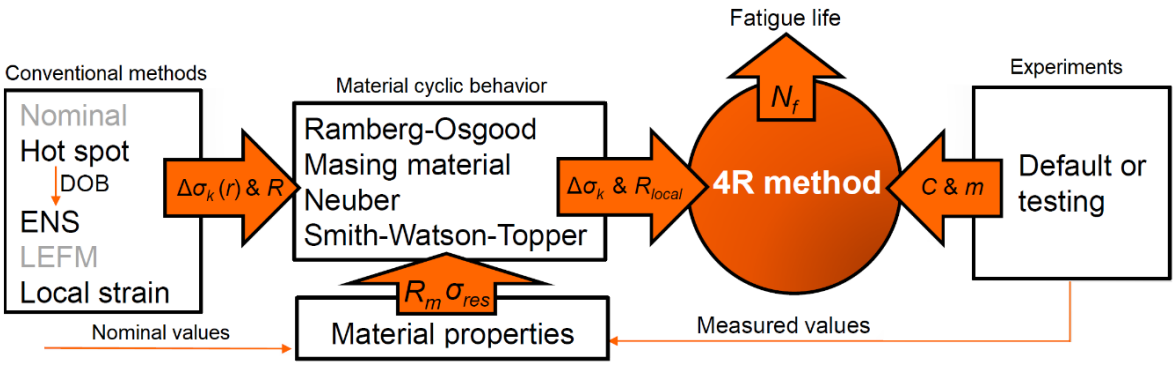

Figure 21. Calculation procedure using the 4R method (Mod. 4R Method 2018, p. 6).

In figure 21, $\Delta\sigma_k$ is effective notch stress range which takes account weld toe radius, R_{local} is local stress ratio, C is fatigue capacity and m is slope of the reference curve. Values for C and m are obtained from earlier fatigue tests. The figure 21 shows that the calculation is based on conventional ENS and local strain methods together with material cyclic behavior related formulas like Ramberg-Osgood relationship, Neuber's theory, Bauschinger's effect and Smith-Watson-Topper (SWT) criterion.

The 4R method enables to exploit the potential of UHSSs because EC3 and IIW gives more conservative fatigue life results than this method which leads to the more competitive structures and post-weld treatments can be taken better into account in calculation. Method can be used to analyze previously obtained fatigue test results and assists to design the tests better in the future. (Mikkonen et al. 2017, p. 30.)

3 EXPERIMENTAL TESTING

This chapter discusses experimental testing. Test specimens, material properties, measurements and results are presented. Fatigue tests were performed in the Laboratory of Steel Structures at Lappeenranta University of Technology. The manufacturing of test specimens and hardness measurements carried out in collaboration with other laboratories at the university.

3.1 Test specimens

Test specimens were laser cut from 8 mm thick steel sheet and specimens were robotized GMAW welded in order to obtain uniform welding quality for all the test specimens with Voestalpine Böhler Welding's Union X96 1 mm diameter filler material. Two butt joints were welded with fiber laser without filler material. Butt joints (BW), non-load carrying T-joints (NLCT), load carrying X-joints (LCX) and longitudinal gusset joints (LG) were investigated under different stress ranges and applied stress ratios. Some of the NLCT and LG-joints were post-weld treated by HiFIT or TIG. Welding parameters are presented in Appendix I. Welding start and stop points were cut and machined away other than LG-joints and then edges were ground and strain gage was attached to test specimen. Each specimen was named so that material, joint type, number of the specimen and possible post-weld treatment can be clarified. Principally two different stress range levels $\Delta\sigma_1$ and $\Delta\sigma_2$ were used for each joint type and two different stress ratios $R_1 = 0.1$ and $R_2 = 0.5$. The total number of specimens was 33. Test matrix for the specimens is shown in table 2.

Table 2. Test matrix for specimens.

Specimen ID	Joint type	Welding process	Post-weld treatment	Stress range	*R*
S11_BW_1	BW	GMAW	no	$\Delta\sigma_1$	0.5
S11_BW_2	BW	GMAW	no	$\Delta\sigma_1$	0.1
S11_BW_3	BW	GMAW	no	$\Delta\sigma_2$	0.1
S11_BW_4	BW	GMAW	no	$\Delta\sigma_2$	0.5
S11_BW_5	BW	GMAW	no	$\Delta\sigma_2$	0.5
S11_BW_6	BW	GMAW	no	$\Delta\sigma_1$	0.1
S11_BW_7	BW	GMAW	no	$\Delta\sigma_1$	0.5

Table 2 continues. Test matrix for specimens.

Specimen ID	Joint type	Weld Process	Post-weld treatment	Stress range	*R*
S11_LW_1	BW	Laser	no	$\Delta\sigma_1$	0.1
S11_LW_2	BW	Laser	no	$\Delta\sigma_1$	0.5
S11_NLCT_1	NLCT	GMAW	no	$\Delta\sigma_1$	0.1
S11_NLCT_2	NLCT	GMAW	no	$\Delta\sigma_1$	0.5
S11_NLCT_3	NLCT	GMAW	no	$\Delta\sigma_1$	0.1
S11_NLCT_4	NLCT	GMAW	no	$\Delta\sigma_1$	0.5
S11_NLCT_5	NLCT	GMAW	no	$\Delta\sigma_2$	0.1
S11_NLCT_6	NLCT	GMAW	no	$\Delta\sigma_2$	0.5
S11_NLCT_7H	NLCT	GMAW	HiFIT	$\Delta\sigma_1$	0.1
S11_NLCT_8H	NLCT	GMAW	HiFIT	$\Delta\sigma_2$	0.1
S11_NLCT_9H	NLCT	GMAW	HiFIT	$\Delta\sigma_1$	0.5
S11_NLCT_10H	NLCT	GMAW	HiFIT	$\Delta\sigma_2$	0.5
S11_NLCT_11T	NLCT	GMAW	TIG	$\Delta\sigma_1$	0.1
S11_NLCT_12T	NLCT	GMAW	TIG	$\Delta\sigma_1$	0.5
S11_NLCT_13T	NLCT	GMAW	TIG	$\Delta\sigma_1$	0.1
S11_NLCT_14T	NLCT	GMAW	TIG	$\Delta\sigma_1$	0.5
S11_LCX_1	LCX	GMAW	no	$\Delta\sigma_1$	0.1
S11_LCX_2	LCX	GMAW	no	$\Delta\sigma_1$	0.5
S11_LCX_3	LCX	GMAW	no	$\Delta\sigma_2$	0.1
S11_LCX_4	LCX	GMAW	no	$\Delta\sigma_2$	0.5
S11_LG_1	LG	GMAW	no	$\Delta\sigma_1$	0.1
S11_LG_2	LG	GMAW	no	$\Delta\sigma_1$	0.5
S11_LG_3	LG	GMAW	no	$\Delta\sigma_2$	0.1
S11_LG_4	LG	GMAW	no	$\Delta\sigma_2$	0.5
S11_LG_5H	LG	GMAW	HiFIT	$\Delta\sigma_1$	0.1
S11_LG_6H	LG	GMAW	HiFIT	$\Delta\sigma_1$	0.5

3.1.1 Strenx® 1100 Plus

SSAB's Strenx® 1100 Plus structural steel was used in test specimens. Toughness of material can be defined with Charpy pendulum impact test where the amount of absorbed energy in to the material is measured (SFS-EN ISO 148-1 2016, p. 5). Mechanical properties of material are shown in table 3.

Table 3. Nominal mechanical properties of Strenx® 1100 Plus (SSAB 2019).

Rolling direction	Yield strength $R_{p0,2}$	Tensile strength R_m	Elongation A_5	Minimum impact energy
0°	≥ 1100 MPa	1130 – 1350 MPa	10 %	27 J/ -40 °C
90°	≥ 1100 MPa	1130 – 1350 MPa	10 %	27 J/ -20 °C

Weldability of steel can be estimated with equivalent carbon content (CEV) which can be calculated from chemical composition of steel (Lukkari 2016, p 20). Chemical composition of the used material is shown in table 4. Cooling time $t_{8/5}$ from 800 °C to 500 °C for the used material is 5-20 s, preheating is not needed and maximum interpass temperature is 150 °C (Björk 2018).

Table 4. Chemical composition of Strenx® 1100 Plus (SSAB 2019).

Content percentage (%)					
C (max)	Si (max)	Mn (max)	P (max)	S (max)	Al (min)
0.20	0.50	1.80	0.020	0.005	0.015

3.1.2 Union X 96 filler material

Union X 96 is Voestalpine Böhler Welding's low-alloyed solid wire filler material for fine grained quenched and tempered high strength structural steels that has good deformability and resistance to cold-cracking despite its mechanical properties (Union X 96 2014). Mechanical properties and chemical composition of Union X 96 are shown in table 5.

Table 5. Nominal mechanical properties and chemical composition of Union X 96 filler material (Mod. Union X 96 2014).

Union X 96					
Yield strength $R_{p0,2}$	Tensile strength R_m	Elongation A	Impact strength		
930 MPa	980 MPa	14 %	47 J/ -50 °C		
Maximum content percentage (%)					
C	Si	Mn	Cr	Mo	Ni
0.12	0.80	1.90	0.45	0.55	2.35

3.1.3 Manufacturing of the test specimens

The test specimens were laser cut from the sheets and cleaned with 10 % citrus acid liquid. The specimens were tack welded from both ends with TIG. All the test specimens were prepared with single-pass welding and the specimen was allowed to cool less than 50 °C between the beads. After welding, in the selected specimens, post-weld treatment was performed for the entire length of the weld excluding LG-specimen where only ends of the gusset were treated. After that, welding start and stop areas were cut and machined away and edges of the specimen were ground to avoid edge cracks. Welding parameters for each pass are presented in Appendix I. Main dimensions and welding sequence of BW GMAW specimen are shown in figure 22.

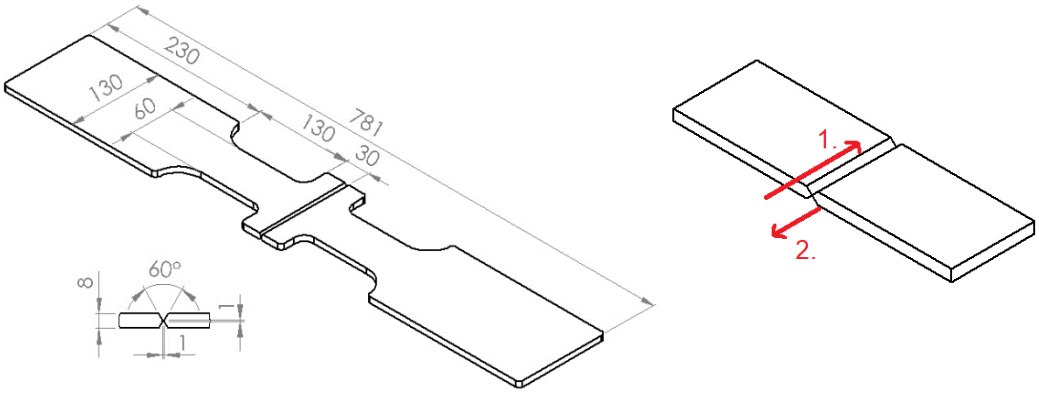

Figure 22. Main dimensions and welding sequence of BW GMAW specimen.

In the case of GMAW butt welds, X-groove with 1 mm root surface, 60 degree angle and air gap of 0 mm (S11_BW_1 - 4) and 1 mm (S11_BW_5 - 7) was used. The tack welded specimens were clamped to the table to avoid angular distortion due to welding as much as possible. For the first bead, 2 mm sheet of steel was added under the specimen to each side

to get advance because second bead will cause more distortion another direction. Root opening was done for the weld after the first bead to make sure that weld was fully penetrated. For the second bead, steel sheets were removed and the specimen was clamped to the table and slightly advance in the same direction as in the first bead was formed due to weld cup. After welding a bead, in both welds, the specimen was allowed to cool before loosen the clamps. Figure 23 shows clamping method of the BW GMAW specimens.

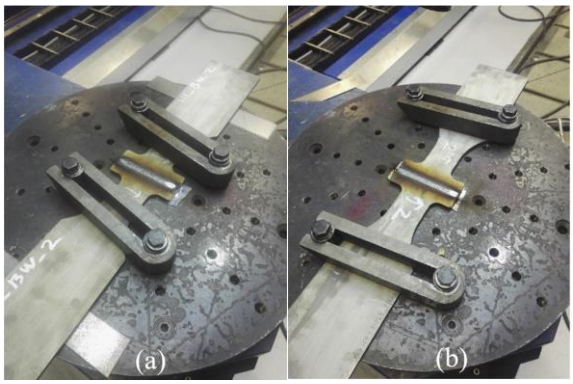

Figure 23. Clamping of the GMAW BW specimen. (a) First weld pass and (b) second weld pass.

In the case of fiber laser butt welds, machined I-groove with no air gap was used. Main dimensions of the specimens were similar to the BW GMAW specimens. The tack welded specimen clamped to the table and let cool down after welding before loosen the clamps. Figure 24 shows clamping method of the specimens.

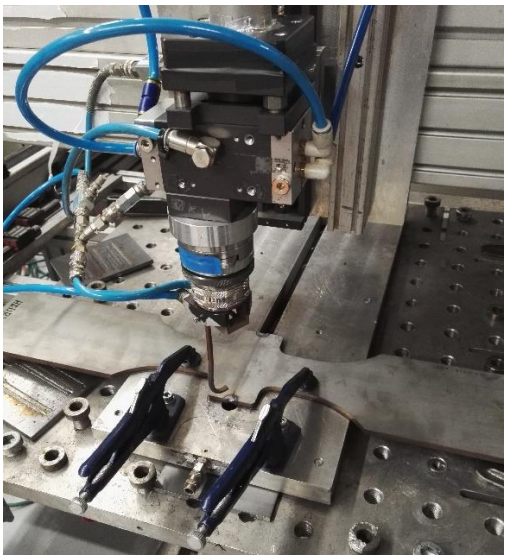

Figure 24. Clamping of the laser welded specimen.

Main dimensions and welding sequences of NLCT- and LCX-specimens are shown in figures 25 and 26.

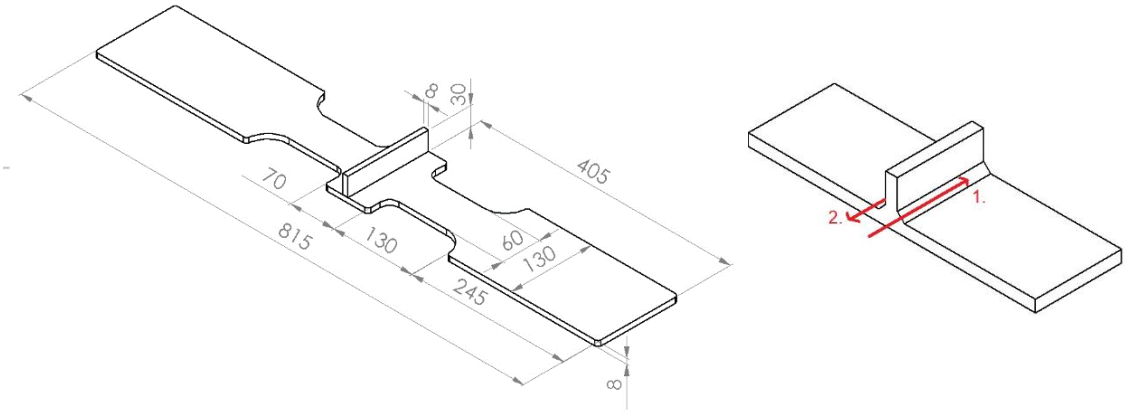

Figure 25. Main dimensions and welding sequence of NLCT-specimen.

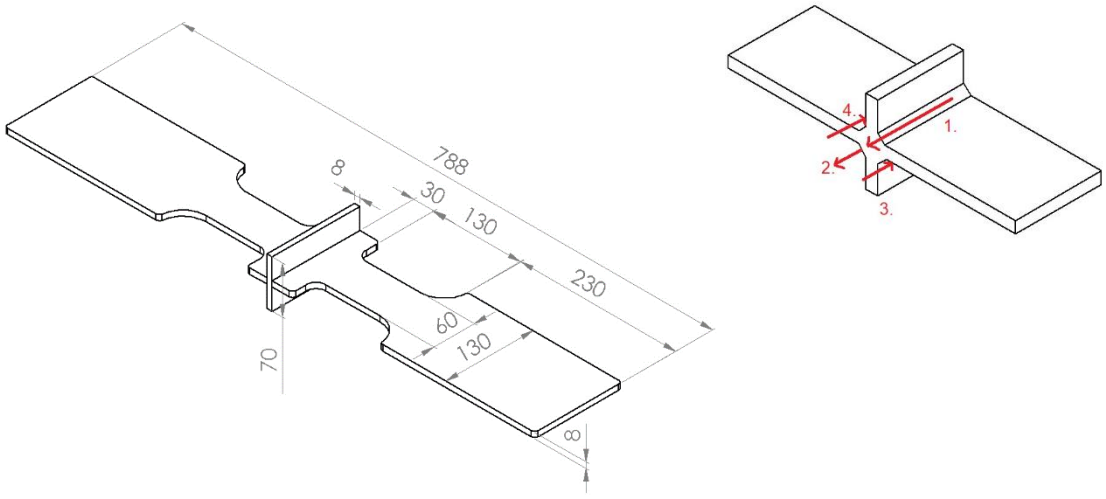

Figure 26. Main dimensions and welding sequence of LCX-specimen.

In the case of the NLCT and LCX -specimens, the tack welded specimen was fastened to a vise. Specimen was allowed to cool less than 50 °C between the beads. HFMI-treatment was performed for the NLCT-joints S11_NLCT_7H - S11_NLCT_10H and TIG-treatment was performed for NLCT-joints S11_NLCT_11T - S11_NLCT_11T before cutting and machining. In order to find out which one is more critical, weld toe or root side, in terms of fatigue strength, no post-weld treatments were performed for the LCX-specimens. Transverse attachment was machined to height of 20 mm in both specimen types to be able

to measure residual stresses at the weld toes. Figure 27 shows fastening of the LCX and NLCT -joint specimens to the vice.

Figure 27. LCX-joint fastened to vise.

Main dimensions and welding sequence of LG-specimen are shown in figure 28.

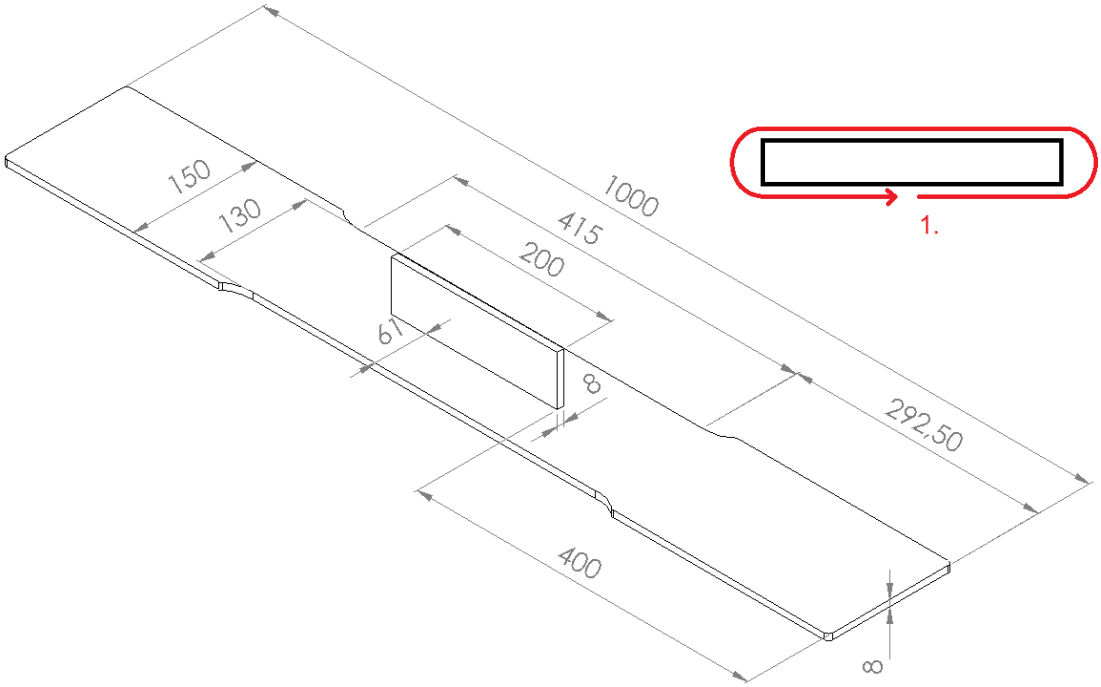

Figure 28. Main dimensions and welding sequence of LG-specimen.

In the case of the LG-specimen, the gusset was tack welded from both sides about 50 mm away from the both ends of the gusset. Tack welded specimens were fastened to table. Gusset was welded at one time so start and stop point was only on the other side of the gusset. Cutting or machining was not needed in this type of specimen, but edges were ground. HFMI-treatment was performed for the LG-specimens S11_LG_5H and S11_LG_6H. Weld toes of the both ends of the gusset were treated around the tip and approximately 25 mm in the longitudinal direction of the specimen. Figure 29 shows fastening of the LG-specimen specimens to the table and HiFIT-treated area.

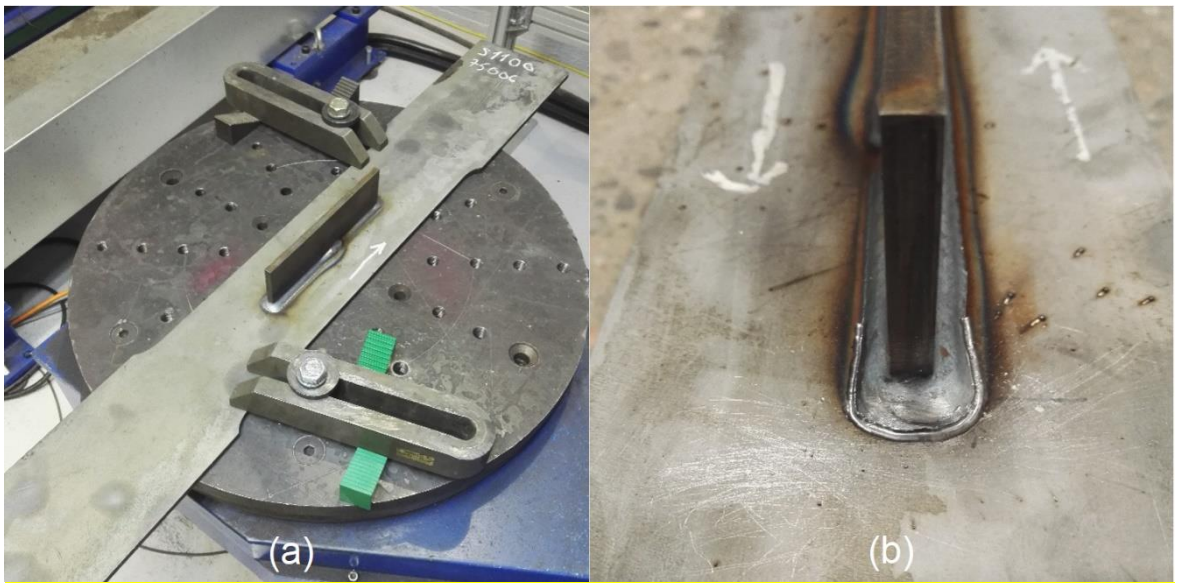

Figure 29. LG-joint fastened to table (a) and HiFIT-treated end of the gusset (b).

3.2 Measurements

Various measurements were carried out after manufacturing of the test specimens. Shape laser 2D measurement was carried out to find out angular distortion, weld geometry and throat thickness of the specimens for the FE-analysis. Measurements were done in the centerline of the specimen. Angular distortion for all specimens and more accurate weld geometry for BW-specimens could be measured at horizontal position which is shown in figure 30a, but the weld geometry for NLCT, LCX and LG -specimens had to be measured at an angle to avoid possible shades due to attachment which is shown in figure 30b. Local weld toe geometry was measured first to get accurate weld toe radius, flank angle and throat thickness of the weld. After that global shape of the specimen was measured to obtain angular distortion of the specimen.

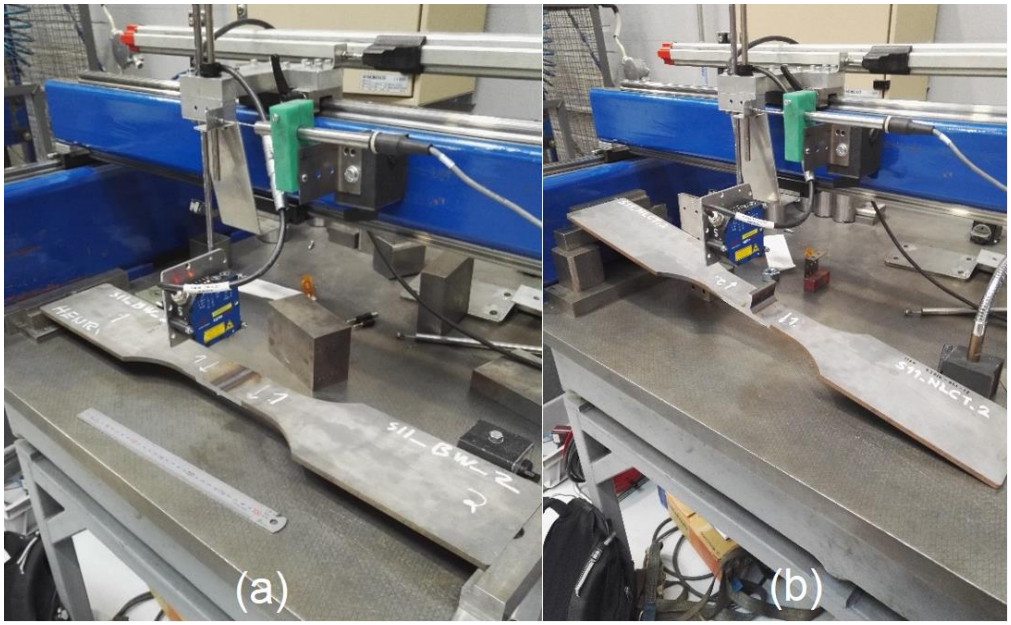

Figure 30. 2D measurement of BW (a) and NLCT -specimen (b).

Measurement data was imported to AutoCAD-software to measure weld toe radius, flank angle, throat thickness and angular distortion for each specimen. Lines and circles were fitted visually to the 2D data points, so that the needed values could be measured. Figure 31 shows an example, how the weld toe radius, flank angle and throat thickness were measured from imported data.

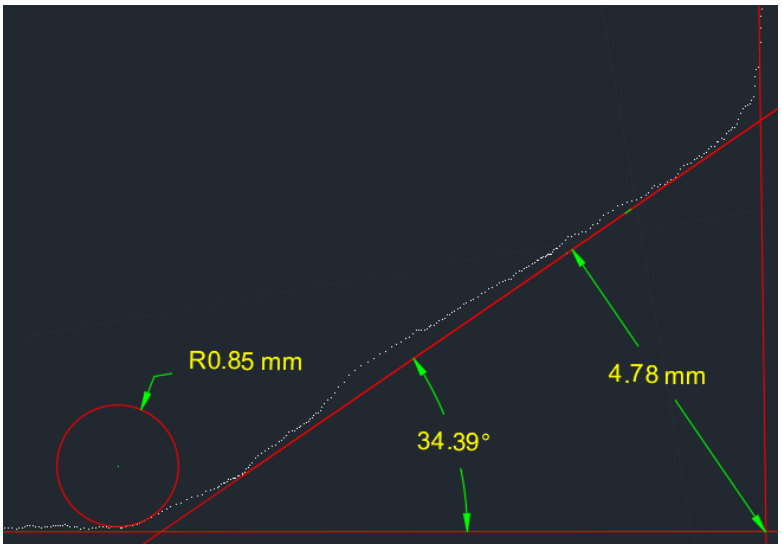

Figure 31. Weld toe radius, flank angle and throat thickness measurement from 2D data of NLCT-specimen.

Angular distortion of the specimen was measured by drawing two hand fitted lines and measuring the angle between these lines. Figure 32 shows how angular distortion was measured from 2D data.

Figure 32. Angular distortion measurement from 2D data of BW-specimen.

Residual stresses were measured by an X-ray diffraction method from the surface of the specimen in a longitudinal direction from the centerline of the specimen. Residual stresses at the fatigue critical weld toes, parallel to the loading direction, were measured from all welds of the all specimens and for one specimen of each joint type, more data points were measured to obtain the distribution of residual stresses on the longitudinal (loading) direction of the specimen. First or the only measurement point (0 mm) was weld toe in ASW-condition, bottom of the treated groove in the HiFIT-treated condition and fusion line towards base material in the TIG-treated condition. The measuring of points was made at 1 mm intervals from 0 to 4 mm and 2 mm intervals from 4 up to 8 or 14 mm, so the total number of measuring points was 7 or 10 points per weld depending of the specimen. Specimens were measured at horizontal position, except LG-joint, which was measured at angle of 10 degrees because of the height of the gusset. Stresstech XSTRESS 3000 with G3-goniometer was used in the measurement. Figure 33 shows the residual stress measurement.

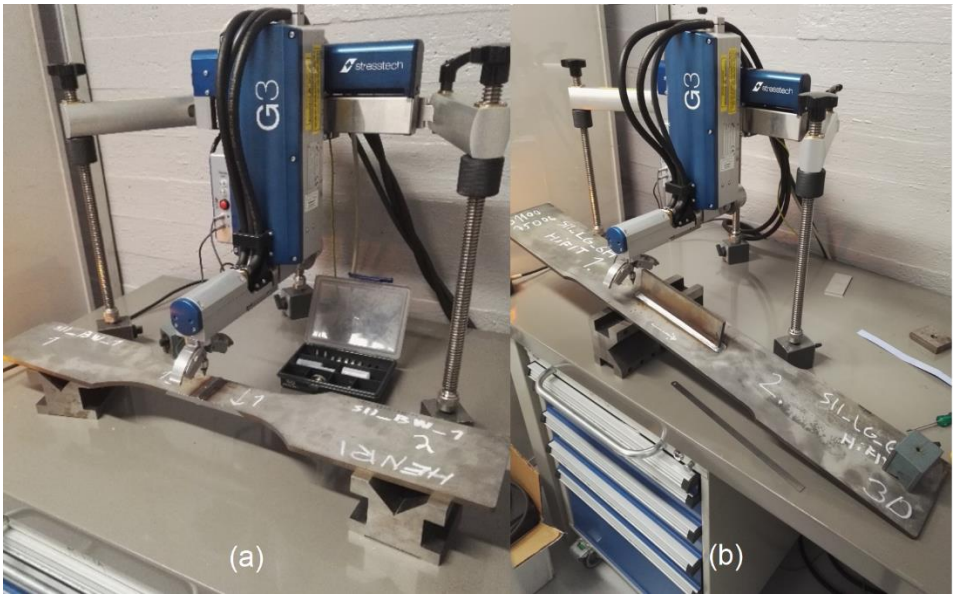

Figure 33. Measurement of residual stresses from (a) BW-specimen and (b) LG-specimen.

Hardness measurement was conducted for each joint type to obtain information about hardness changes due to welding which can affect the overall strength of the welded joint. Extra joints, similar to the actual test specimens, were made for the macrograph and hardness measurement. The Vickers hardness HV 5 test method was used and distance between measuring points was 0.5 mm, excluding LCX-joint, where also 1 mm interval was used. Measurements were performed in the areas sensitive to fatigue failure in the load and through-thickness direction and through the weld. Hardness values were measured at near to the surface in the longitudinal direction and boundary line of the weld in the thickness direction. In the LCX-joint, the hardness was also measured in the direction of the throat thickness of the weld. Macrographs were also taken from each joint type to get information about the welding quality, the penetration of the weld and root gap. In the case of LG-joint, only macrographs were taken from the failed specimen. The hardness measuring points of different specimens are illustrated in figure 34.

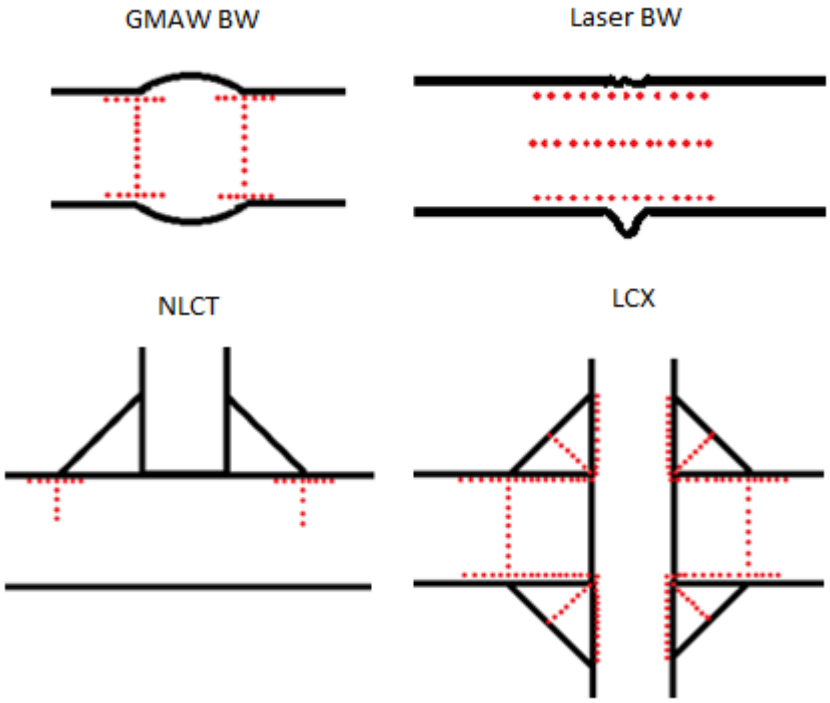

Figure 34. Hardness measurement points in different joint types.

3.3 Fatigue test arrangements

Fatigue tests were performed with servo-hydraulic 750 kN test rig with constant amplitude tensile loading and applied stress ratio of 0.1 and 0.5. Frequency of 1-3 Hz was used depending of the expected fatigue life of the test specimen. Figure 35 shows the test set-up.

Figure 35. BW GMAW -specimen attached to the test rig.

Strain gages were used to define structural stress at the weld toe in order to obtain desired stress range for the test. Stress caused by the clamping of the specimen which is due to the angular distortion of the specimen was also obtained. Structural stress can be defined from strain measured by strain gage (Hobbacher 2016, p. 26):

$$\sigma_{hs} = E * \varepsilon_{hs} \quad (1)$$

In equation 1, σ_{hs} is structural stress, *E is* modulus of elasticity, ε_{hs} is strain obtained by strain gage and simple uniaxial stress state is assumed. Strain gage was used in all of the specimens and located at a distance of 0.4*t* from the weld toe in all other specimens except HiFIT-treated NLCT -specimens where strain gage located at a distance of 1.0*t* from the bottom of the treated groove because the treatment caused small undercut that can affect stress concentration at a distance of 0.4*t*. Strain gage was attached in both ends of the gusset in the LG-specimens. Strain gage was attached to the centerline of the specimen near of that weld toe where the highest stress was expected to occur according to 2D measurement data. Strain gage values are used to calculate fatigue strength by the structural stress method. Recommendation is to use two strain gages at distances 0.4*t* (3.2 mm) and 1.0*t* (8 mm) and use linear extrapolation of the strain gage values to obtain more accurate results by the structural stress method (Hobbacher 2016, p. 25). However, only one strain gage was used to define stress range in this study but the test results were corrected to correspond the stress state on the weld toe later using FE-analysis. Figure 36 shows strain gage locations in different weld toe conditions. Strain gage locations in the LG-specimens shown in figure 37.

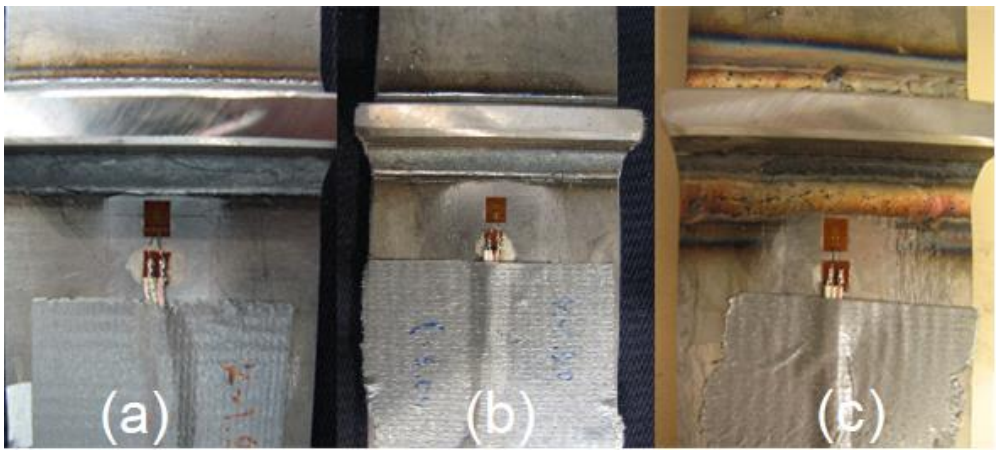

Figure 36. Strain gage location at different weld toe conditions: (a) ASW, (b) HiFIT and (c) TIG.

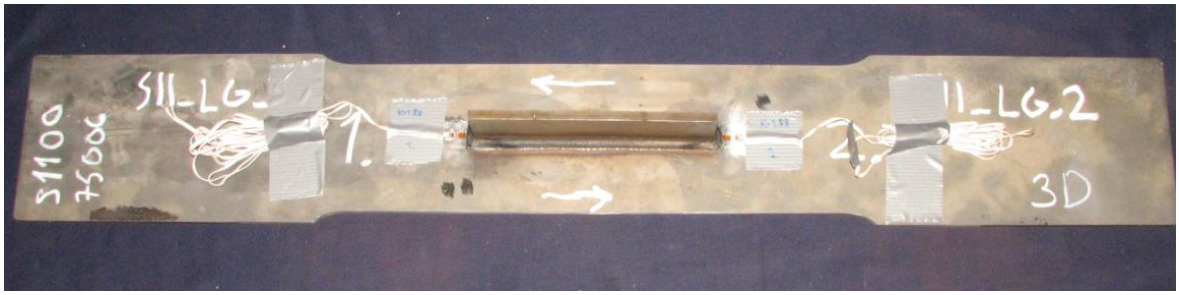

Figure 37. LG-specimen with two strain gages.

3.4 Results

Results of the various measurements and experimental testing are presented in this section. Average values of 2D weld geometry measurement results are presented here and specimen specific 2D measurement data and weld toe residual stress measurement results are shown in the Appendix III. Residual stress diagrams and overview of the results together with examples of macrographs and hardness diagrams are presented in this section and all results are shown in Appendices IV and V. Results of the fatigue tests are presented last.

Shape measurement was performed at the centerline of the specimen for all the test specimens to obtain values for weld geometry and angular distortion. Measured weld geometry values were used later in the FE-analysis. Average values of 2D weld geometry measurement are shown in tables 6 and 7. Root gap width was measured from macrograph.

Table 6. The average values and standard deviations of BW-specimens.

Specimen		Weld toe radius	Weld reinforcement height	Weld reinforcement width	Weld reinforcement diameter	Flank angle
		[mm]	[mm]	[mm]	[mm]	[deg]
BW GMAW	Average	0.72	1.86	6.83	19.29	20.33
	Stdv	0.39	0.18	0.53	1.98	3.30
BW Laser (root side)	Average	0.25	1.02	2.98	1.85	41.19
	Stdv	0.04	0.05	0.14	0.45	2.42

Table 7. The average values and standard deviations of the NLCT, LCX and LG -specimens.

Specimen		Weld toe radius	Throat thickness	Flank angle	Root gap width
		[mm]	[mm]	[deg]	[mm]
NLCT ASW	Average	0.35	4.50	35.81	5.28
	Stdv	0.22	0.06	1.20	0.21
NLCT HiFIT	Average	2.31	4.48	37.14	5.28
	Stdv	0.49	0.09	1.73	0.21
NLCT TIG	Average	6.44	4.59	37.15	5.28
	Stdv	1.82	0.11	1.52	0.21
LCX ASW	Average	0.49	4.66	34.89	5.71
	Stdv	0.28	0.07	1.06	0.27
LG ASW	Average	0.34	4.84	31.07	6.72*
	Stdv	0.11	0.16	1.89	-
LG HiFIT	Average	3.06	4.87	30.30	6.72*
	Stdv	0.57	0.18	0.75	-

* Single measurement result

Residual stresses were measured at the weld toe from all test specimens. Residual stress distributions, starting from the weld toe to the longitudinal direction of the specimen, were measured from specimens: S11_BW_1, S11_LW_2, S11_NLCT_6, S11_NLCT_10H, S11_NLCT_14T and S11_LG_4 and S11_LG_6H. No distribution was taken for the LCX-joint because of the expected root side failure. First measuring point was bottom of the treated groove in the HiFIT-treated specimen and the fusion line of the treated area in the TIG-treated specimens. Variation of the measured values is also shown as error bars in the diagrams. Residual stress diagrams for BW, NLCT and LG -specimens are shown in figures 38, 39 and 40.

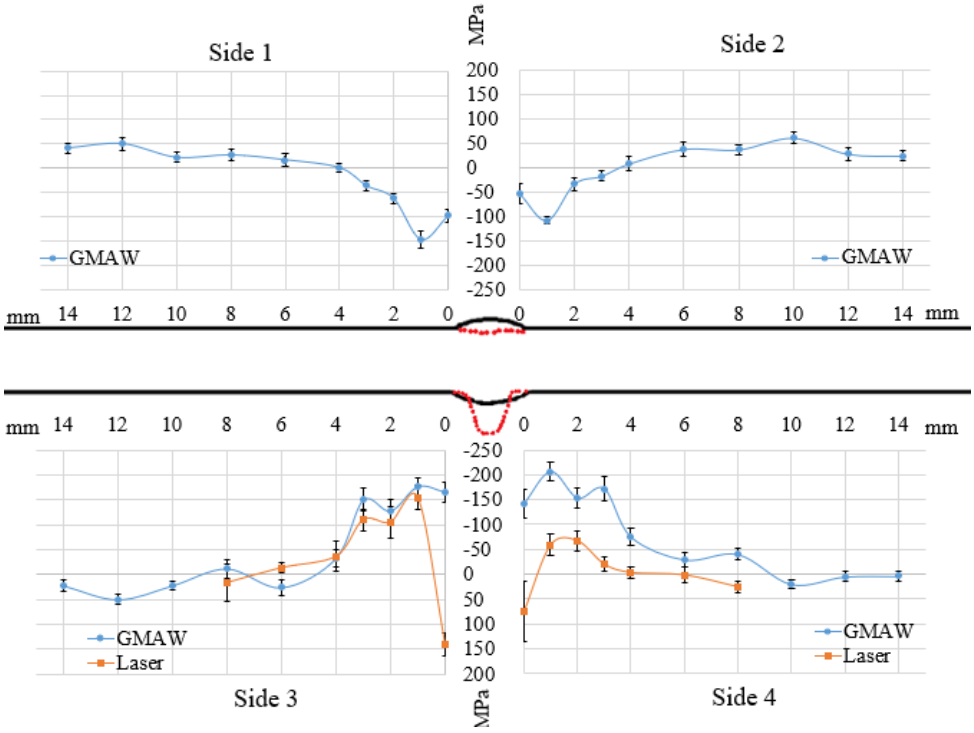

Figure 38. The residual stress diagram of BW-specimens.

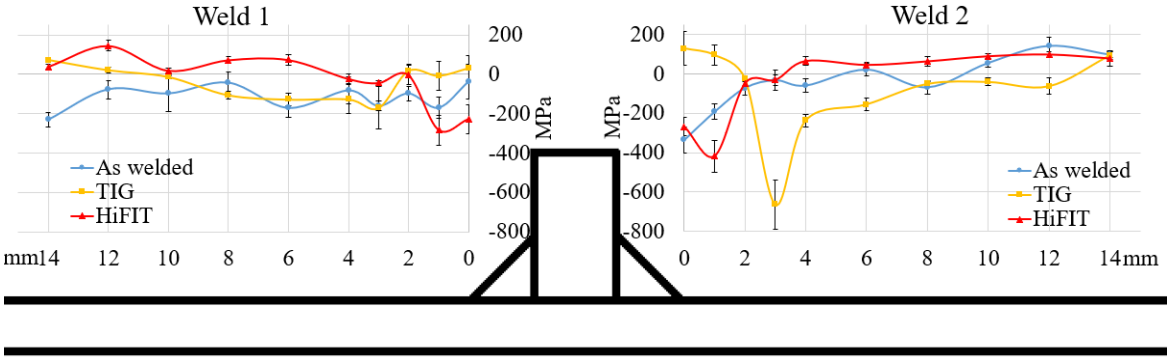

Figure 39. The residual stress diagram of NLCT-specimen in as-welded, HiFIT-treated and TIG-treated conditions.

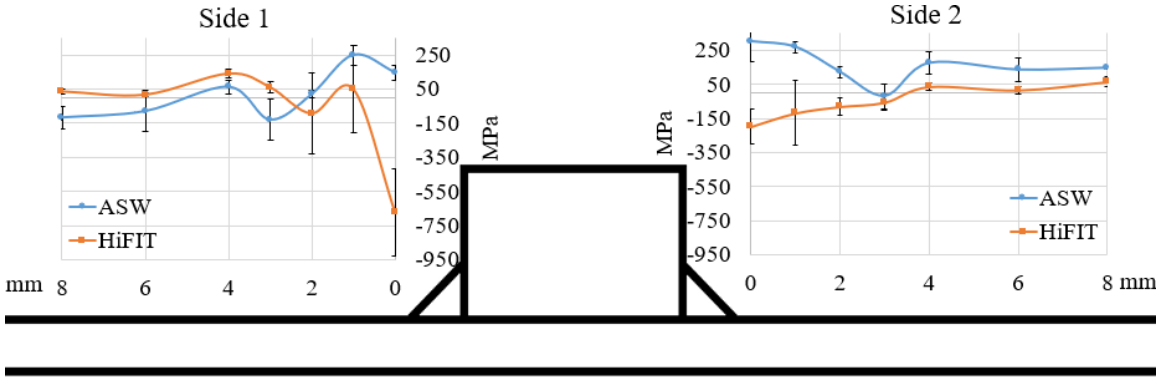

Figure 40. The residual stress diagram of LG-specimen.

Table 8 summarizes the residual stress measurement results from the weld toe of the test specimens. The results in the table are measured values that do not take into account possible error in the measurement which was shown as error bars in the residual stress diagrams.

Table 8. Residual stress measurement results.

Joint type	Condition	$\sigma_{res,min}$	$\sigma_{res,max}$	$\sigma_{res,avg}$	Stdv	No. of measurements
BW GMAW	ASW	-326	-16	-136	79	28
BW laser (root side)	ASW	41	175	108	61	4
NLCT	ASW	-396	42	-171	156	12
	HiFIT	-800	-228	-478	187	8
	TIG	-305	211	52	184	8
LCX	ASW	-173	84	-32	67	16
LG	ASW	147	352	281	65	8
	HiFIT	-671	-30	-335	280	4

Macrograph of each type of specimen with dimensions are shown in Appendix IV. Pores were detected in the root area from macrographs of the NLCT specimens, so there may be pores also in other test specimens. Pores may have an effect to the fatigue strength, especially in the case of the LCX-joint. Example of macrograph where effective throat thickness and root gap width were measured is shown in figure 41.

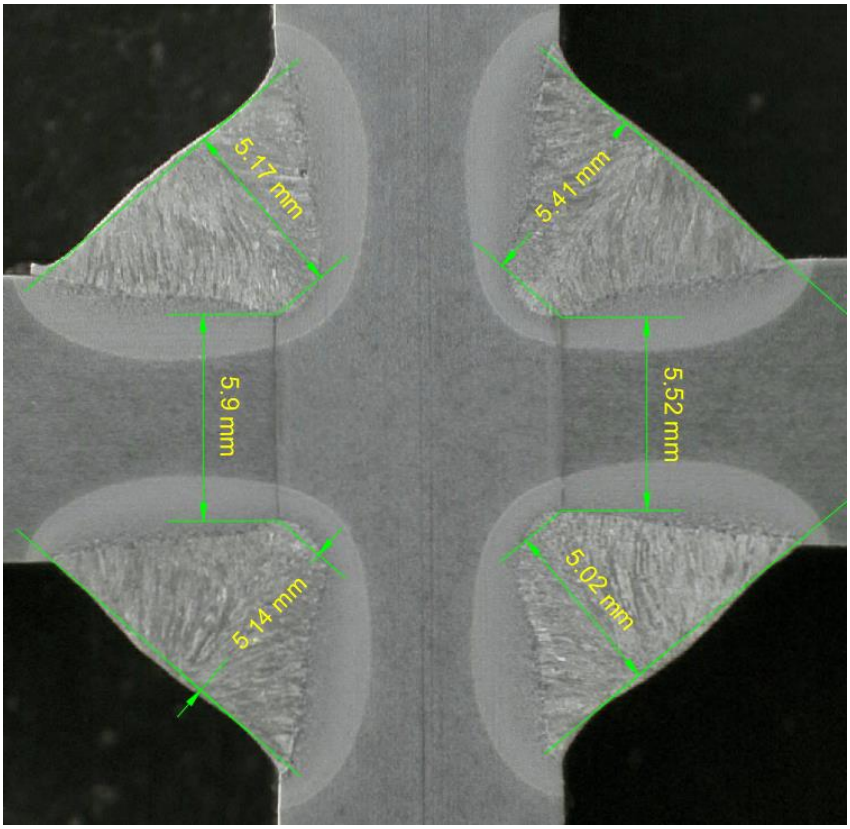

Figure 41. Macrograph of LCX-specimen.

According to the hardness measurement results, the hardness of the base material is between 360-380 HV and softening of the HAZ was not detected. Hardness measurement results are presented in Appendix V. Examples of the hardness measurement results are shown in figures 42 and 43.

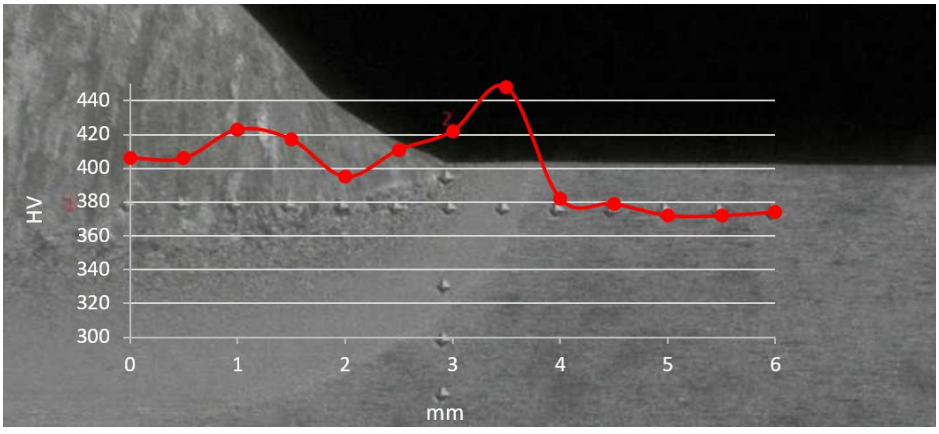

Figure 42. Hardness diagram of NLCT-specimen in ASW-condition in longitudinal direction.

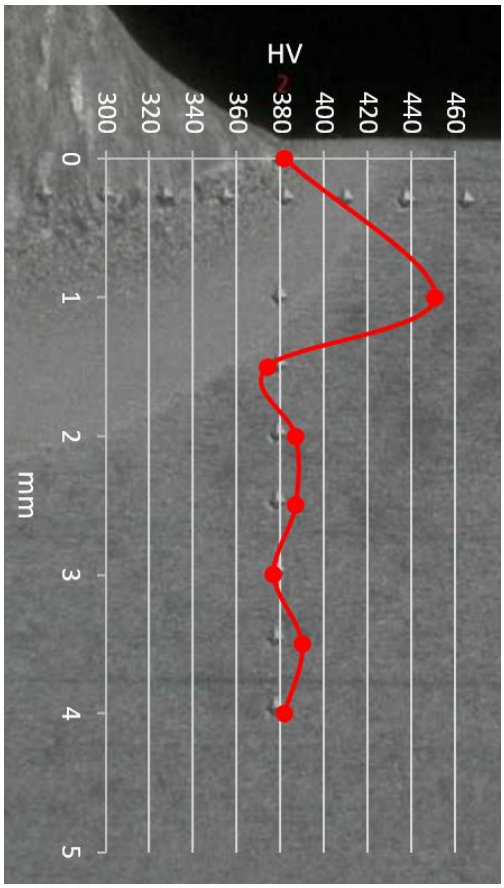

Figure 43. Hardness diagram of NLCT-specimen in ASW-condition in thickness direction.

Experimental results are shown in table 9. Table contains the applied stress ratio, calculated nominal stress, structural stress and ENS range, stress concentration factor for structural stress and ENS, fatigue life and crack initiation location of test specimen. Structural stress range of BW GMAW, NLCT and LG -specimens was fixed by FE-analysis and the procedure is shown in the section 4.

Table 9. Fatigue test results.

Specimen	R	Stress range [MPa]			k_{str}	k_{ens}	Fatigue life N_f	Info
	[-]	Nom[4)]	Str[2)]	ENS	[-]	[-]	[cycles]	[-]
S11_BW_1	0.5	316	-	-	-	-	14 555	root side 2-4
S11_BW_2	0.1	318	-	-	-	-	696 485	root side 1-3
S11_BW_3	0.1	447	504	904	1.13	2.02	83 318	weld toe 4
S11_BW_4	0.5	452	-	-	-	-	1 306	root side 1-3
S11_BW_5	0.5	483	503	914	1.04	1.89	20 297	weld toe 2
S11_BW_6	0.1	387	408	740	1.05	1.91	149 790	weld toe 3
S11_BW_7	0.5	373	415	746	1.11	2.00	46 104	weld toe 2
S11_LW_1	0.1	385	402	633	1.04	1.64	67 524	root side 3
S11_LW_2	0.5	390	403	635	1.03	1.63	76 670	root side 4, weld toe 1
S11_NLCT_1	0.1	311	365	683	1.17	2.20	159 573	weld toe 2 [1)]
S11_NLCT_2	0.5	313	363	680	1.16	2.17	46 422	weld toe 1
S11_NLCT_3	0.1	310	365	683	1.18	2.20	135 643	wed toe 2
S11_NLCT_4	0.5	318	364	681	1.14	2.14	52 181	weld toe 2
S11_NLCT_5	0.1	250	297	558	1.19	2.23	376 238	weld toe 2
S11_NLCT_6	0.5	254	296	554	1.17	2.18	97 383	weld toe 1
S11_NLCT_7H	0.1	339	372	666	1.10	1.96	1 977 793	run out [3)]
	0.1	604	667	1242	1.10	2.06	47 174	corner/edge of groove, side 2 [1)]
S11_NLCT_8H	0.1	526	565	1048	1.07	1.99	116 617	BM failure side 2
S11_NLCT_9H	0.5	465	518	965	1.11	2.08	29 305	bottom of the groove, side 2 [1)]

Table 9 continues. Fatigue test results.

Specimen	R	Stress range [MPa]			k_{str}	k_{ens}	Fatigue life N_f	Info
	[-]	Nom[4)]	Str[2)]	ENS	[-]	[-]	[cycles]	[-]
S11_NLCT_10H	0.5	423	475	888	1.12	2.10	56 474	corner/edge of groove, side 2
S11_NLCT_11T	0.1	446	602	1141	1.35	2.56	67 404	treated area, side 2 [1)]
S11_NLCT_12T	0.5	434	507	950	1.17	2.19	58 140	treated area, side 1 [1)]
S11_NLCT_13T	0.1	289	408	775	1.41	2.68	247 632	treated area, side 1
S11_NLCT_14T	0.5	323	408	768	1.26	2.38	135 812	treated area, side 1
S11_LCX_1	0.1	100	-	406	-	4.06	328 618	root side 1
S11_LCX_2	0.5	138	-	527	-	3.82	63 828	root side 3
S11_LCX_3	0.1	186	-	714	-	3.84	43 393	root side 1/3 (weld toe 3 crack also)
S11_LCX_4	0.5	192	-	733	-	3.82	31 583	root side 2/4
S11_LG_1	0.1	154	288	426	1.87	2.77	217 005	weld toe 1 [1)]
S11_LG_2	0.5	150	278	416	1.85	2.77	197 477	weld toe 1 [1)]
S11_LG_3	0.1	98	173	271	1.77	2.77	1 265 484	weld toe 2 [1)]
S11_LG_4	0.5	100	175	278	1.75	2.78	942 780	weld toe 1 [1)]
S11_LG_5H	0.1	288	491	797	1.70	2.77	580 161	BM, clamp
S11_LG_6H	0.5	277	483	766	1.74	2.77	56 810	weld 2, border line of treated area

[1)] Strain gage same side with crack

[2)] Fixed structural stress values: BW, NLCT and LG -specimens

[3)] Test continued with new values

[4)] Nominal stress in LCX-specimens is calculated using effective throat thickness

Fatigue test results are shown as S-N diagrams in terms of nominal stress, structural stress and ENS in figures 44, 45 and 46. Test specimens with stress ratio R = 0.1 are marked with point and specimens with R = 0.5 are marked with ring. The same colors were used for the same joint type in same condition. S-N curves with fixed slope are shown in the discussion section 6.2 but obtained FAT classes with fixed and free slopes are shown in tables 10 and 11. Slope m = 5 was used for HiFIT-treated and slope m = 4 was used for TIG-treated specimens (Marquis & Barsoum 2016, p.17; Yildirim 2015, p. 44; Skriko 2017, p. 110-114).

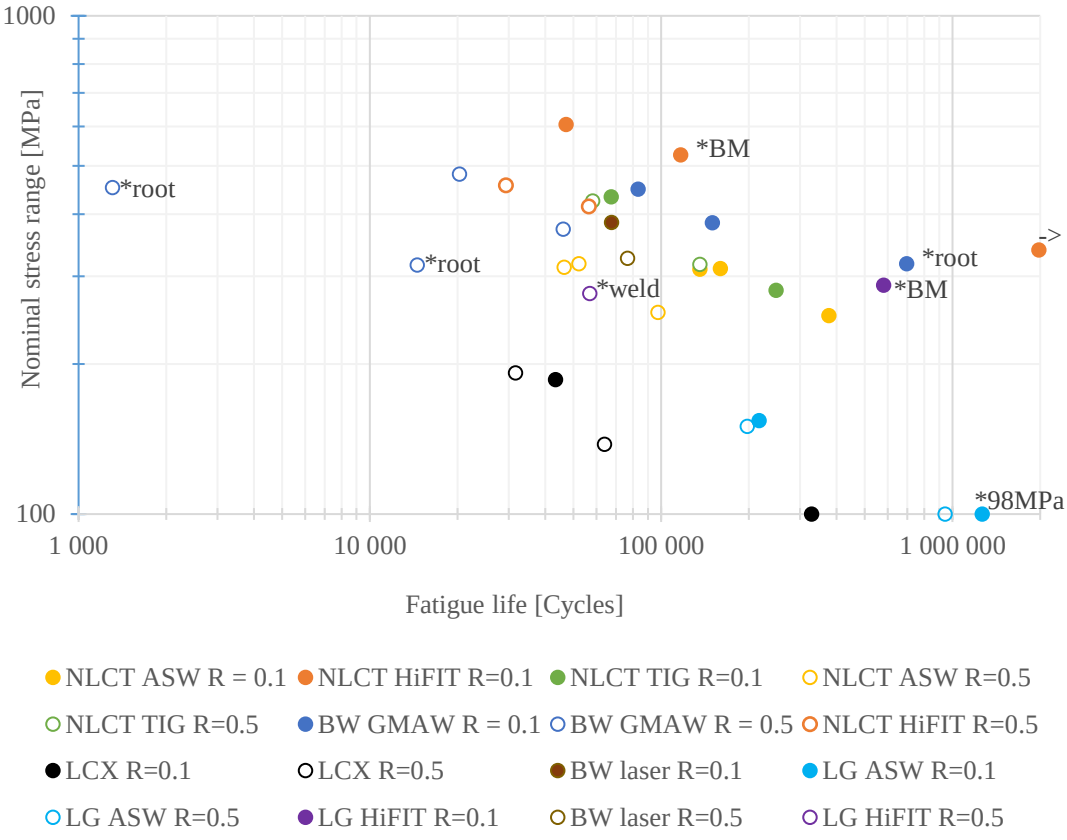

Figure 44. Fatigue test results in terms of nominal stress method.

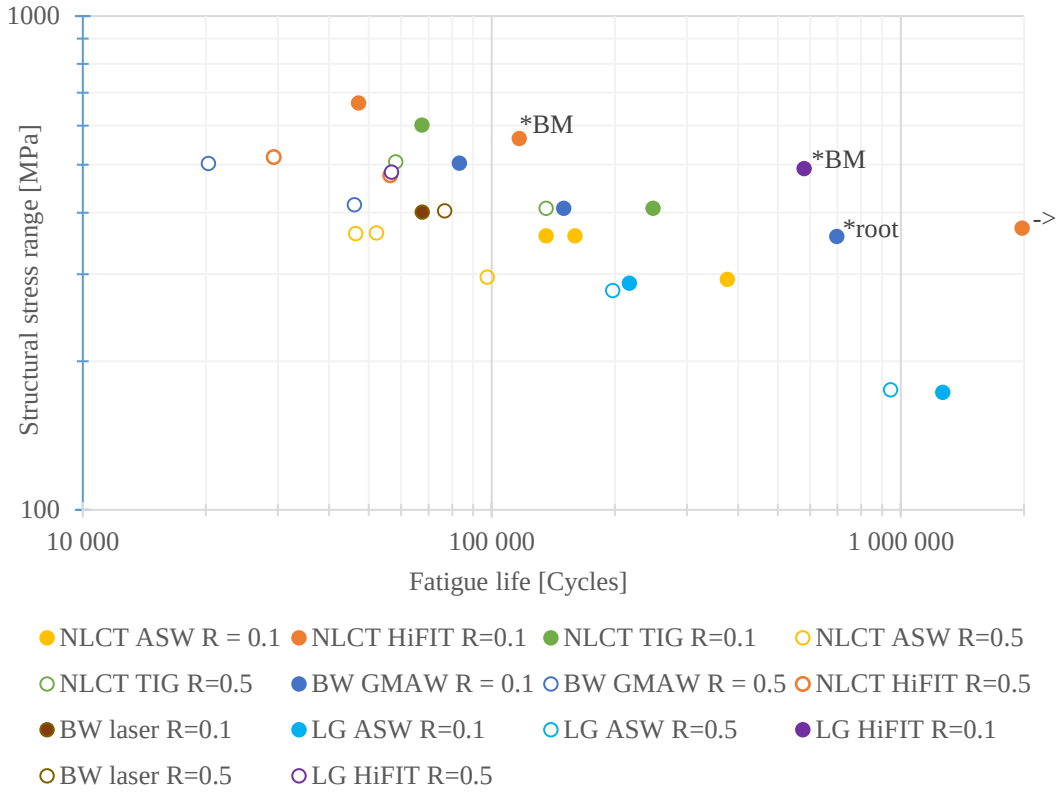

Figure 45. Fatigue test results in terms of structural stress method.

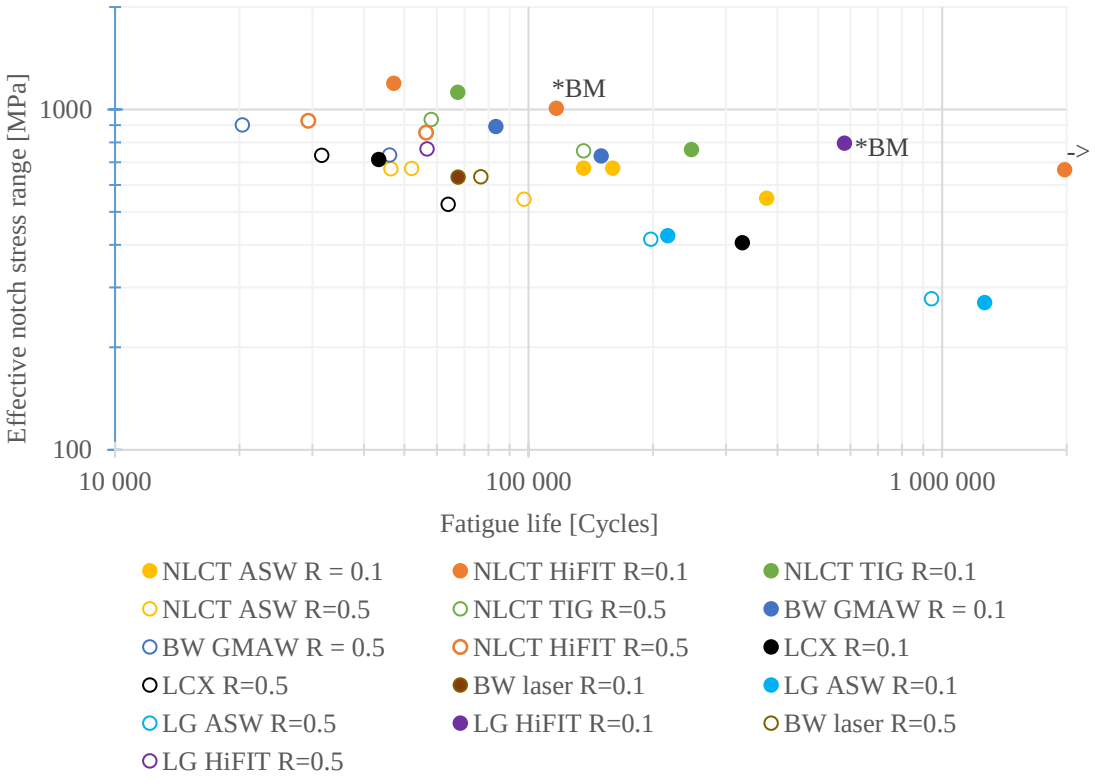

Figure 46. Fatigue test results in terms of ENS method.

Table 10. Obtained mean FAT classes with fixed slope.

Joint	Stress ratio	Fixed slope *m*					
		Nominal		Structural		ENS	
	R	*m*	FAT_{mean}	*m*	FAT_{mean}	*m*	FAT_{mean}
BW GMAW	0.1	3	159	3	173	3	308
	0.5	3	105	3	113	3	202
BW laser	0.1	3	124	3	130	3	204
	0.5	3	132	3	136	3	214
NLCT ASW	0.1	3	134	3	158	3	292
	0.5	3	92	3	107	3	196
NLCT HiFIT	0.1	5	292	5	318	5	568
	0.5	5	204	5	228	5	409
NLCT TIG	0.1	4	181	4	250	4	467
	0.5	4	172	4	209	4	386
LCX	0.1	3	53	-	-	3	210
	0.5	3	46	-	-	3	175
LG	0.1	3	79	3	143	3	217
	0.5	3	73	3	132	3	204
LG HiFIT	0.1	5	225	5	383	5	622
	0.5	5	136	5	237	5	376

Table 11. Obtained mean FAT classes with free slope.

Joint	Stress ratio	Free slope *m*					
		Nominal		Structural		ENS	
	R	*m*	FAT_{mean}	*m*	FAT_{mean}	*m*	FAT_{mean}
BW GMAW	0.1	4.07	205	2.78	160	2.93	301
	0.5	3.17	114	4.27	171	4.03	289
BW laser	0.1	-	-	-	-	-	-
	0.5	-	-	-	-	-	-
NLCT ASW	0.1	4.32	170	4.55	206	4.61	382
	0.5	3.11	96	3.32	119	3.29	217
NLCT HiFIT	0.1	6.55	341	5.45	336	5.35	593
	0.5	6.93	253	7.57	297	8.01	548
NLCT TIG	0.1	3.00	144	3.35	219	3.36	410
	0.5	2.87	127	3.91	205	3.99	385
LCX	0.1	3.26	57	-	-	3.59	245
	0.5	2.13	27	-	-	2.13	105
LG	0.1	3.90	87	3.46	152	3.90	241
	0.5	3.86	82	3.38	140	3.88	229
LG HiFIT	0.1	-	-	-	-	-	-
	0.5	-	-	-	-	-	-

Angular distortion obtained from 2D measurement compared to the strain gage value is shown in figure 47.

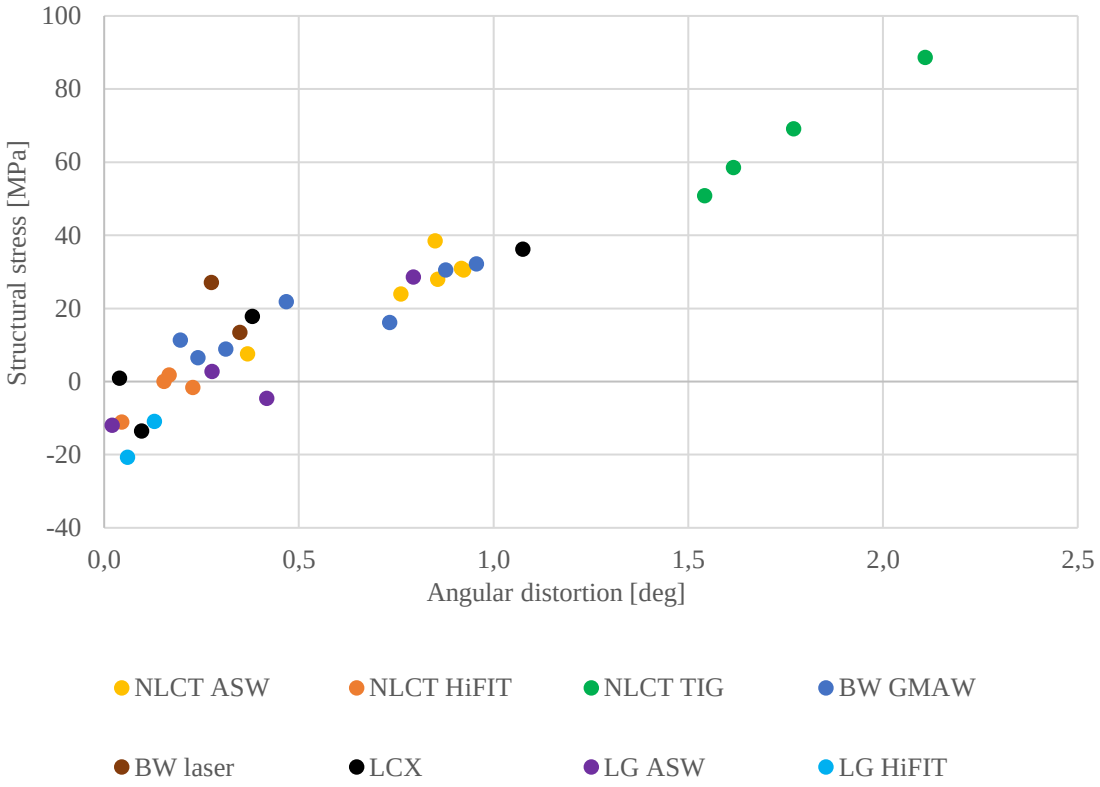

Figure 47. Effect of clamping.

Fatigue crack initiated at the weld toe in the most of the test specimens. Crack initiated at root side in the LCX-specimens as expected, but also part of the GMAW BW-specimens with 0 mm air gap cracked at root side. In the S11_NLCT_8H specimen, base material failure happened side 2 far from the weld at edge of the specimen, but it had also visible crack in the side 1 in edge of the HiFIT-treated groove where S11_NLCT_7H and S11_NLCT_10H specimens failed. Visible cracks were also initiated from edges of treated grooves in other welds of the NLCT HiFIT -treated specimens S11_NLCT_8H-10H. TIG-treated specimens failed from vicinity of the fusion line of TIG-treated area from the side of treated area. In the specimen S11_LW_2 crack initiated both root side 4 and weld toe side 1. Other HiFIT-treated LG specimen failed from base material from clamping and other failed from border line of the treated area from the side of the weld. Fracture surfaces of test specimens are shown in figures 48-51.

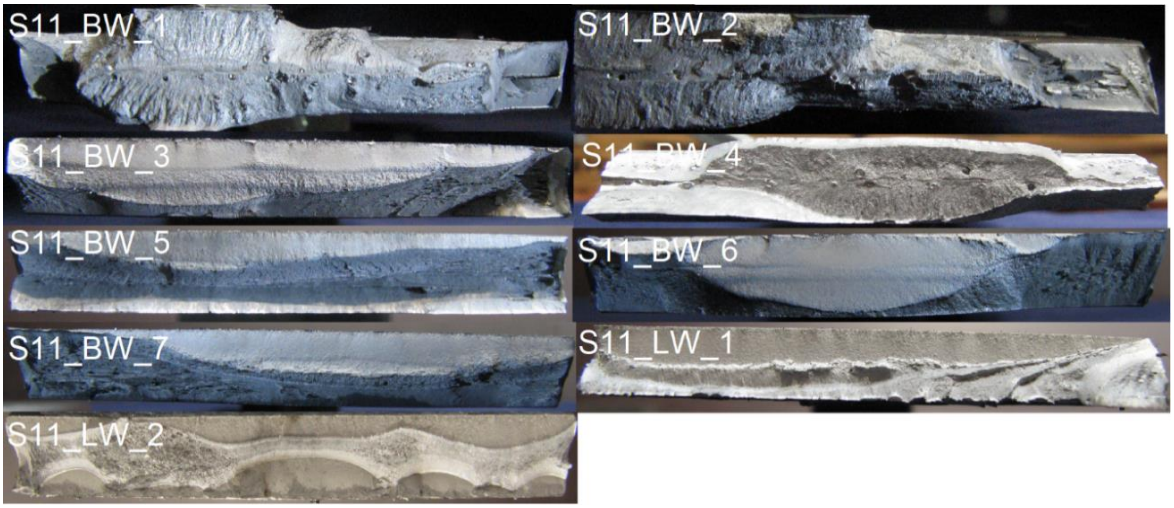

Figure 48. Fracture surfaces of BW-specimens.

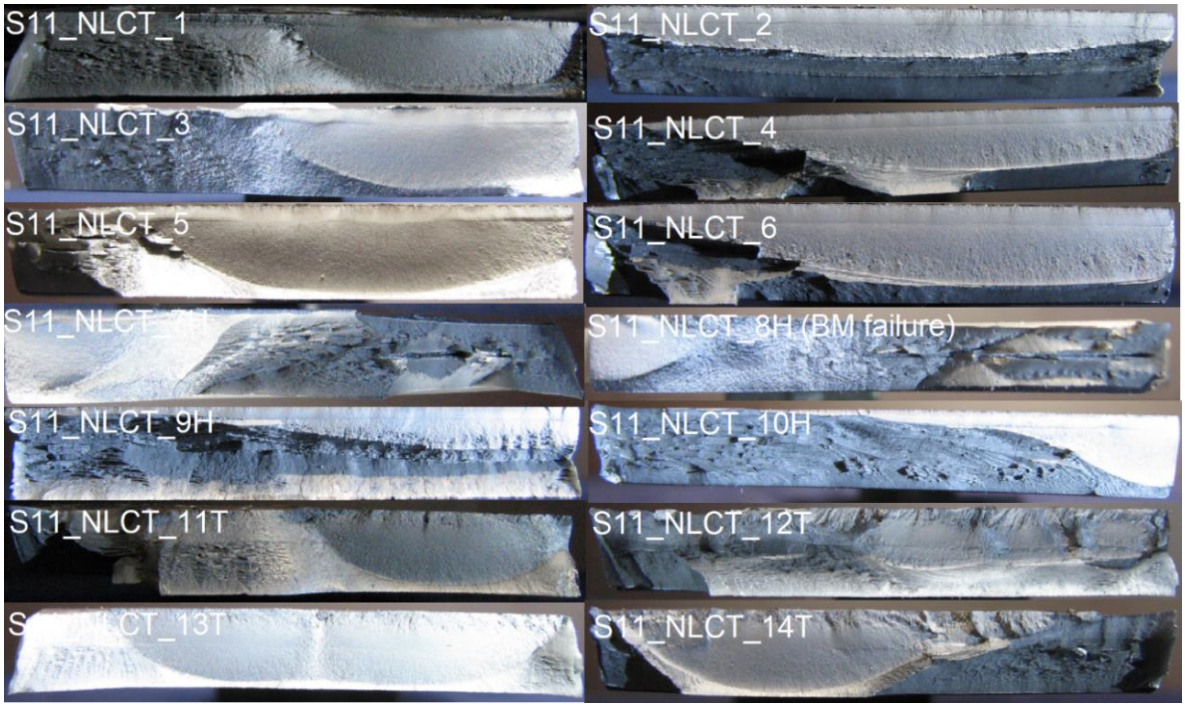

Figure 49. Fracture surfaces of NLCT-specimens.

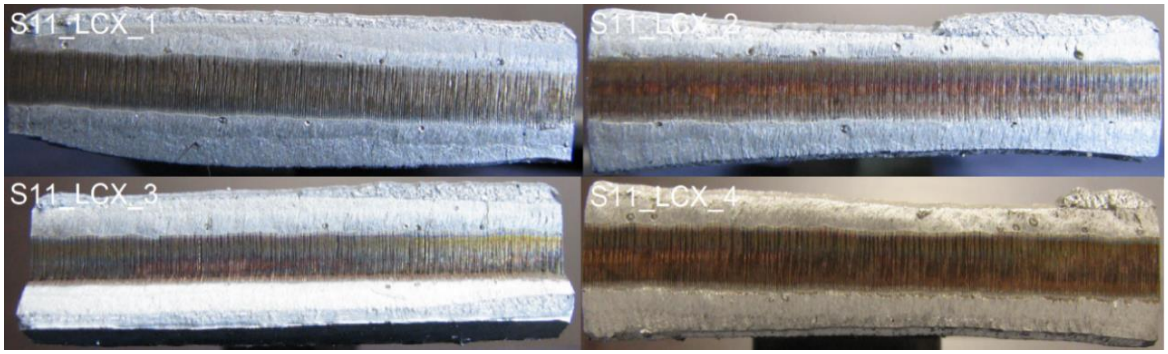

Figure 50. Fracture surfaces of LCX-specimens.

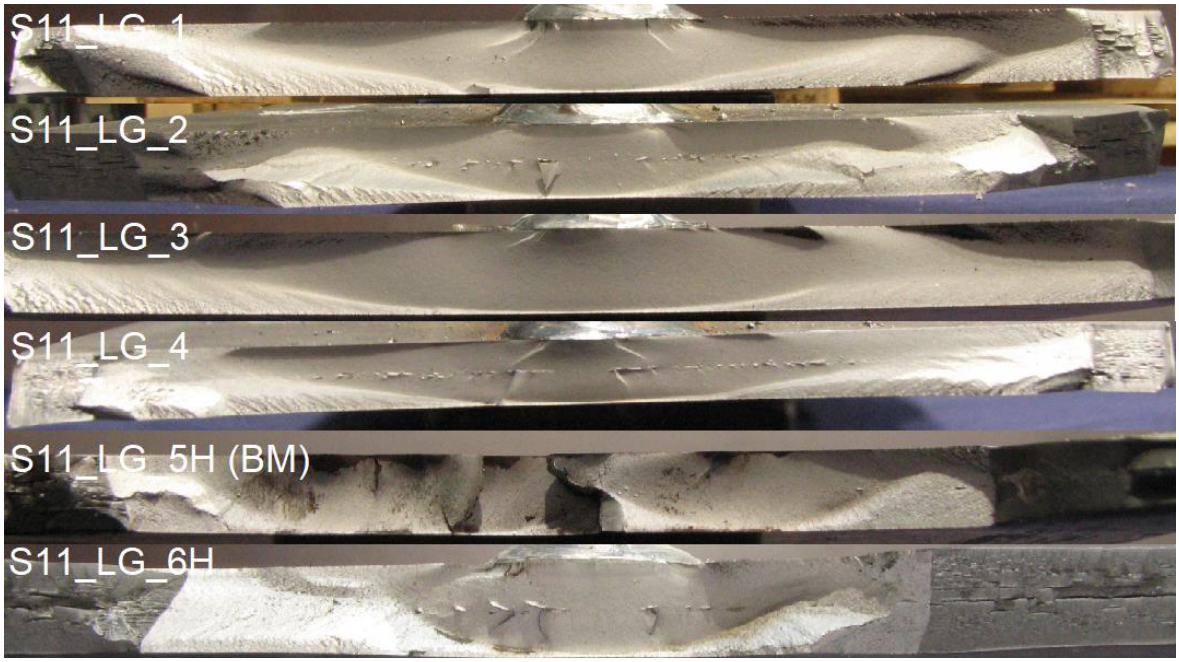

Figure 51. Fracture surfaces of LG-specimens.

4 FE-ANALYSIS

The FE-analysis procedure and the obtained results are shown in this section. Fatigue lives for the test specimens are calculated using four different methods: the nominal stress method, structural stress method, effective notch stress method and 4R method. FE-analyses was performed to obtain stress concentration factors for fatigue life calculations by effective notch stress and 4R methods. In addition, hot spot models were made to fix strain gage values.

4.1 FE-models

Femap version 11.4.0 with NxNastran version 11.1 solver was used for analysis. Material properties with the modulus of elasticity of the material E = 210 GPa and Poisson's ratio v = 0.3 were used and the thickness of the plate was 8 mm. Element size in the vicinity of weld toe and weld root was equal or below 0.05 mm. All the joints were modelled with the reference weld toe and root radius of 1 mm and with the average weld toe radius calculated from 2D measurement data (table 6 and 7). In addition, average values from other weld dimensions were used to reduce the amount of models and workload. Due to robotized welding, variation in the dimensions within the joint type was relatively small. Macrographs were used to measure the penetration of the weld and root gap, so that those dimensions could be taken into account in FE-models. Angular distortion was not modelled in the geometry of the model, but it was taken into account as bending moment. Models were analyzed with linear static analysis separately with tensile and bending loading, which corresponds to 1 MPa stress, to get stress concentration factors for the membrane and bending to calculate ENS range. Before reading the stress concentration factors, maximum principal stresses were converted from elements to nodes.

Weld geometry was modeled based on 2D measurement values presented in chapter 3.2 and root gap height and width was measured from macrograph of the specimen shown in Appendix IV. Measured height of the root gap varied between 0.05 and 0.08 mm depending of the specimen, so it was decided to use value of 0.1 mm in all the models. The fillet method was used to model the weld toe radius in all the cases. Modelled weld toe radius was average of the measured values plus 1 mm, but also reference 1 mm weld toe radius was used.

In the modelling of BW, NLCT and LCX -joints, 2D models were used and symmetry was exploited in the modelling to reduce the counting time. Parabolic plane strain elements were used, constraints were applied to the nodes in the symmetry lines of the model and force was applied to the sheet thickness line at the other end of the model. The membrane loading case was analyzed by a quarter model and it was converted to half model to analyze the bending loading case. In the case of NLCT- and BW laser joints, half model was modelled and only 1 mm weld toe radius was modelled in the root side of the laser weld to test ENS method suitability for laser welded joint. Root radius of 1 mm was used in the both LCX-models. Figure 52 shows used mesh size and constraints in the case of the quarter model of LCX-joint.

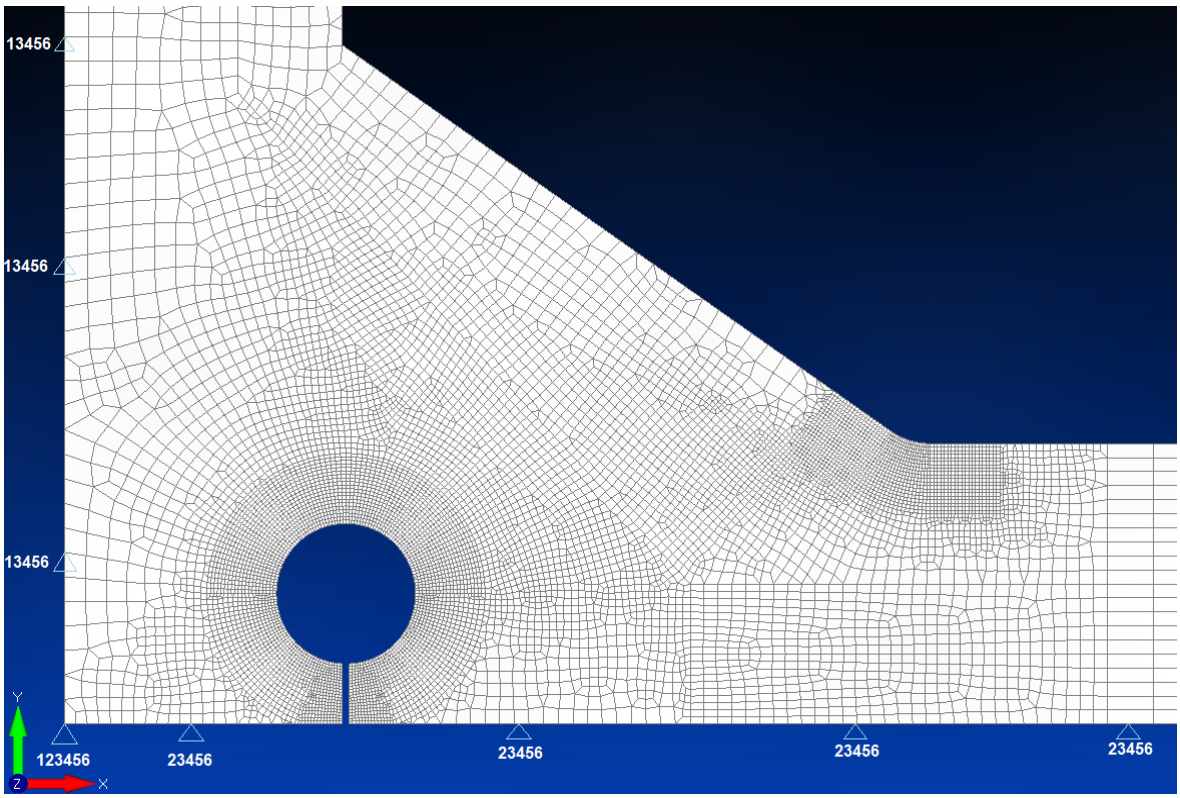

Figure 52. Example of mesh size at the weld toe and root and constraints of the symmetry lines.

In the modelling of LG-specimen, 3D models were used. Quarter of the model was modelled using hexahedral 8-node solid elements. The model was made by using meshed surfaces that were extruded to solid elements. Mesh size at the critical area at the weld toe was 0.05x0.05x0.15 mm. Constraints were applied to the nodes in the symmetry surfaces of the

model and force was applied to the cross-sectional surface the other end of the model. Model was analyzed with membrane and bending loading cases. Global model and mesh area in the weld toe of LG-specimen is shown figures 53 and 54.

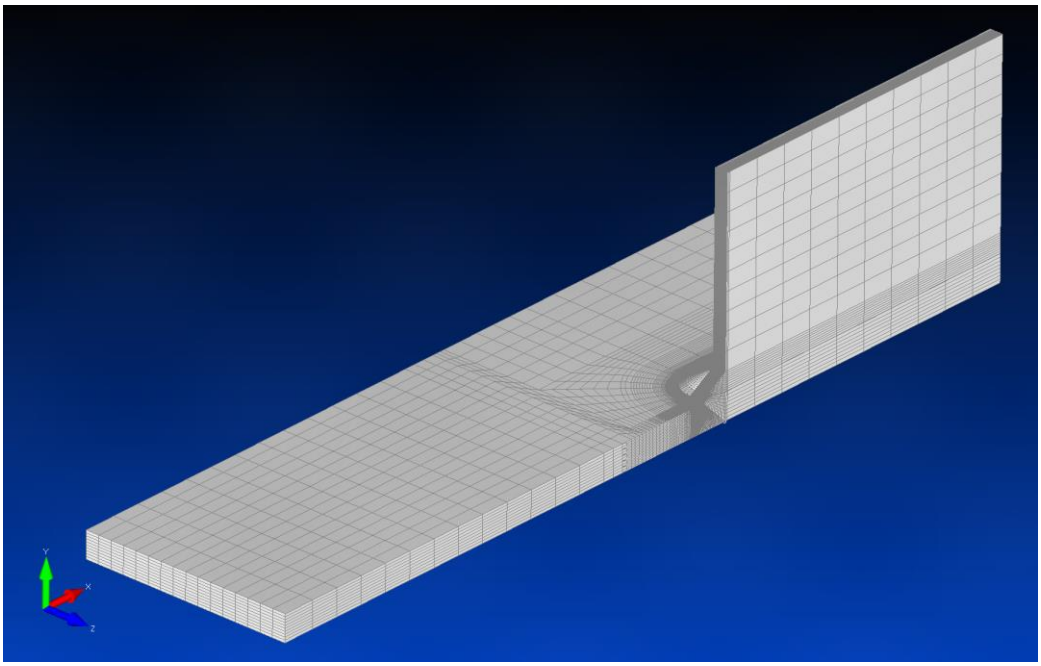

Figure 53. Model of LG-specimen.

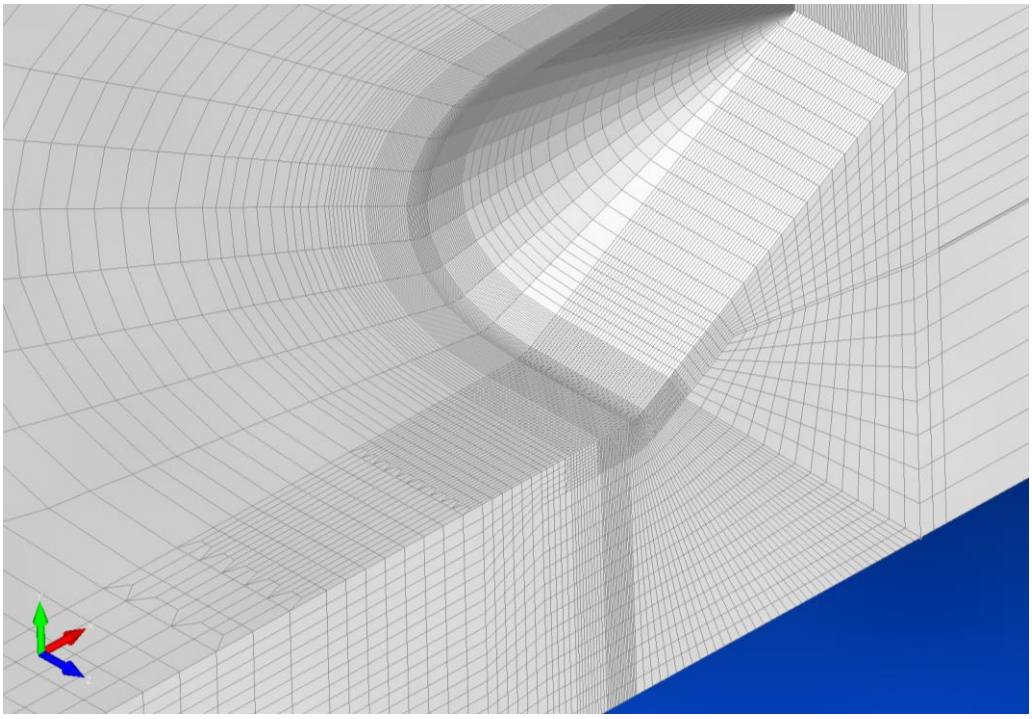

Figure 54. Mesh size at the area of the weld toe.

Recommendation is to use two stain gages and use linear extrapolation to get accurate results as discussed in chapter 3.3. However, one strain gage was used in the fatigue tests so the structural stress results based on one strain gage are slightly lower compared values obtained by linear extrapolation so the results were corrected using FE-analysis. Hot spot -models were made from the BW GMAW, NLCT and LG -joints with typical angular distortion based on 2D measurement data. Otherwise the same measured average values are used in the modelling as in ENS models. Outline of the NLCT hot spot -model is shown in figure 55.

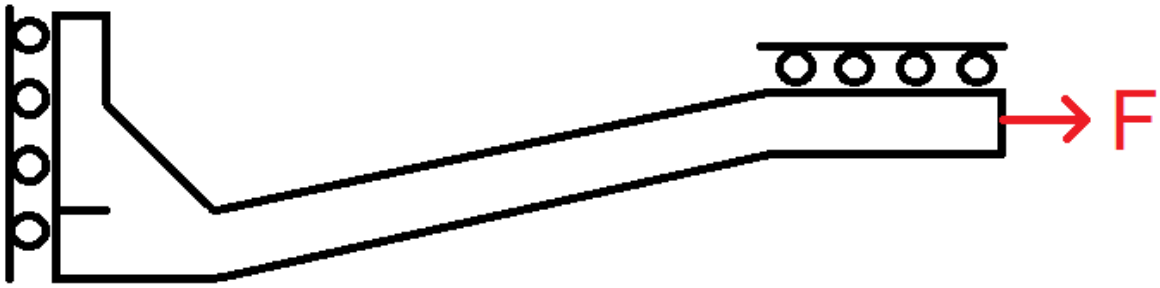

Figure 55. Outline of the NLCT hot spot -model.

Stresses were read from distances 0.4*t* and 1.0*t* from the weld toe after which hot spot stress was calculated using linear extrapolation (Hobbacher 2016 p. 26):

$$\sigma_{hs} = 1.67\sigma_{0.4t} - 0.67\sigma_{1.0t} \quad (2)$$

In equation 2, the σ_{hs} is hot spot stress and the $\sigma_{0.4t}$ and $\sigma_{1.0t}$ are stresses from distances 0.4*t* and 1.0*t* from the weld toe. Obtained stresses from model were divided by extrapolated hot spot stress to get error percentage.

4.2 Results

FE-analyses were performed to obtain stress concentration factors for the fatigue life calculations by ENS and 4R methods. In addition, hot spot models were done to obtain error percentage to fix strain gage values. Obtained stress concentration factors for membrane and bending and error percentages are shown in tables 12 and 13.

Table 12. Stress concentration factors for membrane and bending obtained by FE-analysis.

Specimen	Weld toe radius $r = r_{true,avg} + 1$ mm	$k_{t,m}$	$k_{t,b}$
	[mm]	[-]	[-]
BW GMAW	1.00	1.83	1.53
	1.72	1.66	1.49
BW laser	1.00	1.57	1.69
NLCT ASW	1.00	1.85	2.03
	1.35	1.71	1.87
NLCT HiFIT	3.31	1.38	1.48
NLCT TIG	7.44	1.20	1.24
LCX	1.00	2.49 (2.89)*	1.79 (0.46)*
	1.49	2.22 (2.89)*	1.61 (0.46)*
LG ASW	1.00	2.77	3.82
	1.34	2.57	3.54
LG HiFIT	4.06	1.98	2.69

* Stress concentration factors for root are in brackets and modelled root radius is 1 mm in both cases.

Table 13. Error percentage obtained by FE-analysis and linear extrapolation.

Specimen	Error percentage at distance (%)	
	0.4*t*	1.0*t*
BW GMAW	2.38	3.99
NLCT	1.39	3.46
LG	6.23	15.52

5 FATIGUE STRENGTH ASSESSMENT

Fatigue strength assessment procedures and the obtained results are shown in this section. Fatigue lives for the test specimens were calculated by four different methods: the nominal stress, structural stress, ENS and 4R methods. First, calculation procedures with different methods are explained and then obtained results are presented.

5.1 Nominal stress method

The nominal stress range caused by the force of the test rig to the specimen can be calculated with the basic equation of stress (Hobbacher 2016 p. 12):

$$\Delta\sigma_{nom} = \frac{F_{\max} - F_{\min}}{A} \quad (3)$$

In equation 3, the $\Delta\sigma_{nom}$ is nominal stress range, $F_{\max}$ is maximum and $F_{\min}$ is minimum force affect to the specimen and A is cross-sectional area of the specimen. In the case of LCX-specimen, which failed from root side, effective cross-sectional area of weld is used to calculate the stress range (Hobbacher 2016 p. 51). Fatigue life N_f can be now calculated from equation (Hobbacher 2016 p. 92, 109):

$$N_f = \left(\frac{FAT_{nom}}{\Delta\sigma_{nom}}\right)^m * 2 * 10^6 \quad (4)$$

In equation 4, the FAT_{nom} is the nominal fatigue class of structural detail and m is the slope of the reference curve. Fatigue class values for structural details are presented in IIW document (Appendix II). Fatigue class value can be increased by factor 1.6, if specimen is post-weld treated by hammer peening and by factor 1.5, if specimen is post-weld treated by TIG-dressing but the FAT class that is below the obtained value is used and FAT 125 still is maximum allowable value to use (Haagensen & Maddox 2006, p. 17-18, 24-25).

5.2 Structural stress method

In the structural stress method, structural stress range is used instead of nominal stress range. Structural stress range obtained from strain gage values was used in calculation. Fatigue life N_f can be now calculated as before:

$$N_f = \left(\frac{FAT_{hs}}{\Delta\sigma_{hs}}\right)^m * 2 * 10^6 \quad (5)$$

In equation 5, the FAT_{hs} is fatigue class for structural stress method and $\Delta\sigma_{hs}$ is structural stress range obtained from strain gage values and fixed by FE-analysis. Fatigue class values for structural details are presented in IIW Recommendations (Appendix II). FAT 140 is used for TIG-treated and FAT 160 is used for hammer peened non-load-carrying fillet welded joints, if yield strength of the material is over 350 MPa (Haagensen & Maddox 2006, p. 33).

5.3 Effective notch stress method

In the effective notch stress method, effective notch stress range is used and it can be calculated by using stress concentration factors obtained from FE-analysis. Effective notch stress range can be obtained from the equation (Björk et al. 2018, p. 3):

$$\Delta\sigma_{ens} = k_{t,m} * \Delta\sigma_m + k_{t,b} * \Delta\sigma_b \quad (6)$$

In equation 6, the $\Delta\sigma_{ens}$ is effective notch stress range, $\Delta\sigma_m$ is membrane stress range, $\Delta\sigma_b$ is bending stress range, $k_{t,m}$ is notch stress concentration factor for membrane and $k_{t,b}$ is notch stress concentration factor for bending loading. Because lack of structural membrane stress concentration, stress range for bending can be calculated by reducing nominal stress range from the structural stress range. Fatigue life N_f can be now calculated as before:

$$N_f = \left(\frac{FAT_{ens}}{\Delta\sigma_{ens}}\right)^m * 2 * 10^6 \quad (7)$$

In equation 7, the FAT_{ens} is fatigue class value for ENS method and the value is 225 MPa when using principal stress hypothesis and 200 MPa when using von Mises stress hypothesis. Slope of the reference curve $m = 3$ is used. (Sonsino et al. 2012, p. 4.)

5.4 4R method

Fatigue life calculation by 4R method, originally developed by Nykänen & Björk (Nykänen & Björk 2015), takes into account material strength, weld toe radius, residual stresses and stress ratio in addition to stress range. Effective notch stress is used including the effect of the weld toe radius. Modeled weld toe radius is true weld toe radius plus 1 mm i.e. $r = r_{true,avg}$ + 1 mm (Björk et al. 2018, p. 2). Residual stresses were measured at the weld toe of each specimen, ultimate tensile strength of the material is obtained from material specification and stress ratio can be calculated from maximum and minimum stresses. Effect of clamping can be taken into account in stress ratio. Local stress ratio can be calculated from local maximum and minimum stresses (Björk et al. 2018, p. 4):

$$R_{local} = \frac{\sigma_{\min}}{\sigma_{\max}} \tag{8}$$

In the equation 8, the R_{local} is local stress ratio, $\sigma_{\min}$ is local minimum stress and $\sigma_{\max}$ is local maximum stress considering the elastic-plastic material behavior as illustrated in figure 56. Ramberg-Osgood relationship and Neuber's theory are used to determine the local maximum stress. Ramberg-Osgood relationship is shown in next equation (Björk et al. 2018, p. 3-4):

$$\varepsilon(\sigma_{\max}) = \frac{\sigma_{\max}}{E} + \left(\frac{\sigma_{\max}}{H}\right)^{\frac{1}{n}} \tag{9}$$

In the equation 9, the ε is strain, $\sigma_{\max}$ is maximum stress, E is modulus of elasticity, H is strength coefficient and n is strain hardening exponent. Values E = 210 GPa, $H = 1.65 * R_m$ and n = 0.15 are used in the calculations (Björk et al. 2018, p. 6). Neuber's theory is shown in the following equation and it takes residual stresses in to account (Björk et al. 2018, p. 3-4):

$$\varepsilon(\sigma_{\max}, \sigma_{res}) = \frac{(\sigma_k + \sigma_{res})^2}{\sigma_{\max} E} \tag{10}$$

In the equation 10, the σ_{res} is residual stress and σ_k is effective notch stress. Local maximum stress $\sigma_{\max}$ can be calculated from equations 9 and 10 by combining them and using iterative solver. Local minimum stress can be calculated when local maximum stress and stress range

are known. Bauschinger's effect (kinematic hardening model) have to take into account in the calculation, so Ramberg-Osgood relationship comes to a form (Björk et al. 2018, p. 3-4):

$$\Delta\varepsilon(\Delta\sigma) = \frac{\Delta\sigma}{E} + 2\left(\frac{\Delta\sigma}{2H}\right)^{\frac{1}{n}} \quad (11)$$

In the equation 11, the $\Delta\varepsilon$ is strain range and $\Delta\sigma$ is stress range. Neuber's rule comes to a form (Björk et al. 2018, p. 3-4):

$$\Delta\varepsilon(\Delta\sigma) = \frac{(\Delta\sigma_k)^2}{\Delta\sigma E} \quad (12)$$

In the equation 12, the $\Delta\sigma_k$ is effective notch stress range. Stress range $\Delta\sigma$ can be calculated from earlier equations 11 and 12 by combining them and using solver. Maximum local stress and stress range can be used to calculate local minimum stress $\sigma_{\min}$ and after that local stress ratio R_{local} can be calculated by equation 8. Fatigue life can be calculated with equation (Björk et al. 2018, p. 6):

$$N_f = \frac{C_{ref}}{\left(\frac{\Delta\sigma_k}{\sqrt{1-R_{local}}}\right)^{m_{ref}}} \quad (13)$$

In the equation 13, the C_{ref} is characteristic or mean fatigue capacity and m_{ref} is slope of the reference curve. Characteristic and mean values for fatigue capacity are $C_{char} = 10^{20.83}$ and $C_{mean} = 10^{21.59}$ and slope of reference curve $m = 5.85$ were used in the calculations (Björk et al. 2018, p. 6). Results can be presented in local reference coordinate system using equation (Björk et al. 2018, p. 5):

$$\Delta\sigma_{k,ref} = \Delta\sigma_k \frac{\sqrt{1-R_{local,ref}}}{\sqrt{1-R_{local}}} \quad (14)$$

In the equation 14, the $\Delta\sigma_{k,ref}$ is reference effective notch stress range and $R_{local,ref}$ is reference local stress ratio. Figure 56 clarifies how the R_{local} is calculated in the 4R method.

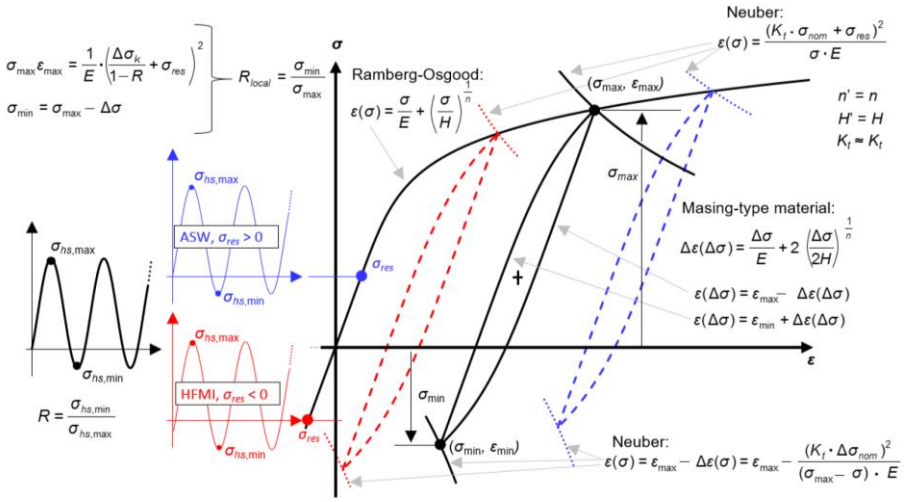

Figure 56. Calculation of R_{local} (Björk et al. 2018, p. 3).

5.5 Results

Fatigue strength assessment was performed with the nominal stress, structural stress, ENS and 4R methods for specimens which failed from weld toe. Specimen S11_NLCT_8H was taken also in the calculation because there was clearly propagated crack at the edge of treated groove though it failed from base material. Calculated results were compared to test results. IIW FAT classes are shown in Appendix II. Mean FAT classes were obtained from characteristic FAT classes with factor 1.37 in nominal, structural and ENS methods (Sonsino et al. 2012. p. 7). An average of the measured weld toe radii summed with 1mm, i.e. $r = r_{true,avg}$ + 1mm was used to calculate ENS in the 4R method. Residual stresses were considered in two different ways. Measured residual stress value from failed weld toe was used in the calculations taking into account possible error. In addition, the maximum value of the measured values of that joint type was used (table 8). Table 14 shows used FAT classes in calculations for different specimen types. Figures 57 and 58 shows calculated fatigue lives compared to test results for test specimens that failed from weld toe.

Table 14. FAT classes used in calculations. FAT_{mean} is obtained from FAT_{char} by factor 1.37.

Method	IIW FAT $m = 3$	BW GMAW	NLCT ASW	NLCT HiFIT	NLCT TIG	LG ASW
Nominal	FAT_{char}	90	80	125	125	63
	FAT_{mean}	123	110	171	171	86
Structural	FAT_{char}	100	100	160	140	90
	FAT_{mean}	137	137	219	191	123
ENS	FAT_{char}	225				
	FAT_{mean}	308				

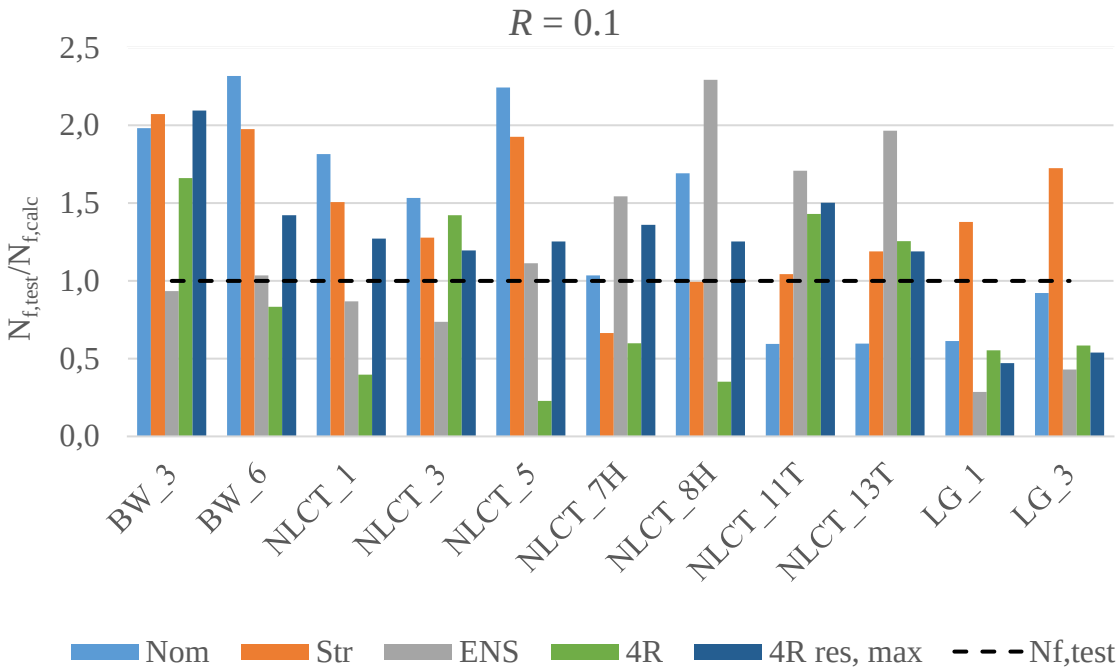

Figure 57. Calculated fatigue lives compared to test results, R = 0.1.

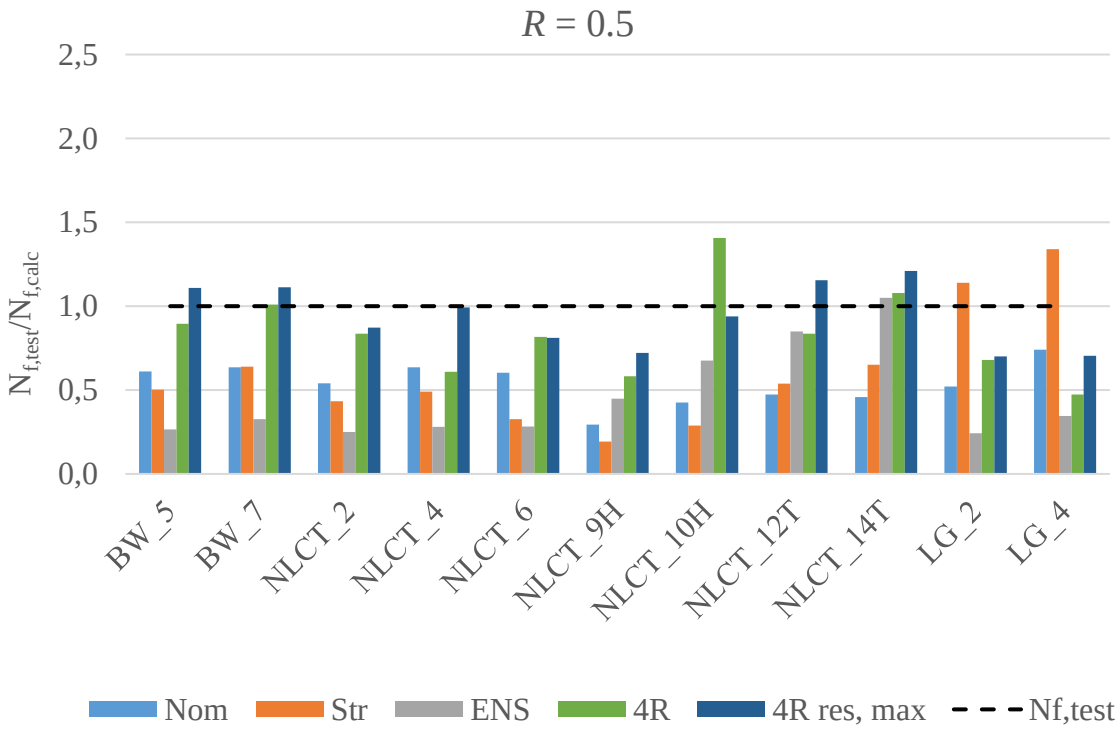

Figure 58. Calculated fatigue lives compared to test results, R = 0.5.

6 DISCUSSION

Results of measurements, fatigue test, FE-analysis and fatigue strength assessment results are discussed in this section. First, measurements before fatigue tests are discussed after which fatigue test results are presented as S-N curves. FE-analysis and fatigue strength assessment results are finally discussed. In addition, obtained results are compared with results of literature.

6.1 Measurements

Residual stress and 2D measurement were performed for each test specimen before fatigue test. Hardness measurement was performed for extra test specimens from which macrographs were also taken. Data of the 2D measurements was used in FE-modeling and fatigue life calculations. Weld geometry and angular distortion were measured from each test specimen using the 2D measurement. Determination of the weld toe radius was not unambiguous in all cases and fitting the circle to the 2D data visually can cause error. Measurement was performed only from the center line of the specimen, so the actual weld toe radius, where the crack was initiated can be different to the measured value but the other hand, robotized welding will decrease the scatter and this characterization based only one point can thus be justified. From the data of NLCT-specimens can be noted that HiFIT-treatment decreases and TIG-treatment increases angular distortion of the specimen and both treatments have clear effect on the geometry of the weld toe.

Residual stresses were measured from all weld toes of each test specimen and distribution along the longitudinal direction of the specimen was measured from each type of the specimen, excluding LCX-specimen, which failed at the weld root. Compressive residual stresses were measured at all of the weld toes of BW and NLCT-specimens in ASW-condition, excluding S11_NLCT_3 where tensile residual stresses were measured at the weld 2. Both, compressive and tensile residual stresses were measured from the weld toes of LCX -specimens. Relatively high tensile residual stresses up to 350 MPa were measured from LG-specimens compared to other specimen types. The highest compressive residual stresses were achieved by HiFIT-treatment up to -800 MPa with the possible error of ± 163 MPa but the other hand, only -30 MPa compression was measured from the side 2 of HiFIT-

treated specimen S11_LG_5H. One of the TIG-treated specimens had compressive residual stresses but others were on tensile side. Residual stress was measured from fusion line of the TIG-treated area while the specimens did not fail exactly in this location but in the vicinity of the fusion line from the side of treated area so the assumption of residual stress can be wrong. Generally, relatively large variations in the residual stress results were observed with all the specimen types. According to residual stress distributions, the greatest variations in residual stresses occurred at distance of 0 mm to 4 mm from the weld toe after which large variations in the results no longer occurred. As in 2D measurement, measurements have been performed only at the centerline of the specimen so the result can be different in the location of the crack and it can easily predict too optimistic assumption of the residual stress state of the specimen.

According to hardness measurement results, HAZ softening was not detected. Hardness of the base material was between 360-380 HV and usually hardness increases quickly at the HAZ even to value 450 HV, after which the hardness decreases being still higher or equal to the hardness of base material. Macrographs showed that pores were left on the root side of the weld in the NLCT-specimens, so it is reasonable to assume that there might be pores also in the other specimens, which may have an effect on the root side fatigue strength.

6.2 Fatigue tests

Fatigue test results are presented as S-N curves where mean curves were fitted by standard procedure with fixed slope to the test data points because of the small number of specimens. The slope of $m = 5$ is used for HiFIT-treated, $m = 4$ is used for TIG-treated and $m = 3$ is used for ASW-specimens. However, FAT classes obtained by fixed and free slopes were presented earlier in chapter 3.4. S-N curves were done by means of nominal stress, structural stress and ENS methods. Results are compared with IIW FAT classes and effect of post-weld treatments and the applied stress ratio to the fatigue strength are discussed.

All results are not shown in the same S-N diagram for the sake of clarity. The diagrams are divided into the following three groups: BW, NLCT and LCX/LG -specimens. Mean FAT classes are obtained from characteristic FAT classes by factor 1.37 as mentioned in Chapter 5.5. Figures 59-61 shows the test results of BW-specimens. Specimens that failed from the root side are marked in the nominal stress S-N curve.

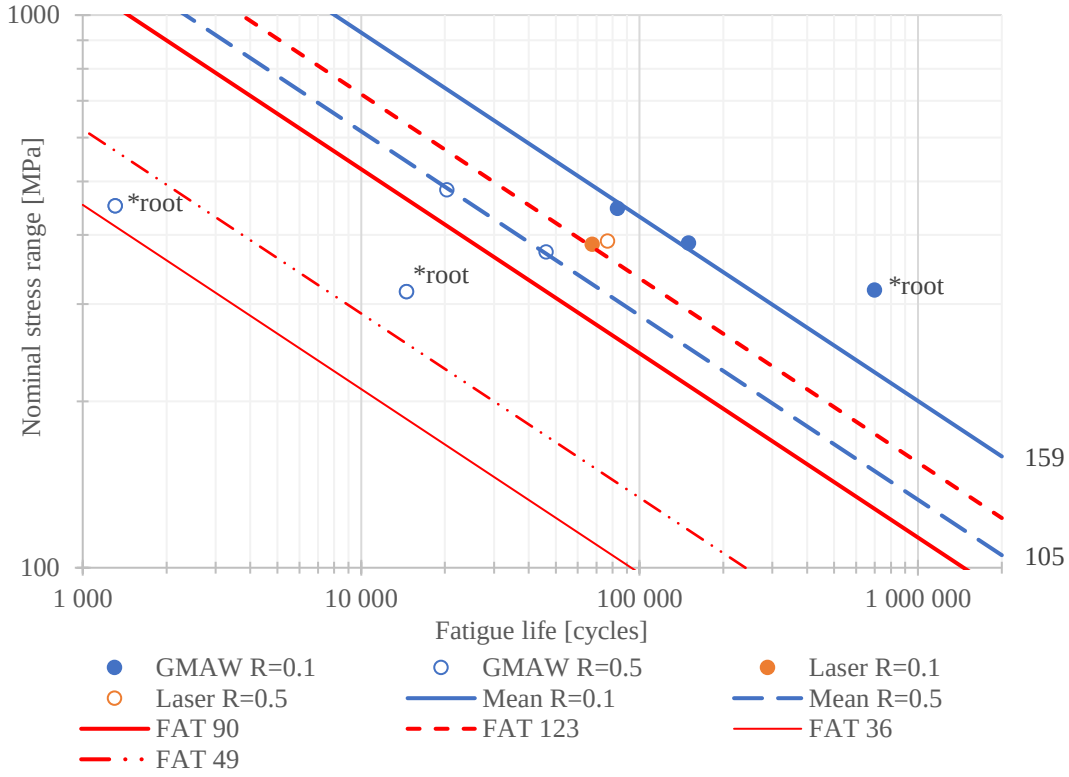

Figure 59. Nominal stress results for BW-specimens as S-N curves.

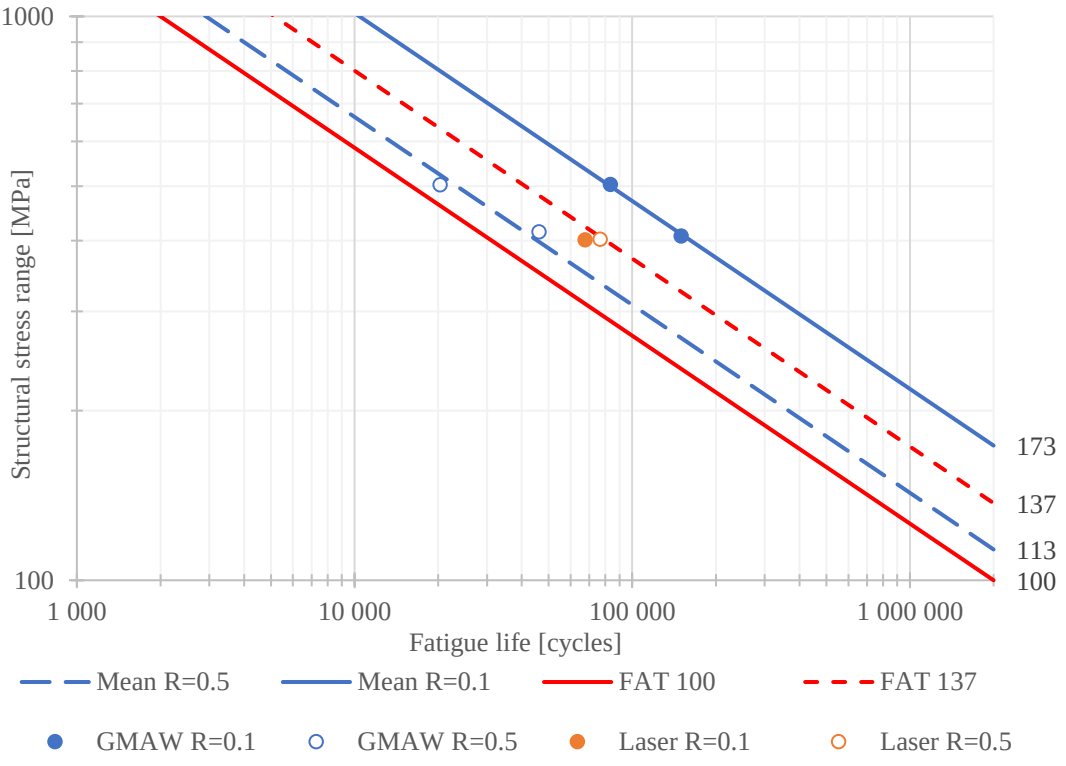

Figure 60. Structural stress results for BW-specimens as S-N curves.

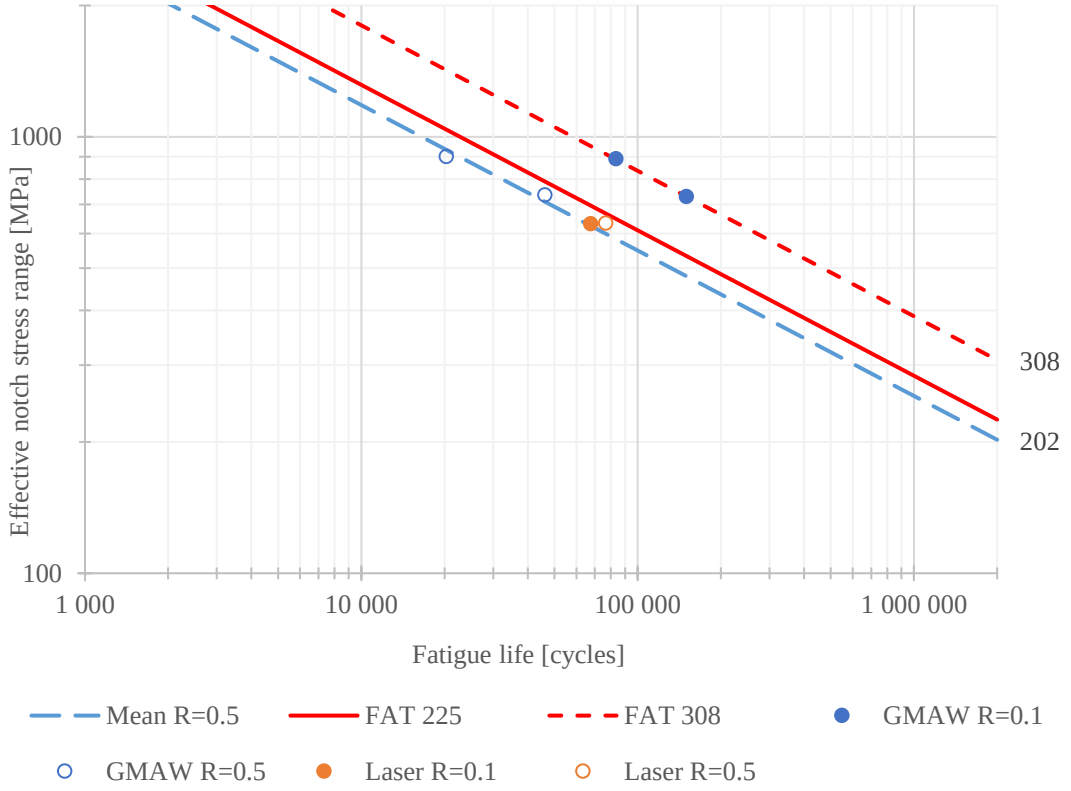

Figure 61. ENS results for BW-specimens as S-N curves.

Based on the results, the applied stress ratio has significant effect on the fatigue strength of GMAW BW-specimens. FAT class decreases over 30% between stress ratios R = 0.1 and R = 0.5. FAT_{mean} value can be considered conservative for R = 0.1 but non-conservative for R = 0.5 in terms of nominal and structural stresses. However, all the results are above the FAT_{char} values. Laser welded specimens are in good relation with FAT_{mean} in terms of nominal and structural stress. Contrary to expectations the higher stress ratio specimen had better fatigue strength than the lower stress ratio specimen which may refer to variation in welding quality or then stress ratio does not have effect on the fatigue strength of laser welded joint. In the ENS results, both laser specimens and GMAW R = 0.5 specimens are below FAT_{char} 225, but GMAW R = 0.1 specimens are in line with the FAT_{mean} 308. One of the GMAW BW specimens, which failed at root side, had better fatigue strength than specimens failed from weld toe. That might mean other R = 0.1 specimen lasted less some reason. Based on Leitner et al. (2017 p. 166) results, also knee-point for this type of joint can be earlier which can explain the result. So it seems that FAT_{mean} can be more conservative at in higher cycles in terms of nominal and structural stresses. However, more tests need to be done to make better conclusions. Results of the root side failed specimens

are above the FAT_{char} 36. FAT_{mean} classes obtained from test results with fixed slope are compared to IIW FAT_{mean} values and comparison between applied stress ratios was done. Comparison of FAT classes is shown in table 15.

Table 15. FAT class comparison of BW-specimens.

Joint type	Method	$FAT_{R=0.1}/FAT_{mean}$	$FAT_{R=0.5}/FAT_{mean}$	$FAT_{R=0.5}/FAT_{R=0.1}$
BW GMAW	Nominal	1.29	0.85	0.66
	Structural	1.26	0.82	0.65
	ENS	1.00	0.66	0.66
BW laser	Nominal	1.01	1.07	1.06
	Structural	0.95	0.96	1.05
	ENS	0.66	0.69	1.05

Figures 62-64 shows test results of NLCT-specimens as S-N curves. The slope m = 5 is used for HiFIT-treated and m = 4 is used for TIG-treated specimens. HiFIT-treated specimen which failed from base material is marked to the S-N curves.

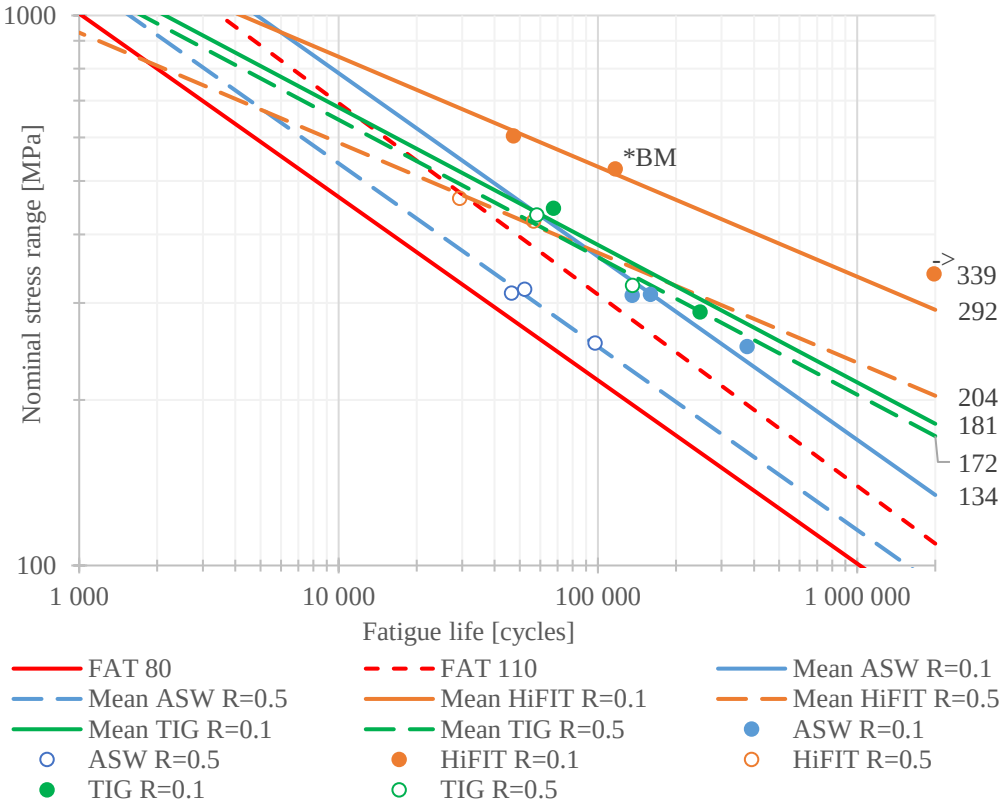

Figure 62. Nominal stress results for NLCT-specimens as S-N curves.

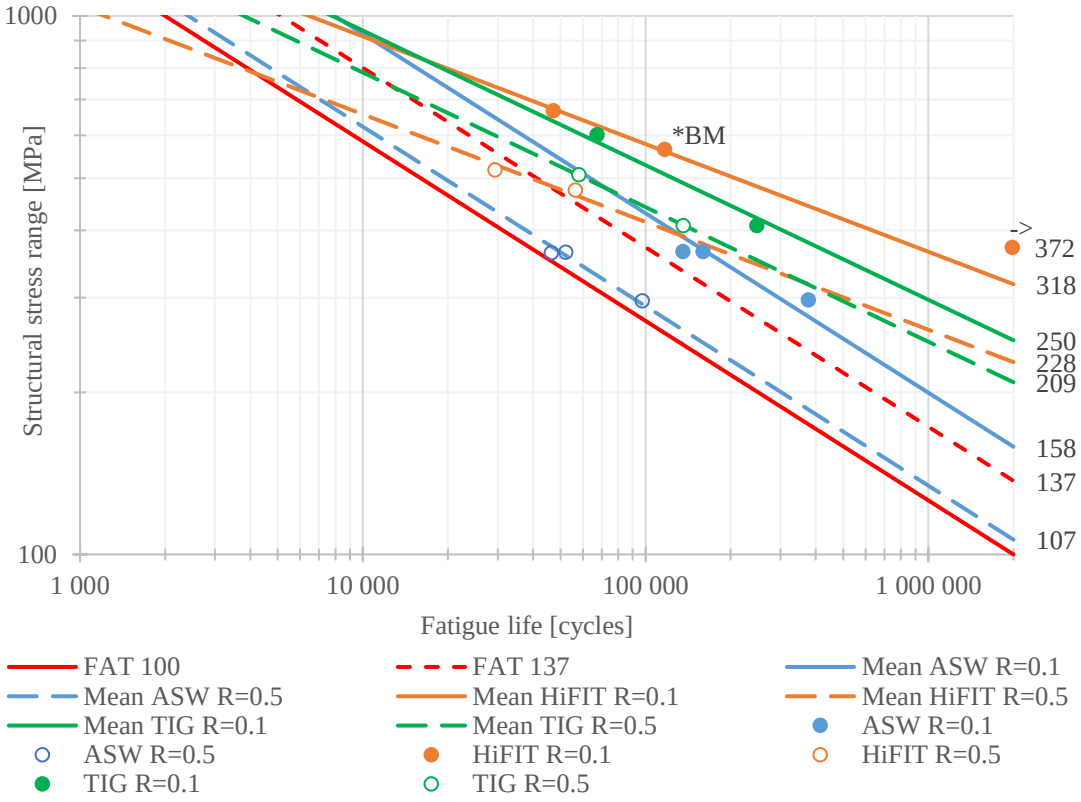

Figure 63. Structural stress results for NLCT-specimens as S-N curves.

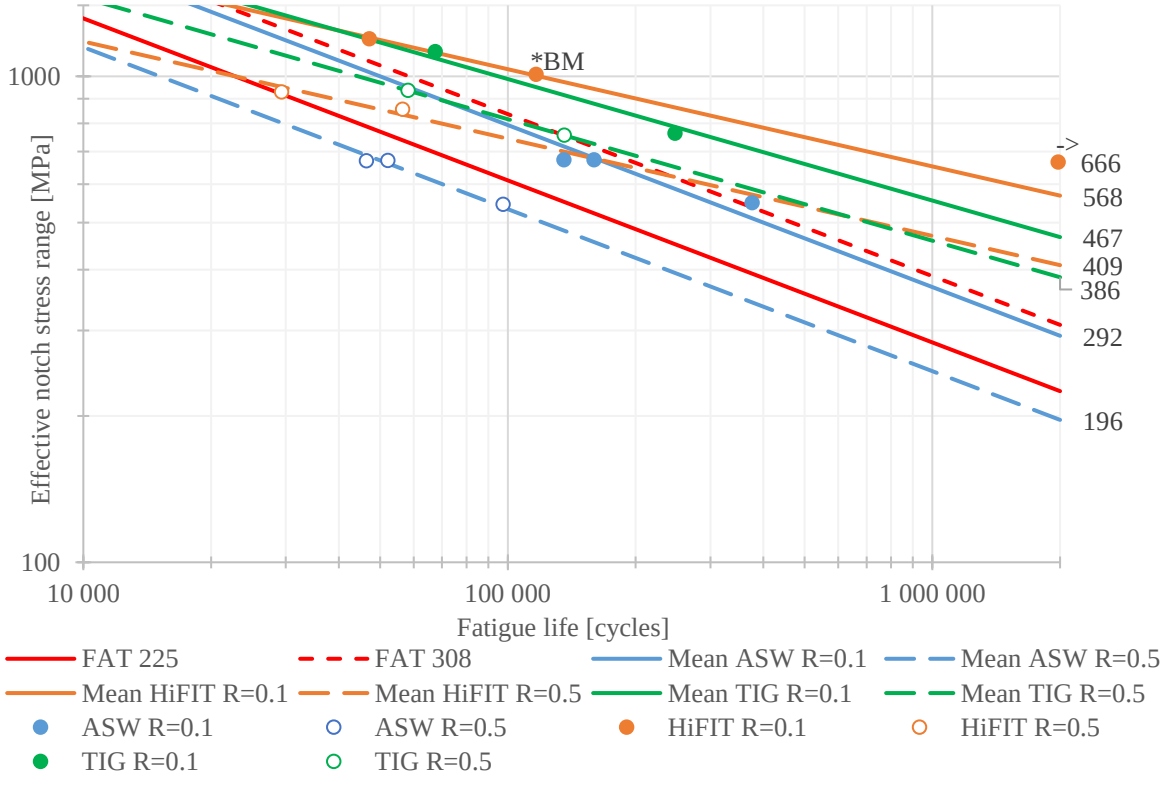

Figure 64. ENS results for NLCT-specimens as S-N curves.

According to the results, the applied stress ratio has effect on the fatigue strength of NLCT-specimens. FAT class decreases about 30% between stress ratios R = 0.1 and R = 0.5 in ASW and HiFIT-conditions and about 20% in TIG-treated condition. FAT class for HiFIT-treated specimen is approximately two times higher than in ASW-condition with both stress ratios. Benefit of the TIG-treatment was especially visible with the R = 0.5 when FAT class increased about 1.9 times with R = 0.5 and approximately 1.5 times with R = 0.1. FAT_{mean} value can be considered as conservative for ASW-specimens with the low stress ratio but very optimistic with the high stress ratio in terms of nominal and structural stress. However, all the results are above the FAT_{char} value also with these specimens. In the ENS results, ASW-condition specimens with R = 0.5 are below FAT_{char} 225 value. The rest of the results are near of the FAT_{mean} 308 value and post-weld treated specimens with R = 0.1 are clearly above that. The ENS method seems to be working well for specimens in ASW-condition with R = 0.1 and specimens in treated condition with R = 0.5 while post-weld treated specimens with the lower stress ratio are clearly above the FAT_{mean} 308.

Generally, post-weld treated specimens are at same level or above the FAT_{mean} value also with the higher stress ratio. The slope m = 5 appears to be proper for HiFIT-treated specimens as recommended and slope m = 4 seems to be suitable for TIG-treated specimens. The slope m = 4 could be considered for ASW R = 0.1 specimens. According to Yildirim (2015, p. 44) the slope m = 4 is preferable for TIG-treated specimens with CAL but more research is needed and also Skriko et al. (2017, p. 114) received such results. Based on the Leitner et al. (2017 p. 165-167) and the results of this study, sc. knee-point of HiFIT-treated specimens is clearly before 2 million, even before a million cycles, so the actual FAT class can be better than obtained class based on tests. In addition, part of the HiFIT-treated specimens failed from the edge of treated groove which could have been affected the results so paying attention to the grinding of the edges of test specimens is important. FAT class could be increased if post-weld treatment was used according to the IIW Recommendations. FAT_{mean} class for HiFIT-treated specimen was FAT_{mean} 171 in nominal stress and FAT_{mean} 219 in structural stress method and for TIG-treated specimen FAT_{mean} 171 in nominal stress and FAT_{mean} 191 in structural stress method. FAT_{mean} class for HiFIT-treated specimen is conservative at least with higher cycles and low stress ratio in terms of nominal and structural stress methods. FAT_{mean} class for TIG-treated specimen is optimistic in terms of nominal

stress and seems to be reasonable in terms of structural stress. Comparison of FAT classes is shown in table 16 and the effect of post-weld treatment is shown in table 17.

Table 16. FAT class comparison of NLCT-specimens.

Joint type	Method	$FAT_{R=0.1}/FAT_{mean,asw}$	$FAT_{R=0.5}/FAT_{mean,asw}$	$FAT_{R=0.5}/FAT_{R=0.1}$
NLCT ASW	Nominal	1.22	0.84	0.69
	Structural	1.15	0.78	0.68
	ENS	0.95	0.64	0.67
NLCT HiFIT	Nominal	2.65	1.85	0.70
	Structural	2.32	1.66	0.72
	ENS	1.84	1.33	0.72
NLCT TIG	Nominal	1.65	1.56	0.83
	Structural	1.82	1.53	0.84
	ENS	1.52	1.25	0.83

Table 17. Effect of post-weld treatments to FAT class of NLCT-specimens.

Method	HiFIT R = 0.1	HiFIT R = 0.5	TIG R = 0.1	TIG R = 0.5
	FAT_{HiFIT}/FAT_{asw}	FAT_{HiFIT}/FAT_{asw}	FAT_{TIG}/FAT_{asw}	FAT_{TIG}/FAT_{asw}
Nominal	2.18	2.22	1.35	1.87
Structural	2.01	2.13	1.58	1.95
ENS	1.95	2.09	1.60	1.97

Figures 65-67 shows the test results of LCX and LG -specimens as S-N curves. Nominal stress was calculated as weld stress using effective throat thickness obtained from macrograph (figure 41). Because of the root side failure in LCX-specimens, those results are not shown in the structural stress S-N curve. The slope m = 5 was used for LG HiFIT-treated specimens and otherwise m = 3 was used. Neither of the HiFIT-treated LG-specimens failed from weld toe but still they are marked to the S-N curves for comparison.

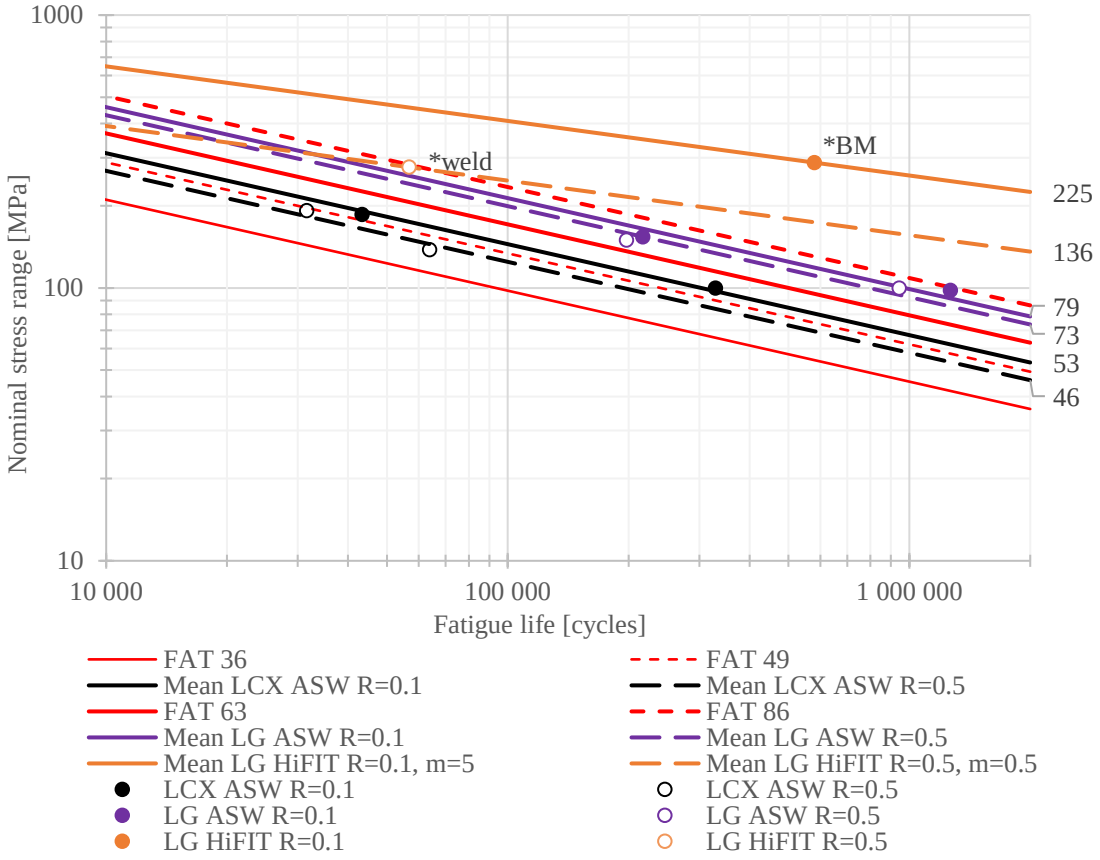

Figure 65. Nominal stress results for LCX and LG -specimens as S-N curves.

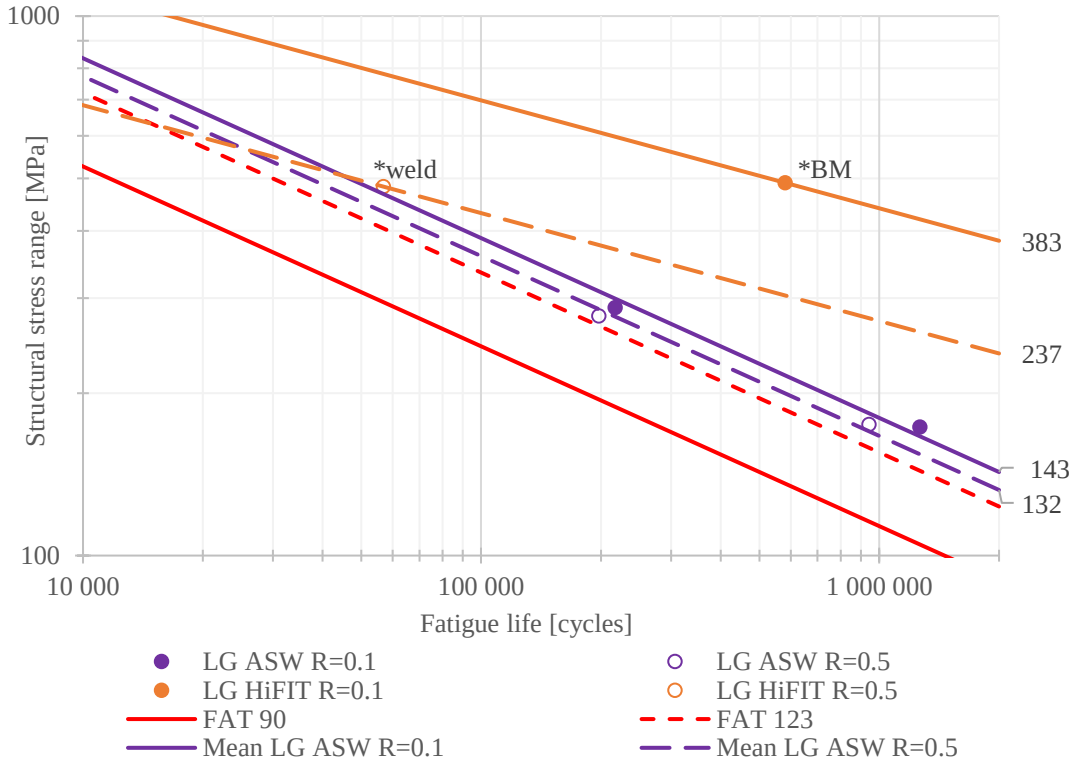

Figure 66. Structural stress results for LG-specimens as S-N curves.

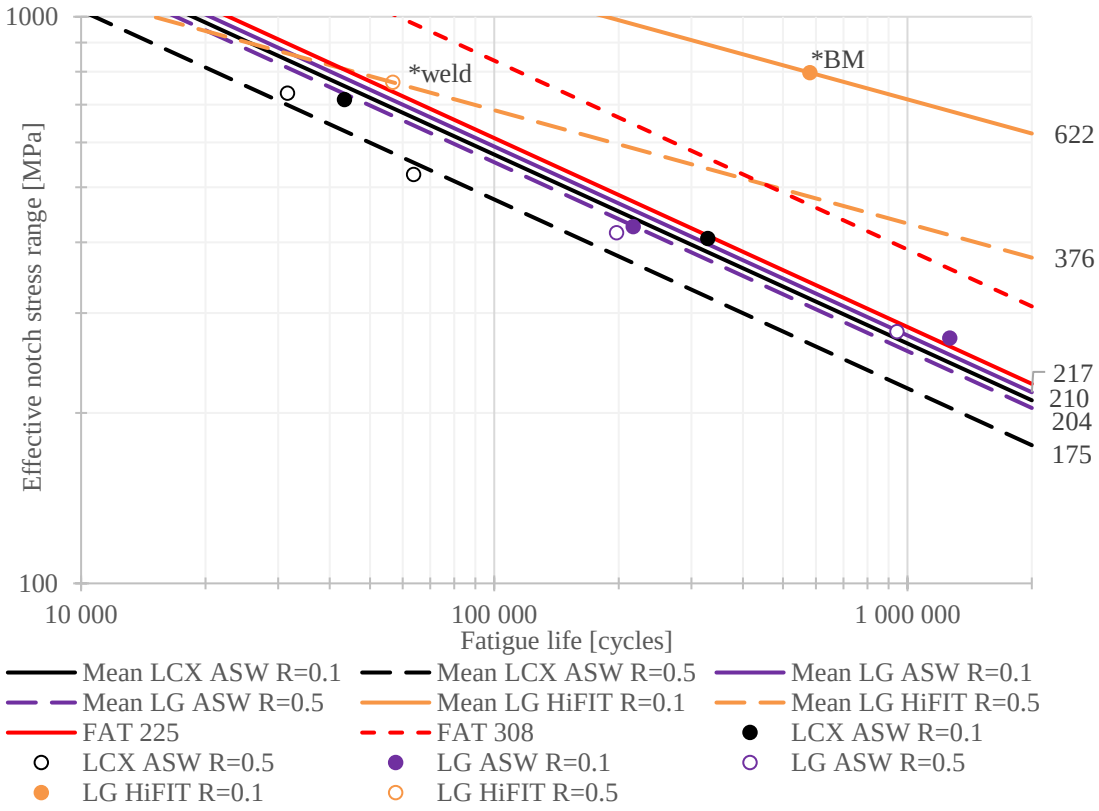

Figure 67. ENS results for LCX and LG -specimens as S-N curves.

The applied stress ratio have an effect on the fatigue strength of LCX and LG -specimens although in the case of LG-specimen effect is clearly less in the ASW-condition. FAT class decreases about 15% in LCX-specimens and 10% in LG-specimens between stress ratios R = 0.1 and R = 0.5. In the case of HiFIT-treated LG-specimen, the decrease is about 40% between stress ratios and FAT class clearly increased more with HiFIT-treatment in LG-specimens compared to NLCT-specimens. FAT class for HiFIT-treated specimen is over 2.5 times higher than in ASW-condition with R = 0.1 and almost 2 times higher with R = 0.5 but due to the number of tests and the failure mode the improvement is questionable. Obtained results refers to that at least HiFIT-treatment can eliminate the fatigue failure from weld toe. The situation could be same with HiFIT-treated NLCT-specimens if cracks at the edge of the treated groove could be avoided. In the nominal stress method, results of the LG-specimen are between FAT_{mean} 86 and FAT_{char} 63, but in structural stress method, results are clearly above the FAT_{mean} 123 with both stress ratios. FAT_{mean} is optimistic based on nominal stress but conservative based on structural stress. FAT_{mean} 49 seems to be reasonable for LCX-specimens in nominal stress method. Specimen S11_LCX_3 had offset based on 2D measurement data which is certainly affected to fatigue strength of the specimen, so FAT_{mean}

value for LCX-specimens with R = 0.1 could be better and then free slope of the curves would match better between stress ratios. That specimen had also crack at the weld toe that was propagated almost at that root of the weld where specimen failed. In the ENS method, almost all the ASW-condition results are below FAT_{char} 225, so the FAT class is unsafe for these specimens. Comparison of FAT classes is shown in table 18 and the effect of post-weld treatment is shown in table 19.

Table 18. FAT class comparison of LCX and LG-specimens.

Joint type	Method	$FAT_{R=0.1}/FAT_{mean,asw}$	$FAT_{R=0.5}/FAT_{mean,asw}$	$FAT_{R=0.5}/FAT_{R=0.1}$
LCX	Nom	1.08	0.94	0.87
	Str	-	-	-
	ENS	0.68	0.57	0.83
LG ASW	Nom	0.92	0.85	0.92
	Str	1.16	1.07	0.92
	ENS	0.70	0.66	0.94
LG HiFIT	Nom	2.62	1.58	0.60
	Str	3.11	1.93	0.62
	ENS	2.02	1.22	0.60

Table 19. Effect of HiFIT-treatment to FAT class of LG-specimen.

Method	R = 0.1	R = 0.5
	FAT_{HiFIT}/FAT_{asw}	FAT_{HiFIT}/FAT_{asw}
Nominal	2.85	1.86
Structural	2.68	1.80
ENS	2.87	1.84

According to Yildirim & Marquis (2012 p. 8) the major benefit of HFMI-treatment is obtained when $R \leq 0.15$ but results within this study indicates that FAT of NLCT-specimens decreases about same 30% between both stress ratios in HiFIT and ASW -conditions. In the case of the LG-specimen the situation seems to be different but the due to the number of tests analyzing is difficult. Based on Berg and Stranghoener (2014 p. 76) results fatigue

strength at least doubles as a result of hammer peening with applied stress ratio $R = 0.1$ same kind of results were obtained also in this study. According to Leitner (2017 p. 169) in the case of longitudinal stiffener the FAT increased 2.46 times when hammer peening was used with $R = 0.1$ and similar result was obtained in this study with one specimen. When comparing obtained fatigue strength results of this study with test data of literature review, clear improvement in fatigue strength between S1100 and S960 cannot be observed. However, there is limited amount of S960 test results in the literature review, so more research is needed.

From the results of effect of clamping (figure 47) can be noted that if specimen was very straight the strain gage indicated compression. Results might indicate that the clamps are not absolutely straight against each other. However, this may also be due to that the ends of the specimen are bend which causes compression at small angular distortions. Clamping has effect to stress ratio at the weld toe especially if the specimen is distorted a lot.

6.3 FE-analysis and fatigue strength assessment

FE-analysis was made to obtain stress concentration factors for fatigue strength assessment with the ENS and 4R methods. Models were modelled based on 2D measurement data and average values were used in the modelling. For more accurate results, each model could have been made with specimen specific values but it would have increased the workload significantly, so it was decided to use average values. In addition, fillet method was used in the modelling of the weld toe radius even though post-weld treated specimens have a very small undercut. However, measured values are only from center line of the specimen so correct value to be used is difficult to know as mentioned previously. Weld toe radius could have possibly been measured more accurately from the point where crack was initiated by using 3D scan but it was not used in this study.

Mean FAT classes were used in the fatigue life calculations. Nominal and structural stress methods produced conservative results with stress ratio $R = 0.1$ in ASW-condition. The ENS method worked fine in those circumstances with BW GMAW and NLCT -specimens. Some cases these methods produced reasonable results also for post-weld treated specimens. Situation is totally different with $R = 0.5$ wherein the methods provide optimistic results especially the ENS method. Based on the results 4R method seems to be very sensitive to

residual stress assumption and the benefit of the 4R method is particularly evident at higher stress ratio where also effect of residual stress assumption is clearly reduced. For example, specimens NCLT_1, NLCT_5 and NLCT_7H failed from side where clearly higher compressive residual stresses were measured compared to other weld toe of the specimen based on measurement data. Effect of the residual stress assumption is shown with these specimens with the R = 0.1 in the figure 57. The figure 58 shows that the effect of residual stress assumption is clearly decreased with R = 0.5. Björk et al. (2018 p. 16) have made same observations about 4R method in earlier studies. Results of the 4R method were converted to reference coordinate system using equation 14 and own Master Curve was made with minimization of sum of squared perpendicular distances (MSSPD) -method also known as Deming regression. Results in reference coordinate systems with different residual stress assumptions are shown in figures 68 and 69.

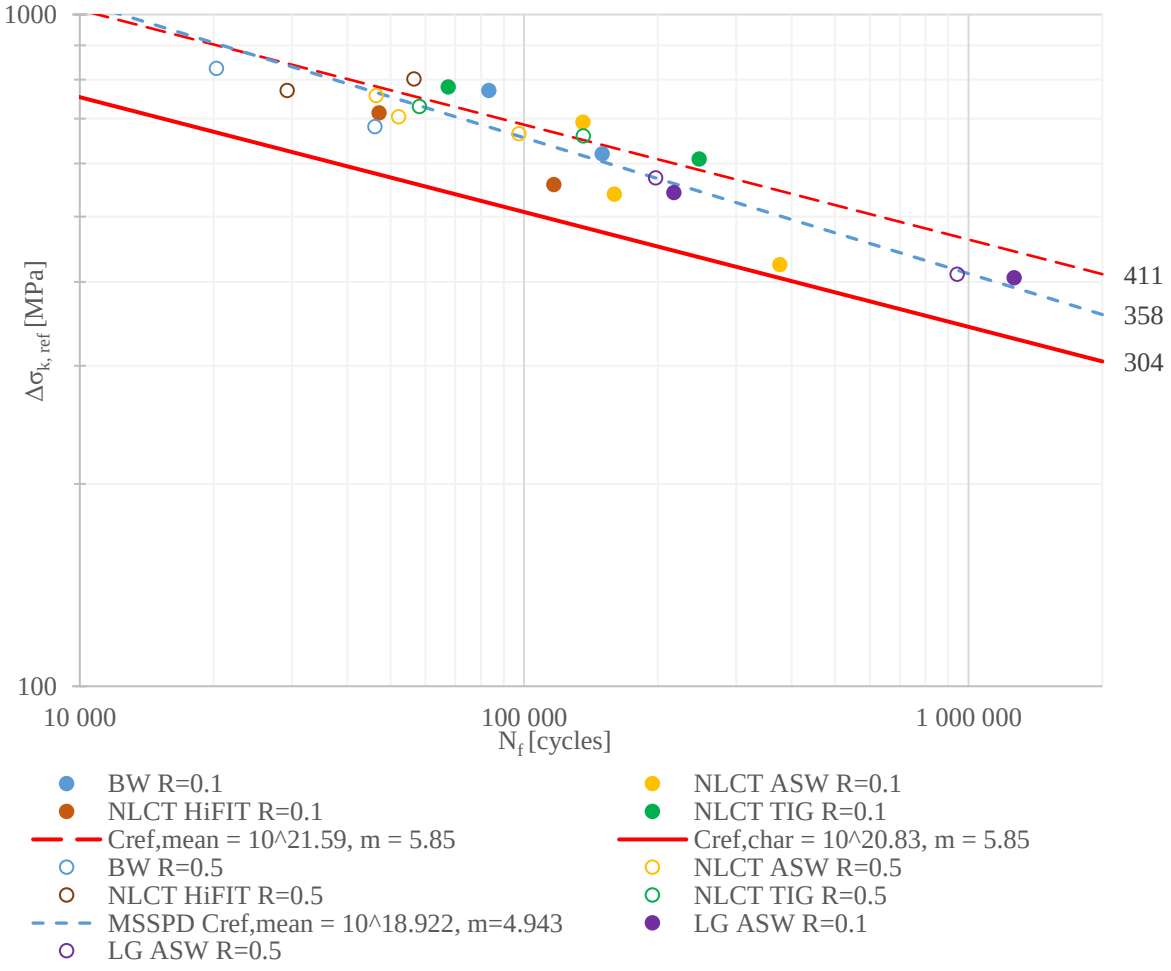

Figure 68. Reference coordinate system, $R_{local,\ ref}$ = 0. Residual stress specific to the specimen.

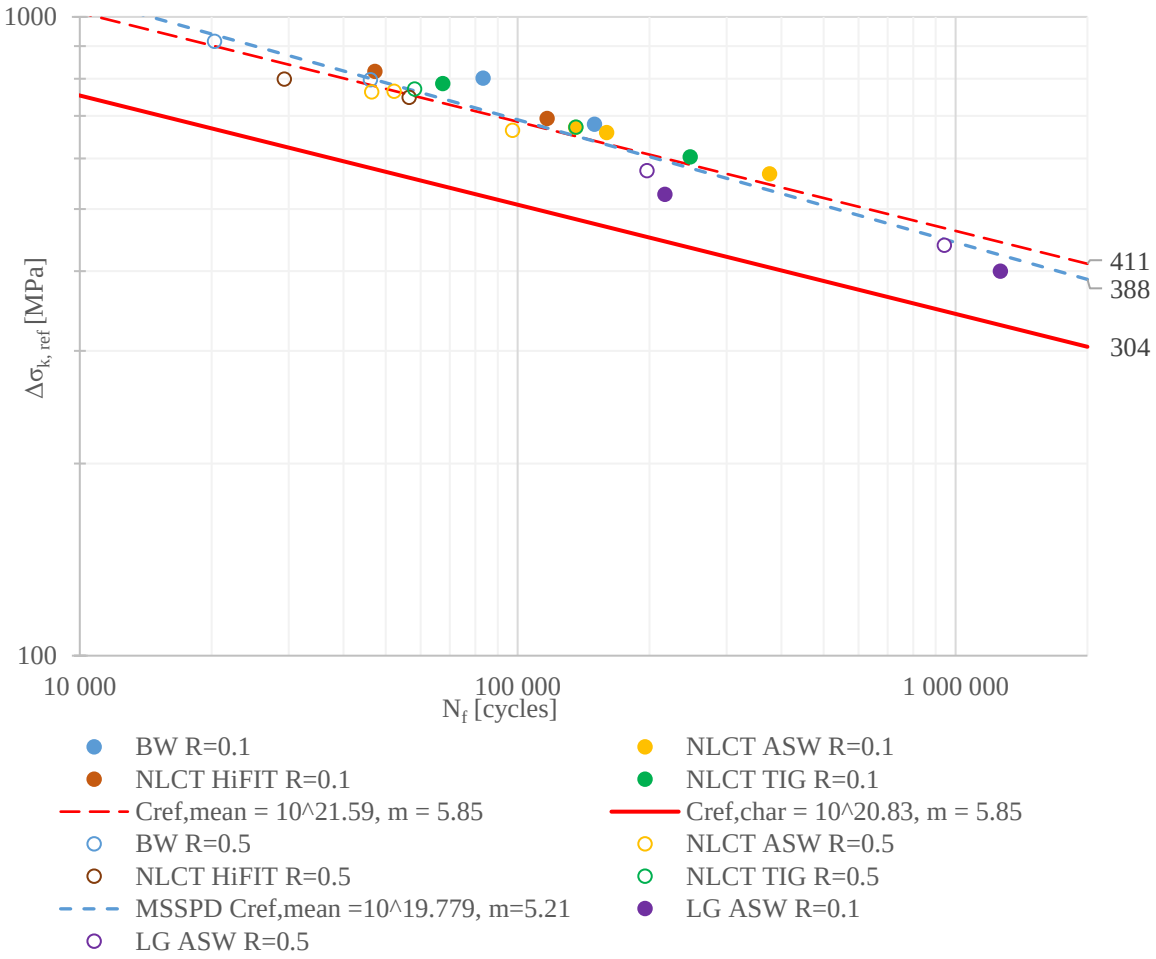

Figure 69. Reference coordinate system, $R_{local,\,ref}$ = 0. Maximum residual stress value to the specimen type.

Based on the results, the original Master Curve works well and it works even better when maximum residual stress value to the specimen type is used. Residual stress assumption can be too optimistic if only one point is measured from the center line of the specimen as already said so it seems that it is better to use maximum value of the measured values of population in the calculation.

Calculation of ENS for the LG-specimens, only nominal stress was used. According to 2D data no angular distortions were found and thus, this simplification was made. Evaluation of secondary bending stress would have been more difficult in this case because the structural stress is due to angular distortion of the specimen and geometric discontinuity of the gusset. Effect assumed to be minor but it would have increased the ENS and the result of fatigue

life calculation would have been smaller i.e. closer to the test result using ENS and 4R methods.

In the future, more fatigue tests could be done to find out the actual slope of the S-N curve. In addition, the effect of post-weld treatments for other joint types could be investigated excluding the LCX-joint. It should be also examined that can fatigue strength be improved by changing the welding parameters. Residual stresses could be measured more than one point though it is time consuming. Fatigue tests under variable amplitude loading could be performed and also fatigue strength of the weld root could be investigated more. However, it is clear that more tests are needed to make better conclusion.

7 SUMMARY AND CONCLUSIONS

Fatigue strength of typical welded joints made of SSAB's Strenx® 1100 Plus structural steel was studied in this work. Butt welded joints (BW), non-load carrying T-joints (NLCT), load carrying X-joints (LCX) and longitudinal gusset joints (LG) were investigated. All the test specimens were welded with robotized GMAW except of two butt joints that were welded by fiber laser. Some of the NLCT- and LG-joints were post-weld treated by HiFIT-treatment or TIG-treatment. Fatigue tests were performed with CAL and with applied stress ratios R = 0.1 and R = 0.5. Experimental fatigue test results were compared with results of FE-analysis and fatigue strength assessment by the nominal stress, structural stress, ENS and 4R methods. In addition, 2D measurements, residual stress measurements and hardness measurements were carried out. The research questions of this work were:

- What is the fatigue strength of the test specimens and how it differ from fatigue strength of lower strength steels such as S960?
- Can accurate fatigue strength results be obtained by finite element analysis (FEA) and analytic calculations for welded joints made of S1100?
- How post-weld treatments, such as HiFIT-treatment and TIG-dressing, affect the fatigue strength capacity?
- How test results differ from fatigue strength estimations obtained by the 4R method?

Obtained FAT classes in this study with fixed and free slopes are presented in chapter 3.4. There was no unambiguous improvement in fatigue strength between S1100 and S960 when obtained FAT classes were compared with test data of literature review. However, there was limited amount of S960 test results in the literature review, so more research is needed. Generally, nominal and structural stress methods provided conservative results with applied stress ratio R = 0.1 but with R = 0.5 test results were below FAT_{mean} values even vicinity of FAT_{char} values. For LCX-specimens, nominal FAT_{mean} 49 seems to be reasonable. The ENS method produced accurate results for GMAW BW and ASW NLCT-specimens with R = 0.1 when in other cases FAT_{char} 225 was unsafe in ASW-condition. Benefit of the 4R method was that it takes account applied stress ratio and residual stresses but it was sensitive to residual stress assumption. The 4R method was clearly more accurate than other methods

when the applied stress ratio was R = 0.5. Post-weld treatments significantly increased the fatigue strength of test specimens. HiFIT-treatment increased fatigue strength of NLCT-specimens over 2 times with both stress ratios R = 0.1 and R = 0.5 and with TIG-treatment, the increase was approximately 1.5 times with R = 0.1 and 1.9 times with R = 0.5. Improvement in LG-specimen with applied stress ratio R = 0.1 was over 2.5 times and with R = 0.5 was about 1.8 times with HiFIT-treatment although the improvement was questionable due to the number of tests and the failure mode of the specimens. Based on the results of this study following conclusions were made:

- Applied stress ratio has significant effect on the fatigue strength of the test specimens.
- Post-weld treatment by HiFIT or TIG improved fatigue strength of the test specimens with both stress ratios. In addition, HiFIT-treatment can eliminate weld toe failure at low stress ratios.
- IIW FAT_{mean} classes are conservative at low stress ratios in terms of nominal and structural stress methods. However, the FAT_{char} classes can be even unsafe in some cases at high stress ratios.
- The ENS method predicted accurate results for BW GMAW and NLCT-specimens in ASW-condition with low stress ratios but IIW FAT_{char} 225 is unsafe in other cases in ASW-condition.
- Benefit of the 4R method compared with other fatigue strength assessment methods was that it takes account the applied stress ratio and effect of residual stresses which resulted in more accurate results especially at high stress ratios compared to other methods.

LIST OF REFERENCES

4R Method, 2018. Laboratory of Steel Structures. Lappeenranta University of Technology. Updated version, 13.2.2018. 54 p.

Berg, J. & Stranghoener, N. 2014. Fatigue strength of welded ultra high strength steels improved by high frequency hammer peening. In: Procedia Materials Science. 20th European Conference on Fracture (ECF20). Volume III. Elsevier Ltd. Pp. 71-76.

Björk, T. 2018. ST 1100 Plus [private e-mail]. Receivers: Antila Antti, Koskimäki Matti, Kärmeniemi Mika, Yusuf Ahmed (cc), Khan Udoy (cc). Sent 9.4.2018, 17.28 o'clock (GMT +0200).

Björk, T., Mettänen, H., Ahola, A., Lindgren, M & Terva, J. 2018. Fatigue Strength Assessment of Duplex and Super-Duplex Stainless Steels by 4R Method. In: Welding in the world, Vol: 62: 6. Pp. 1285-1300.

Climate guide, 2018. Finnish meteorological institute, Finland's Environment Institute, Aalto University. Material efficiency. [Climate guide webpage]. [Referred 10.7.2018]. Available: https://ilmasto-opas.fi/en/ilmastonmuutos/hillinta/-/artikkeli/38393e35-469e-4b53-8a31-15fbebab897c/materiaalitehokkuus.html

Dowling, N. E. 2013. Mechanical Behavior of Materials. Engineering Methods for Deformation, Fracture, and Fatigue. 4th edition. Pearson Education Limited, England. 954 p.

Finnish Standards Association SFS. 2018. Terässtandardit [web document] [Referred 25.7.2018]. Available in PDF-file: https://www.sfs.fi/files/1483/Terasstandardit.pd.pdf

Goss, C. & Marecki, P. 2012. Fatigue Test Welded Joints Steel S960QL. In: Materials Science Forum, Vol. 726. Trans Tech Publications, Switzerland. Pp. 93-99.

Haagensen, P. J. & Maddox, S. J. 2006. IIW Recommendations on Post Weld Improvement of Steel and Aluminium Structures. IIW Commission XIII. The International Institute of Welding. 39 p.

Hobbacher, A. F. 2016. Recommendations for Fatigue Design of Welded Joints and Components. Springer International Publishing, Switzerland. IIW Collection, Second edition. 143 p.

ISO 12106. 2017. Metallic materials – Fatigue testing – Axial-strain-controlled method. 2nd edition. Genève: International Organization for Standardization. 37 p.

Kah, P., Pirinen, M., Suoranta, R. & Martikainen, J. 2014. Welding of Ultra High Strength Steels. In: Advanced Materials Research, Vol. 849. Trans Tech Publications, Switzerland. Pp. 358-365.

Kauppi, T. & Kesti, V. 2016. Ultralujat teräkset kestävän kehityksen kärjessä. AMK-lehti/UAS journal. n:o 4/2016. Available: https://uasjournal.fi/tutkimus-innovaatiot/ultralujat-terakset-kestavan-kehityksen-karjessa/#1458134585005-b3f22396-5506

Leitner, M. 2017. Influence of effective stress ratio on the fatigue strength of welded and HFMI-treated high-strength steel joints. In: International Journal of Fatigue, Vol: 102. Elsevier Ltd. Pp. 158-170.

Leitner, M., Gerstbrein, S., Ottersböck, M. & Stoschka, M. 2015. Fatigue strength of HFMI-treated and stress-relief annealed high-strength steel weld joints. In: Procedia Engineering. Fatigue Design 2015, 6th Fatigue Design conference, held at Senlis, France 18-19 November, 2015. Vol. 133. Elsevier Ltd. Pp. 477-484.

Lukkari, J., Kyröläinen, A. & Kauppi, T. 2016. Hitsauksen materiaalioppi, osa 2: Metallit ja niiden hitsattavuus. Orivesi: Oriveden kirjapaino. Suomen Hitsausteknillinen Yhdistys r.y. (SHY). 364 p.

Marquis, G. B. & Barsoum, Z. 2016. IIW Recommendations on High Frequency Mechanical Impact (HFMI) Treatment for Improving the Fatigue Strength of Welded Joints. Springer Science+Business Media, Singapore. IIW Collection. 34 p.

Mikkonen, P., Björk, Timo., Skriko, T. & Tuominen, N. 2017. Ultralujien terästen ominaisuudet lopputuotteeseen osaavan suunnittelun ja valmistuksen avulla. Hitsaustekniikka, n:o 1. Pp. 26-30.

Möller, B., Wagener, R., Hrabowski, J., Ummenhofer, T. & Melz, T. 2015. Fatigue life of welded high-strength steels under Gaussian loads. In: Procedia Engineering. VAL2015, 3rd International Conference on Material and Component Performance. Vol. 101. Elsevier Ltd. Pp. 293-301.

Nykänen, T. & Björk, T. 2015. Assessment of fatigue strength of steel buttwelded joints in as-welded condition - Alternative approaches for curve fitting and mean stress effect analysis. In: Marine Structures, Vol. 44. Pp.288-310.

Pijpers, R. J. M., Kolstein, M. H., Romeijn, A. & Bijlaard, F. S. K. 2009. Fatigue experiments on very high strength steel base material and transverse butt welds. In: Advanced Steel Construction, Vol. 5: 1. Pp. 14-32.

Radaj, D., Sonsino, C. M. & Fricke, W. 2006. Fatigue assessment of welded joints by local approaches. 2nd edition. Woodhead Publishing Limited. Cambridge, England. 639 p.

Ruoppa, R., Keltamäki, K., Tolppila, R. & Kesti, V. 2016. Research of ultra-high-strength and wear-resistant steels using advanced techniques. Proceedings of the METNET Seminar 2016 in Castellon. Universitat Jaume I (UJI), Castellon, Spain. 11-12.10.2016. Pp. 31-42.

Scopus. 2018. Analyze search results. [Scopus webpage]. [Referred 19.12.2018]. Available: https://www.scopus.com/term/analyzer.uri?sid=d27a6954d831e1a9b810b14643654ab3&origin=resultslist&src=s&sort=plff&sdt=a&sot=a&sessionSearchId=d27a6954d831e1a9b810b14643654ab3&count=794&analyzeResults=Analyze+results&cluster=scosubtype%2c%22ar%22%2ct%2c%22cp%22%2ct%2bscosubjabbr%2c%22ENGI%22%2ct%2c%22MAT

E%22%2ct%2bscopubyr%2c%222018%22%2ct%2c%222017%22%2ct%2c%222016%22%2ct%2c%222015%22%2ct%2c%222014%22%2ct%2c%222013%22%2ct%2c%222012%22%2ct%2c%222011%22%2ct%2c%222010%22%2ct%2c%222009%22%2ct%2c%222008%22%2ct%2c%222007%22%2ct%2c%222006%22%2ct%2c%222005%22%2ct%2c%222004%22%2ct%2c%222003%22%2ct%2c%222002%22%2ct%2c%222001%22%2ct%2c%222000%22%2ct%2bscoexactkeywords%2c%22Ultra+High+Strength+Steel%22%2ct&txGid=6aef0430447f3bf4c3776e90479882c6

SFS 3099. 1974. General principles for fatigue testing of metals. Helsinki: Finnish Standards Association SFS. 13 p. Approved 15.8.1974.

SFS-EN 1993-1-9. 2005. Eurocode 3: Design of steel structures. Part 1-9: Fatigue. Helsinki: Finnish Standards Association SFS. 41 p. Approved 15.8.2005.

SFS-EN 1993-1-12. 2007. Eurocode 3: Design of steel structures. Part: 1-12: Additional rules for extension of EN 1993 up to steel grades S700. Helsinki: Finnish Standards Association SFS. 9 p. Approved 16.4.2007.

SFS-EN ISO 148-1. 2016. Metallic materials. Charpy pendulum impact test. Part 1: Test method. Helsinki: Finnish Standards Association SFS. 33 p. Approved 2.12.2016.

SFS-EN ISO 4136. 2012. Destructive tests on welds in metallic materials. Transverse tensile test. Helsinki: Finnish Standards Association SFS. 9 p. Approved 10.12.2012.

SFS-EN ISO 6892-1. 2016. Metallic materials. Tensile testing. Part 1: Method of test at room temperature. Helsinki: Finnish Standards Association SFS. 83 p. Approved 5.8.2016.

SFS-EN ISO 9018. 2015. Destructive tests on welds in metallic materials. Tensile test on cruciform and lapped joints. Helsinki: Finnish Standards Association SFS. 24 p. Approved 20.11.2015.

SFS-ISO 1099. 2017. Metallic materials. Fatigue testing. Axial force-controlled method. Helsinki: Finnish Standards Association SFS. 28 p. Approved 22.12.2017.

Skriko, T., Ghafouri, M. & Björk, T. 2017. Fatigue strength of TIG-dressed ultra-high-strength steel fillet weld joints at high stress ratio. In: International Journal of Fatigue, Vol: 94. Pp. 110-120.

Sonsino, C. M., Fricke, W., de Bruyne, F., Hoppe, A., Ahmadi, A. & Zhang, G. 2012. Notch Stress Concepts for the Fatigue Assessment of Welded Joints - Background and Applications. In: International Journal of Fatigue, Vol: 34: 1. Pp. 2–16.

SSAB. 2018. Image Bank. [SSAB webpage]. [Referred 30.7.2018]. Available: https://imagebank.ssab.com/SSAB/#1532949241602_49

SSAB. 2019. Strenx® 1100 Plus. [SSAB webpage]. [Referred 21.1.2019]. Available: https://www.ssab.com/products/brands/strenx/products/strenx-1100-plus

Union X 96. 2014. [www- data sheet]. (Publishing place unknown): Böhler Welding by Voestalpine, 12/2014. [Referred 13.8.2018] Available: http://www.alruqee.com/Userfiles/Product/TablePdf/19042016000000T_Union%20X%2096_solid%20wire.pdf

van Es, S. H. J., Kolstein, M. H., Pijpers, R. J. M. & Bijlaard, F. S K. 2013. TIG-dressing of high strength butt welded connections – Part 2: physical testing and modelling. In. Procedia Engineering, Vol. 66. Elsevier Ltd. Pp. 126-137.

Yildirim, H. C. 2015. Review of fatigue data for welds improved by tungsten inert gas dressing. In: International Journal of Fatigue, Vol. 79. Elsevier Ltd. Pp. 36-45.

Yildirim, H. C. & Marquis, G. B. 2012. Fatigue strength improvement factors for high strength steel welded joints treated by high frequency mechanical impact. In: International Journal of Fatigue. Elsevier Ltd. 9p.

Welding parameters

Specimen ID	Weld ID	Wire feed rate	Travel speed	Current	Arc voltage	Free wire length	Angle of burner	Angle of tilt
		m/min	mm/s	A	V	mm	[deg]	[deg]
S11_BW_1	1	10.0	6.2	216	26.5	18	90	5 pushing
	2	10.0	6.2	213	26.4	18	90	5 pushing
S11_BW_2	1	10.0	6.2	216	26.6	18	90	5 pushing
	2	10.0	6.2	215	26.5	18	90	5 pushing
S11_BW_3	1	10.0	6.2	215	26.6	18	90	5 pushing
	2	10.0	6.2	217	26.5	18	90	5 pushing
S11_BW_4	1	10.0	6.2	215	26.6	18	90	5 pushing
	2	10.0	6.2	213	26.5	18	90	5 pushing
S11_BW_5	1	10.0	6.2	214	26.2	18	90	5 pushing
	2	10.0	6.2	222	26.3	18	90	5 pushing
S11_BW_6	1	10.0	6.2	216	26.4	18	90	5 pushing
	2	10.0	6.2	218	26.3	18	90	5 pushing
S11_BW_7	1	10.0	6.2	217	26.4	18	90	5 pushing
	2	10.0	6.2	219	26.2	18	90	5 pushing
BW 1 (microsection)	1	10.0	6.2	225	26.0	18	90	5 pushing
	2	10.0	6.2	214	26.4	18	90	5 pushing

Welding parameters

Specimen ID	Weld ID	Wire feed rate	Travel speed	Current	Arc voltage	Free wire length	Angle of burner	Angle of tilt
		m/min	mm/s	A	V	mm	[deg]	[deg]
S11_NLCT_1	1	11.0	7.8	220	26.7	18	45	18 pushing
	2	11.0	7.8	220	26.7	18	45	18 pushing
S11_NLCT_2	1	11.0	7.8	220	27.0	18	45	18 pushing
	2	11.0	7.8	220	26.8	18	45	18 pushing
S11_NLCT_3	1	11.0	7.8	222	26.7	18	45	18 pushing
	2	11.0	7.8	219	26.8	18	45	18 pushing
S11_NLCT_4	1	11.0	7.8	221	26.6	18	45	18 pushing
	2	11.0	7.8	220	26.9	18	45	18 pushing
S11_NLCT_5	1	11.0	7.8	222	26.8	18	45	18 pushing
	2	11.0	7.8	220	26.9	18	45	18 pushing
S11_NLCT_6	1	11.0	7.8	222	26.8	18	45	18 pushing
	2	11.0	7.8	220	26.8	18	45	18 pushing
S11_NLCT_7H	1	11.0	7.8	220	26.9	18	45	18 pushing
	2	11.0	7.8	219	26.9	18	45	18 pushing
S11_NLCT_8H	1	11.0	7.8	220	26.8	18	45	18 pushing
	2	11.0	7.8	220	26.9	18	45	18 pushing
S11_NLCT_9H	1	11.0	7.8	221	26.8	18	45	18 pushing
	2	11.0	7.8	219	26.8	18	45	18 pushing

Welding parameters

Specimen ID	Weld ID	Wire feed rate	Travel speed	Current	Arc voltage	Free wire length	Angle of burner	Angle of tilt
		m/min	mm/s	A	V	mm	[deg]	[deg]
S11_NLCT_10H	1	11.0	7.8	221	26.7	18	45	18 pushing
	2	11.0	7.8	220	26.9	18	45	18 pushing
S11_NLCT_11T	1	11.0	7.8	222	26.8	18	45	18 pushing
	2	11.0	7.8	219	27.0	18	45	18 pushing
S11_NLCT_12T	1	11.0	7.8	222	26.8	18	45	18 pushing
	2	11.0	7.8	220	26.9	18	45	18 pushing
S11_NLCT_13T	1	11.0	7.8	222	26.7	18	45	18 pushing
	2	11.0	7.8	220	26.8	18	45	18 pushing
S11_NLCT_14T	1	11.0	7.8	222	26.7	18	45	18 pushing
	2	11.0	7.8	221	26.7	18	45	18 pushing
S11_NLCT_15 (microsection)	1	11.0	7.8	222	26.6	18	45	18 pushing
	2	11.0	7.8	221	26.7	18	45	18 pushing
S11_NLCT_16 (microsection)	1	11.0	7.8	224	26.5	18	45	18 pushing
	2	11.0	7.8	222	26.7	18	45	18 pushing
S11_NLCT_17 (microsection)	1	11.0	7.8	225	26.6	18	45	18 pushing
	2	11.0	7.8	223	26.7	18	45	18 pushing

Welding parameters

Specimen ID	Weld ID	Wire feed rate	Travel speed	Current	Arc voltage	Free wire length	Angle of burner	Angle of tilt
		m/min	mm/s	A	V	mm	[deg]	[deg]
S11_LCX_1	1	11.0	7.8	220	26.8	18	45	18 pushing
	2	11.0	7.8	220	26.6	18	45	18 pushing
	3	11.0	7.8	219	26.9	18	45	18 pushing
	4	11.0	7.8	221	26.7	18	45	18 pushing
S11_LCX_2	1	11.0	7.8	220	26.7	18	45	18 pushing
	2	11.0	7.8	220	26.6	18	45	18 pushing
	3	11.0	7.8	221	26.8	18	45	18 pushing
	4	11.0	7.8	221	26.8	18	45	18 pushing
S11_LCX_3	1	11.0	7.8	221	26.7	18	45	18 pushing
	2	11.0	7.8	221	26.6	18	45	18 pushing
	3	11.0	7.8	220	26.7	18	45	18 pushing
	4	11.0	7.8	220	26.8	18	45	18 pushing
S11_LCX_4	1	11.0	7.8	220	26.7	18	45	18 pushing
	2	11.0	7.8	221	26.7	18	45	18 pushing
	3	11.0	7.8	220	26.8	18	45	18 pushing
	4	11.0	7.8	221	26.7	18	45	18 pushing
S11_LCX_5 (microsection)	1	11.0	7.8	221	26.6	18	45	18 pushing
	2	11.0	7.8	224	26.5	18	45	18 pushing
	3	11.0	7.8	220	26.5	18	45	18 pushing
	4	11.0	7.8	217	26.8	18	45	18 pushing

Welding parameters

Specimen ID	Weld ID	Wire feed rate	Travel speed	Current	Arc voltage	Free wire length	Angle of burner	Angle of tilt
		m/min	mm/s	A	V	mm	[deg]	[deg]
S11_LG_1	1	11.0	7.8	224	26.8	18	45	18 pushing
S11_LG_2	1	11.0	7.8	223	26.7	18	45	18 pushing
S11_LG_3	1	11.0	7.8	225	26.7	18	45	18 pushing
S11_LG_4	1	11.0	7.8	226	26.8	18	45	18 pushing
S11_LG_5H	1	11.0	7.8	224	26.6	18	45	18 pushing
S11_LG_6H	1	11.0	7.8	222	26.6	18	45	18 pushing

Specimen ID	Weld ID	Travel speed	Welding power
		[m/min]	[kW]
S11_LW_1	1	1.0	7.8
S11_LW_2	1	1.0	7.8
Laser 1 (microsection)	1	1.0	7.8

FAT classes for nominal stress method (Hobbacher 2016, p. 44-45, 51, 53-54).

No.	Structural Detail	Description (St. = steel; Al. = aluminium)	FAT St.	FAT Al.	Requirements and remarks
212	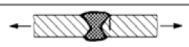	Transverse butt weld made in shop in flat position, NDT weld reinforcement <0.1 A thickness	90	36	Weld run-on and run-off pieces to be used and subsequently removed. Plate edges ground flush in direction of stress. Welded from both sides. Misalignment <5 % of plate thickness
213		Transverse butt weld not satisfying conditions of 212, NDT Al.: Butt weld with toe angle ≤ 50° Butt welds with toe angle > 50°	80	 32 25	Weld run-on and run-off pieces to be used and subsequently removed. Plate edges ground flush in direction of stress. Welded from both sides. Misalignment <10 % of plate thickness
217	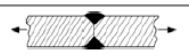	Transverse partial penetration butt weld, analysis based on stress in weld throat sectional area, weld overfill not to be taken into account	36	12	The detail is not recommended for fatigue loaded members Assessment by notch stress or fracture mechanics is preferred
511	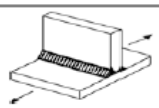	Transverse non-load-carrying attachment, not thicker than main plate K-butt weld, toe ground Two sided fillets, toe ground Fillet weld(s), as welded thicker than main plate	 100 100 80 71	 36 36 28 25	Grinding marks normal to weld toe An angular misalignment corresponding to k_m = 1.2 is already covered
413	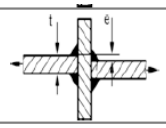	Cruciform joint or T-joint, fillet welds or partial penetration K-butt welds, potential failure from weld toe Single sided T-joints	63 71	22 25	Advisable to ensure that intermediate plate was checked against susceptibility to lamellar tearing Misalignment < 15 % of primary plate thickness in cruciform joints Also to be assessed as 414
414	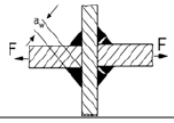	Cruciform joint or T-joint, fillet welds or partial penetration K-butt welds including toe ground joints, potential failure from weld root For a/t <=1/3	36 40	12 14	Analysis based on stress in weld throat $\sigma_w = F/\sum (a_w \cdot l)$ l = length of weld, a_w = load carrying weld throat. Also to be assessed as 413
521	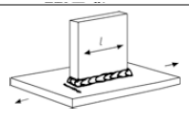	Longitudinal fillet welded gusset of length l. Fillet weld around end l < 50 mm l < 150 mm l < 300 mm l > 300 mm	 80 71 63 50	 28 25 20 18	For gusset on edge: see detail 525 Particularly suitable for assessment on the basis of structural hot spot stress approach

FAT classes for structural stress method (Hobbacher 2016, p. 61).

No.	Structural detail	Description	Requirements	FAT Steel	FAT Alu.
1	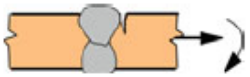	Butt joint	As welded, NDT	100	40
3	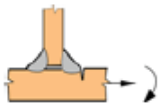	Non load-carrying fillet welds	Transverse non-load carrying attachment, not thicker than main plate, as welded	100	40
6	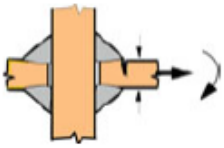	Cruciform joints with load-carrying fillet welds	Fillet welds, as welded	90	36
9	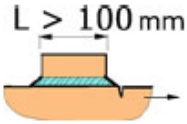	Type “b” joint with long attachment	Fillet or full penetration weld, as welded	90	36

2D- and residual stress measurement

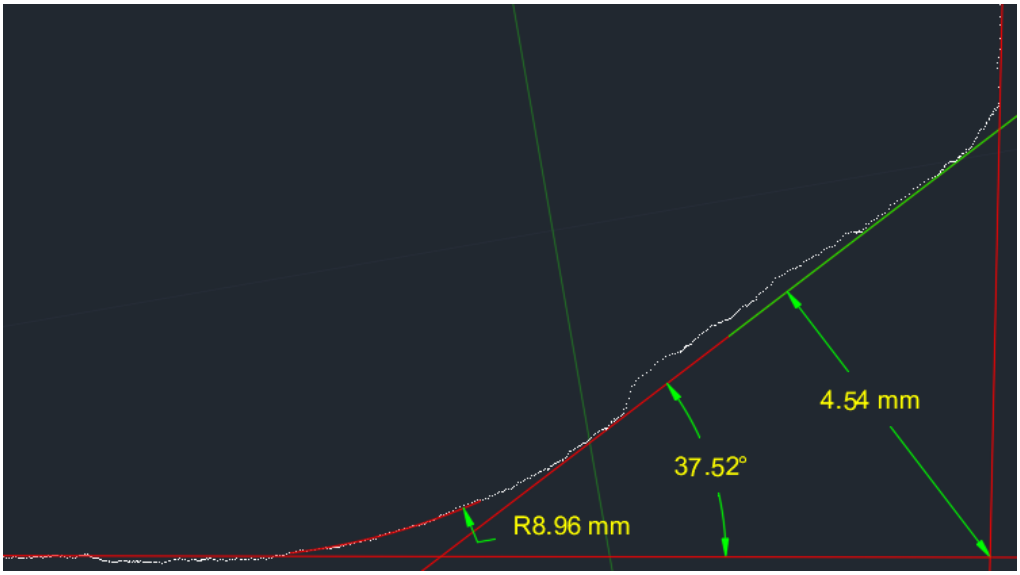

Figure III.1. Weld toe radius, weld angle and throat thickness measurement from 2D data of TIG-treated specimen.

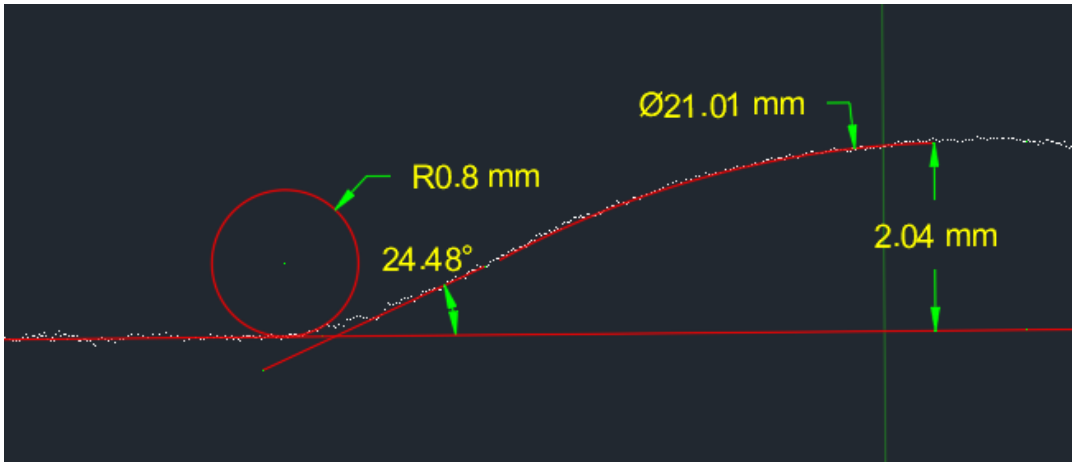

Figure III.2. Weld toe radius, flank angle, weld cup height and weld cup diameter measurement from 2D data.

2D- and residual stress measurement

Specimen	Weld toe	Weld toe radius	Flank angle	Cup width	Cup height	Cup diameter	Angular distortion	SG	Residual stress at weld toe	Error
	ID	[mm]	[deg]	[mm]	[mm]	[mm]	[deg]	ID	[MPa]	(+/-)
S11_BW_1	1	1.50	22.56	13.46	2.15	18	0.88 *	2	-98	11.9
	2	0.42	24.89						-53	20.9
	3	1.92	21.28	13.52	1.73	22			-166	20.1
	4	0.28	19.85						-142	28.2
S11_BW_2	1	0.56	24.70	13.68	2.18	20	0.73 *	1	-16	27
	2	0.68	24.06						-107	7.4
	3	0.47	19.09	14.01	1.79	20			-70	17.6
	4	0.22	16.50						-129	24.5
S11_BW_3	1	0.80	24.48	14.20	2.05	21	0.31 *	1	-161	8.3
	2	1.25	25.37						-78	15.7
	3	0.48	17.80	13.36	1.74	18			-53	16.8
	4	1.22	17.12						-148	16.9
S11_BW_4	1	0.86	24.56	13.75	1.96	20	0.96 **	4	-259	17.7
	2	0.87	23.89						-210	20.3
	3	0.54	22.99	14.34	2.00	17			-66	20
	4	0.86	19.68						-153	13.2
S11_BW_5	1	0.46	20.36	13.48	1.79	19	0.24 *	1	-169	15.9
	2	0.63	20.45						-326	19.7
	3	1.05	19.59	12.74	1.77	19			-45	21.1
	4	0.35	20.99						-92	12.1
S11_BW_6	1	0.46	19.65	13.64	1.82	20	0.20 *	2	-267	44.6
	2	0.51	20.11						-284	19.7
	3	0.68	18.41	12.65	1.77	17			-187	12
	4	0.99	17.34						-44	24.7
S11_BW_7	1	0.52	19.22	14.42	1.65	16	0.47 *	1	-159	19.3
	2	0.71	17.52						-132	10.3
	3	0.67	13.54	13.93	1.6	23			-93	6.6
	4	0.31	13.12						-92	15.4
Average	-	0.72	20.33	13.66	1.86	19.29	0.54	-	-135.68	18.14

* First bead side (Weld ID 1 & 2)

** Second bead side (Weld ID 3 & 4)

2D- and residual stress measurement

Specimen	Weld side	Weld toe radius	Flank angle	Cup width	Cup height	Cup diameter	Angular distortion	SG	Residual stress at weld toe/root	Error
	ID	[mm]	[deg]	[mm]	[mm]	[mm]	[deg]	Weld ID	[MPa]	(+/-)
S11_LW_1	1	0.25	-	-	-	-	0.28	2	-159	10
	2	0.30	-						-282	20.4
	3	0.21	40.24	2.88	1.05	2			41	10
	4	0.29	40.00						175	29
S11_LW_2	1	-	-	-	-	-	0.35	2	-	-
	2	0.22	-						-	-
	3	0.25	44.80	3.08	0.98	2			140	23.3
	4	0.22	39.72						76	60.9
Average	-	0.25	41.19	2.98	1.02	1.85	0.31	-	-1.5	25.6

Specimen	Weld	Weld toe radius	Throat thickness	Flank angle	Angular distortion	Strain gage	Residual stress at weld toe	Error
	ID	[mm]	[mm]	[deg]	[deg]	Weld ID	[MPa]	(+/-)
S11_LCX_1	1	0.84	4.65	35.38	1.08	2	-173	22.1
	2	0.59	4.64	35.37			-45	29.2
	3	0.66	4.68	34.57			-55	55.8
	4	0.61	4.61	33.62			78	14
S11_LCX_2	1	0.49	4.62	37.09	0.38	2	39	39.4
	2	0.11	4.59	34.49			-60	27.9
	3	0.15	4.8	35.74			8	23.7
	4	1.17	4.72	34.26			84	18.7
S11_LCX_3	1	0.82	4.63	34.38	0.09 (offset 0.39)	4	-46	19.3
	2	0.23	4.71	34.2			-38	14.7
	3	0.27	4.81	36.4			-47	31.1
	4	0.3	4.67	34.85			14	9.9
S11_LCX_4	1	0.4	4.6	35.62	0.04	4	-13	52.1
	2	0.33	4.62	35.31			-119	44.7
	3	0.36	4.54	32.78			-51	23.4
	4	0.49	4.71	34.22			-84	81.1
Average	-	0.49	4.66	34.89	0.50	-	-31.75	31.69

2D- and residual stress measurement

Specimen	Weld	Weld toe radius	Throat thickness	Flank angle	Angular distortion	Strain gage	Residual stress at weld toe	Error
	ID	[mm]	[mm]	[deg]	[deg]	Weld ID	[MPa]	(+/-)
NLCT_1	1	0.35	4.62	37.76	0.37	2	-14	37.2
	2	0.57	4.42	34.79			-301	55.2
NLCT_2	1	0.20	4.52	36.29	0.76	2	-26	22.3
	2	0.85	4.51	34.39			-9	26.9
NLCT_3	1	0.10	4.46	35.59	0.92	1	-129	28.3
	2	0.39	4.46	35.36			42	81.7
NLCT_4	1	0.31	4.57	37.04	0.92	1	-275	14.1
	2	0.14	4.48	35.95			-396	28.3
NLCT_5	1	0.24	4.53	37.58	0.86	1	-257	124.7
	2	0.18	4.47	34.72			-313	42.8
NLCT_6	1	0.55	4.58	36.09	0.85	2	-39	88.5
	2	0.36	4.41	34.21			-335	67.8
NLCT_7H	1	1.60	4.48	39.91	0.17	2	-408	188.7
	2	1.71	4.50	35.29			-644	166.4
NLCT_8H	1	2.62	4.48	39.26	0.23	1	-530	57.6
	2	3.03	4.37	36.22			-800	162.7
NLCT_9H	1	2.65	4.63	37.68	0.05	2	-490	49.6
	2	2.50	4.55	36.16			-457	53.3
NLCT_10H	1	2.27	4.49	37.21	0.15	1	-228	73.8
	2	2.13	4.36	35.36			-268	45.5
NLCT_11T	1	8.86	4.56	37.10	1.54	2	211	34
	2	4.57	4.79	36.17			142	32.4
NLCT_12T	1	5.09	4.53	38.23	1.62	1	-305	160.6
	2	4.59	4.51	35.61			-144	135.2
NLCT_13T	1	6.31	4.62	36.35	1.77	2	165	72.5
	2	7.32	4.61	39.24			186	41.7
NLCT_14T	1	9.10	4.64	39.09	2.11	2	31	65.2
	2	5.64	4.42	35.43			130	83.8
Average	ASW	0.35	4.50	35.81	0.78	-	-171.00	51.48
	HiFIT	2.31	4.48	37.14	0.15	-	-478.13	99.70
	TIG	6.44	4.59	37.15	1.76	-	52.00	78.18

2D- and residual stress measurement

Specimen	Weld toe	Weld toe radius	Throat thickness	Flank angle	Angular distortion	Strain gage	Residual stress at weld toe	Error
	ID	[mm]	[mm]	[deg]	[deg]	Weld ID	[MPa]	(+/-)
S11_LG_1	1	0.20	5.01	33.67	0.42	1&2	344	81.1
	2	0.26	4.56	34.45			352	134
S11_LG_2	1	0.35	5.01	29.28	0.02	1&2	268	60.6
	2	0.23	4.75	29.31			308	85.7
S11_LG_3	1	0.41	4.97	31.63	0.66	1&2	275	56.1
	2	0.35	4.74	30.17			250	127.4
S11_LG_4	1	0.36	4.95	31.51	0.22	1&2	147	42.8
	2	0.53	4.76	31.62			304	118.8
S11_LG_5H	1	3.72	5.09	30.72	0.13	1&2	-440	73.4
	2	2.52	4.79	31.04			-30	73.1
S11_LG_6H	1	3.33	4.92	29.33	0.06	1&2	-671	254.7
	2	2.66	4.68	30.12			-198	100.4
Average	ASW	0.34	4.84	31.07	0.25	-	75.75	100.68
	HiFIT	3.06	4.87	30.30	0.09	-	-334.75	125.40

Macrographs and dimensions

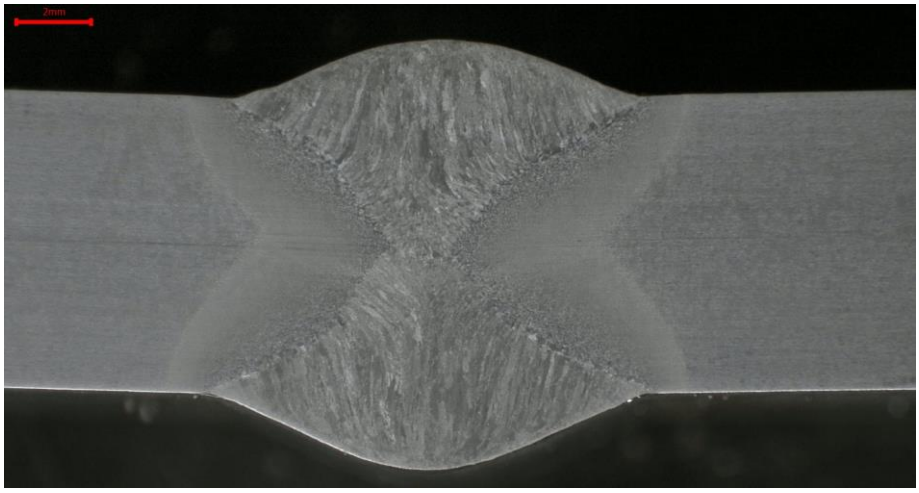

Figure IV.1. Macrograph of GMAW BW-specimen (air gap of 0 mm).

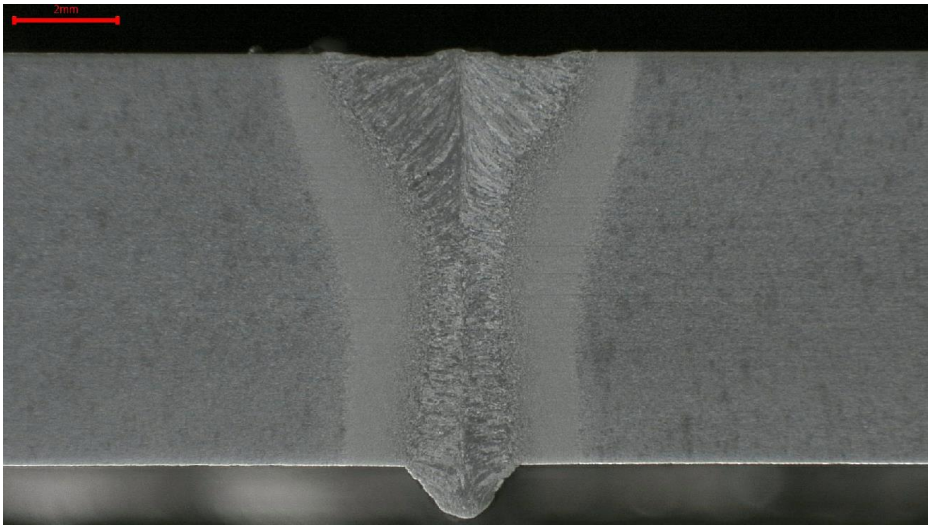

Figure IV.2. Macrograph of LW-specimen.

Macrographs and dimensions

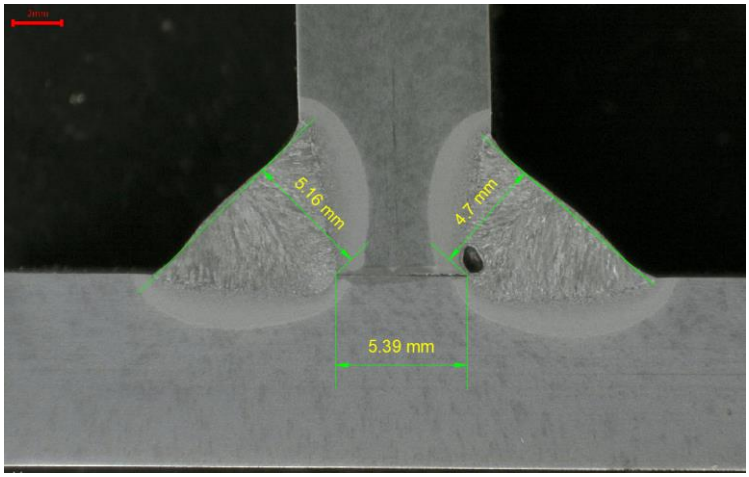

Figure IV.3. Macrograph of NLCT ASW-specimen.

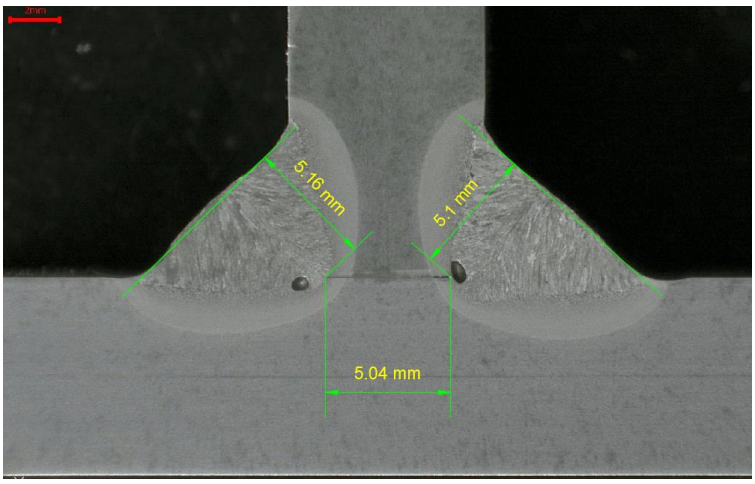

Figure IV.4. Macrograph of NLCT HiFIT-treated specimen.

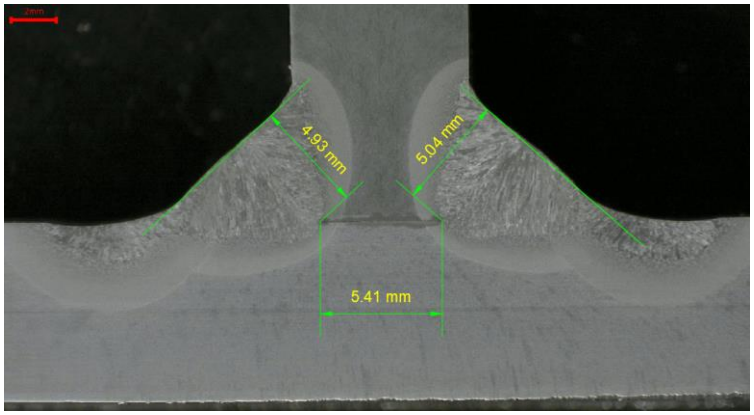

Figure IV.5. Macrograph of NLCT TIG-treated specimen.

Macrographs and dimensions

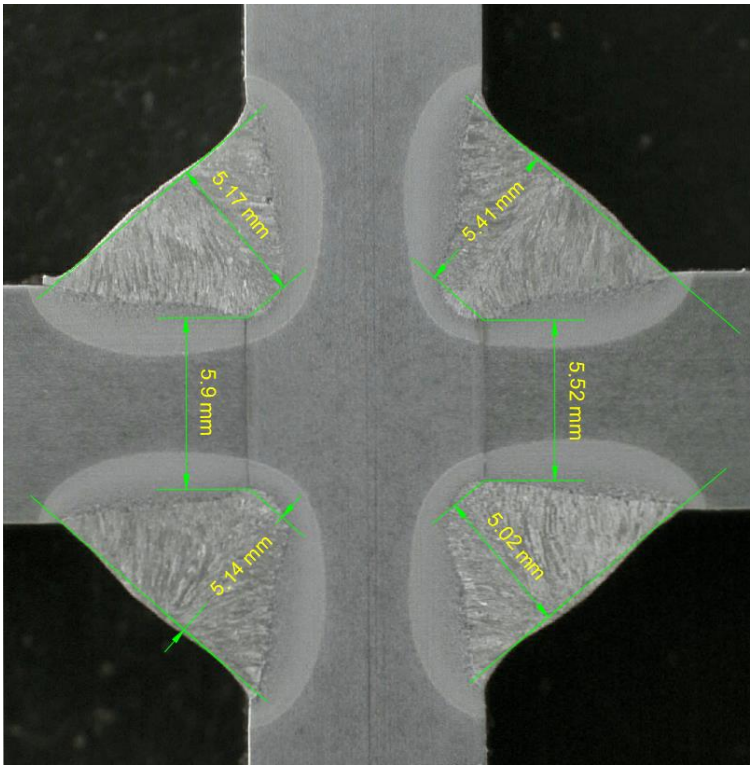

Figure IV.6. Macrograph of LCX-specimen.

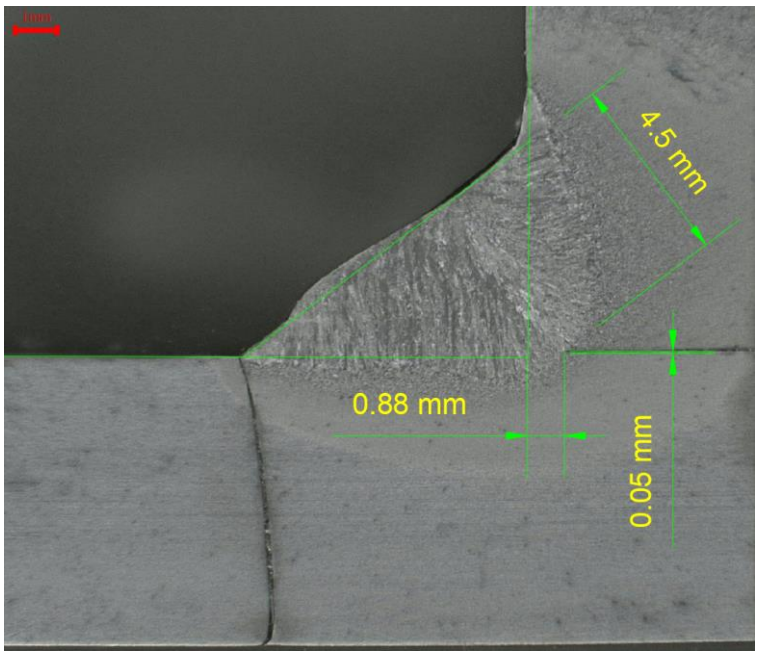

Figure IV.7. Macrograph of LG-specimen from the end of the gusset.

Macrographs and dimensions

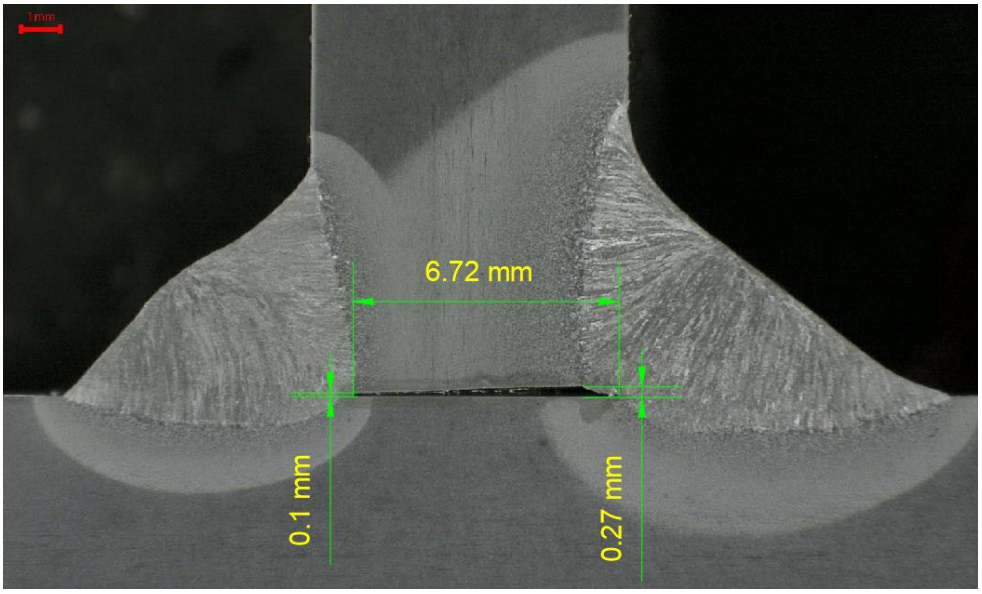

Figure IV.8. Macrograph of LG-specimen in transverse direction of the gusset.

Hardness measurement

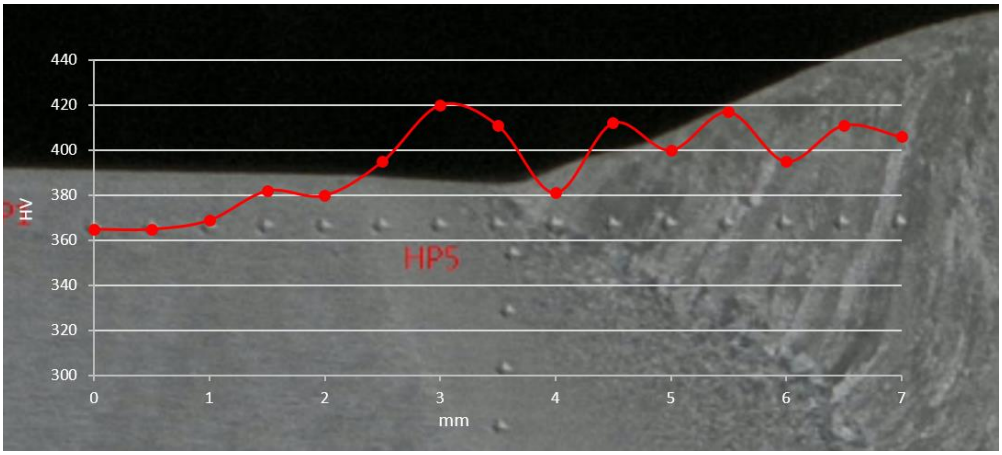

Figure V.1. Hardness diagram of GMAW BW-specimen in longitudinal direction.

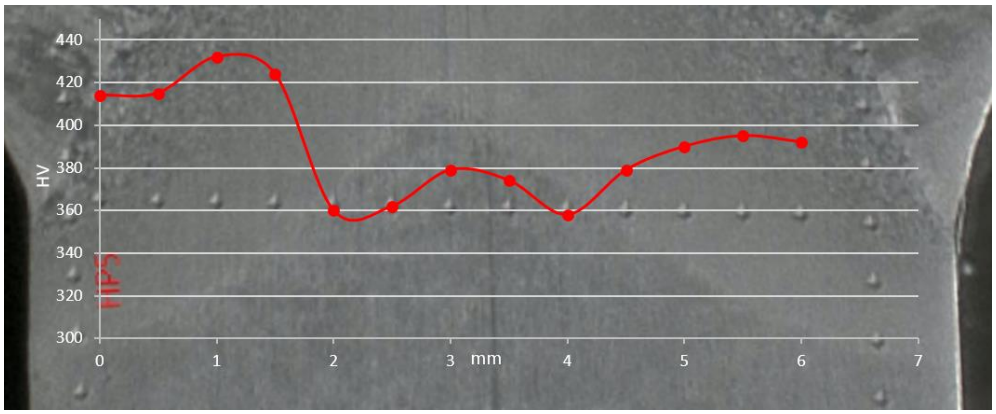

Figure V.2. Hardness diagram of GMAW BW-specimen in thickness direction.

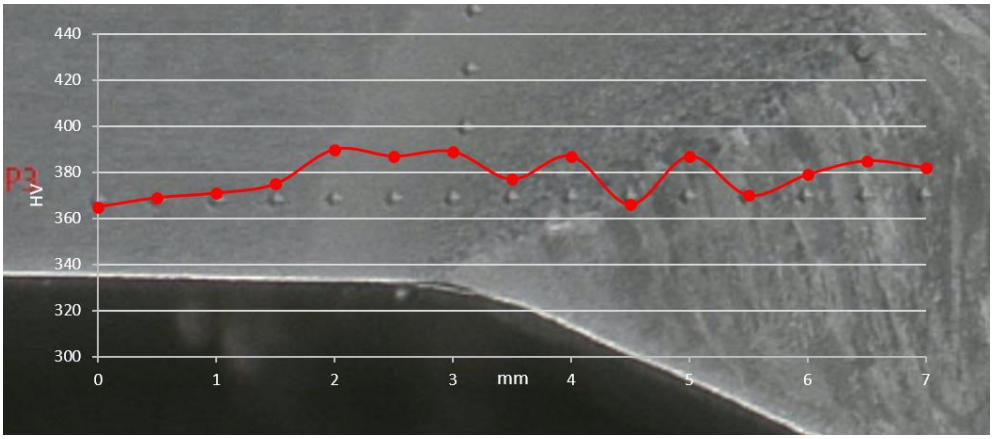

Figure V.3. Hardness diagram of GMAW BW-specimen in longitudinal direction.

Hardness measurement

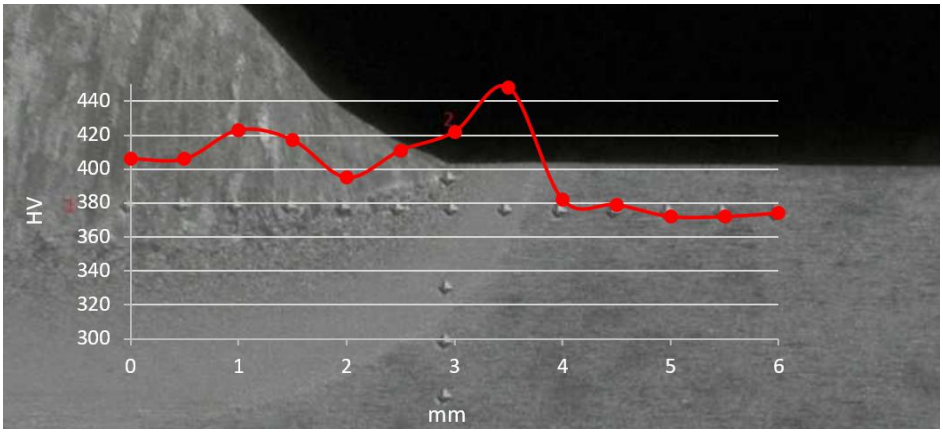

Figure V.4. Hardness diagram of NLCT ASW-specimen in longitudinal direction.

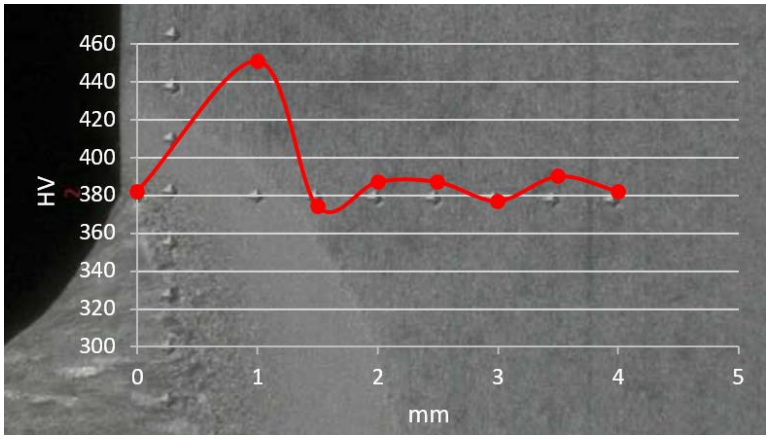

Figure V.5. Hardness diagram of NLCT ASW-specimen in thickness direction.

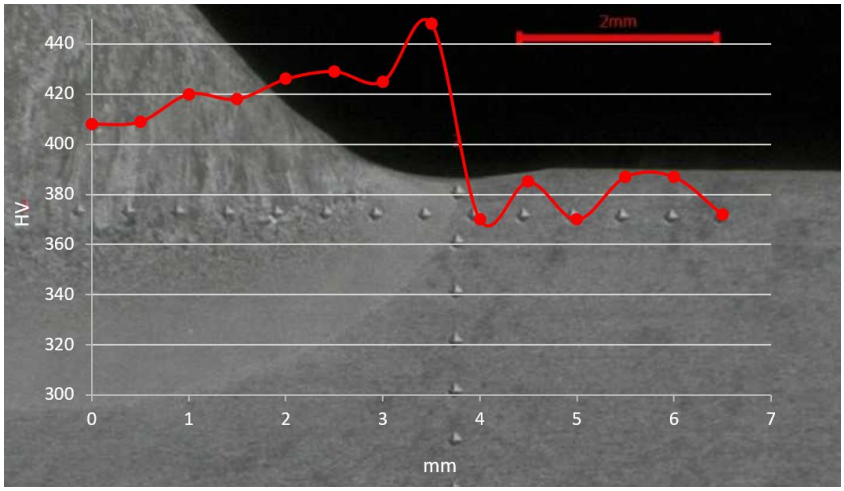

Figure V.6. Hardness diagram of NLCT HiFIT-treated specimen in longitudinal direction.

Hardness measurement

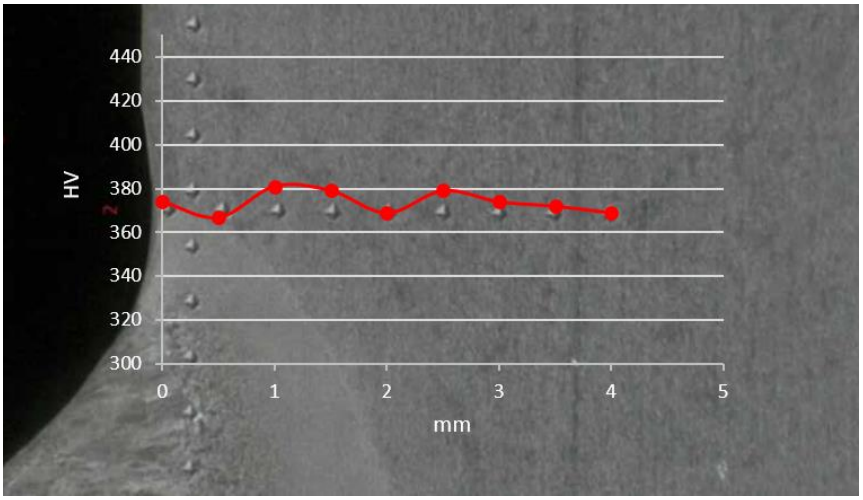

Figure V.7. Hardness diagram of NLCT HiFIT-treated specimen in thickness direction.

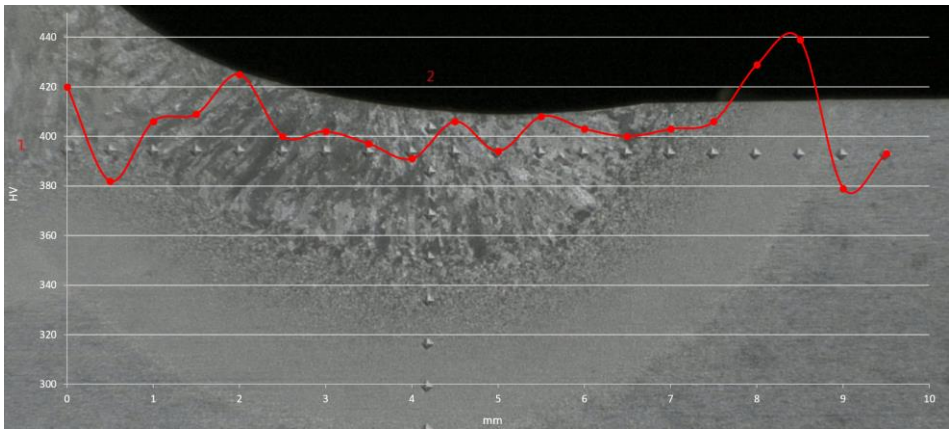

Figure V.8. Hardness diagram of NLCT TIG-treated specimen in longitudinal direction.

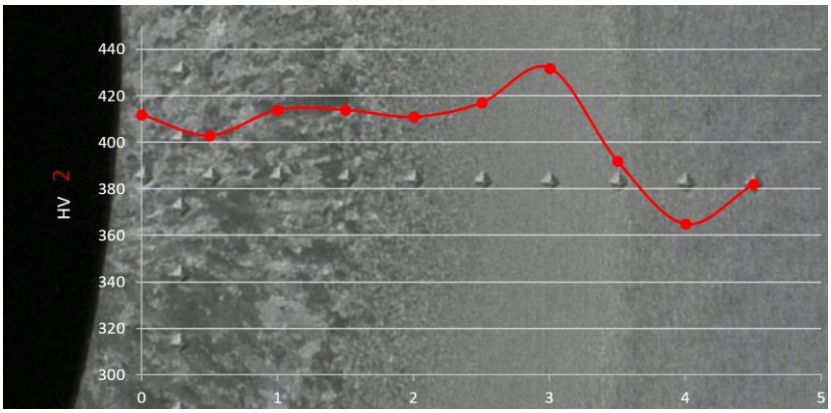

Figure V.9. Hardness diagram of NLCT TIG-treated specimen in thickness direction.

Hardness measurement

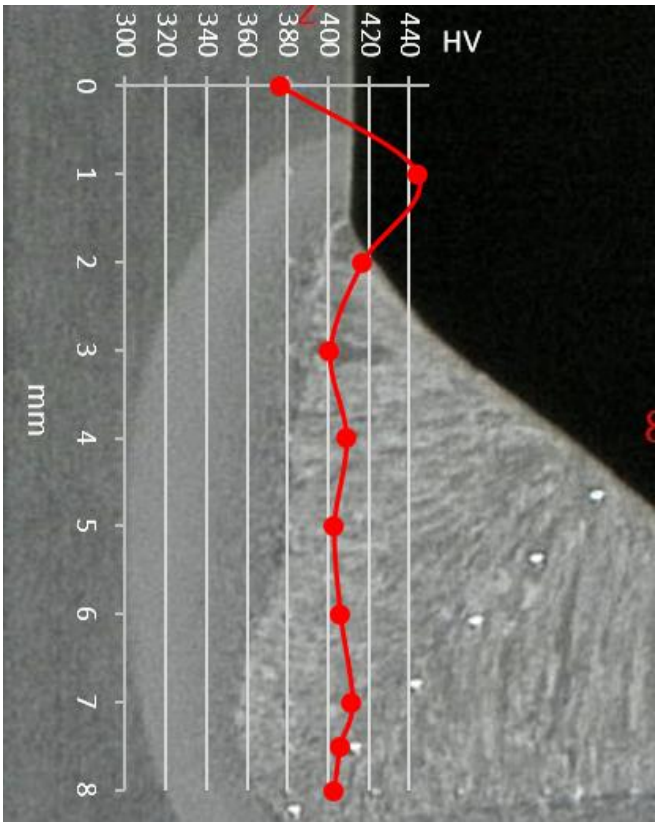

Figure V.10. Hardness diagram of LCX-specimen in vertical direction.

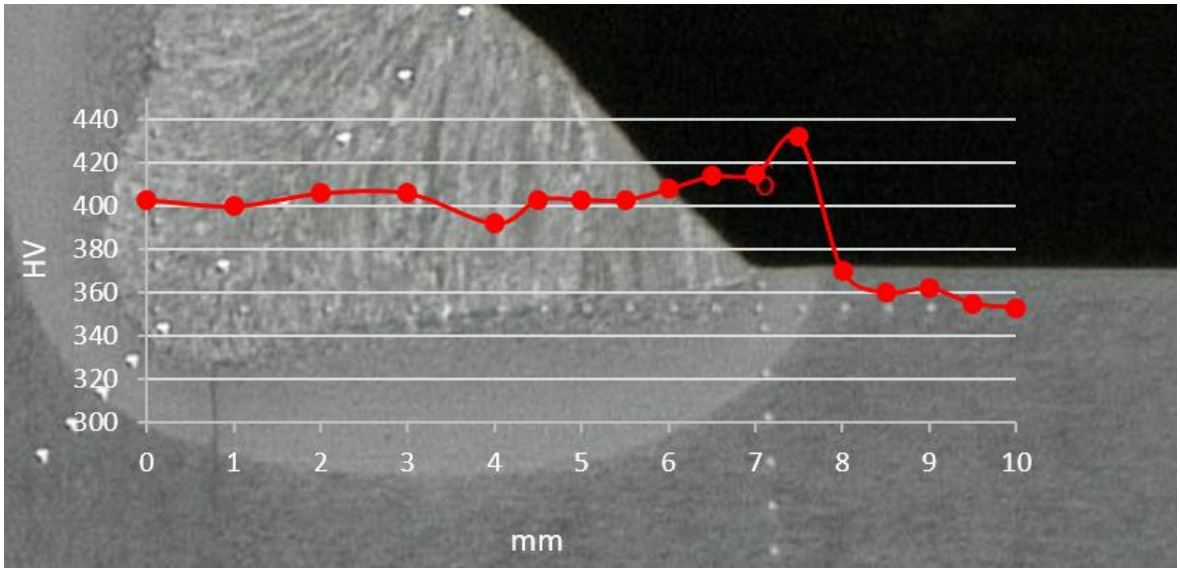

Figure V.11. Hardness diagram of LCX-specimen in longitudinal direction.

Hardness measurement

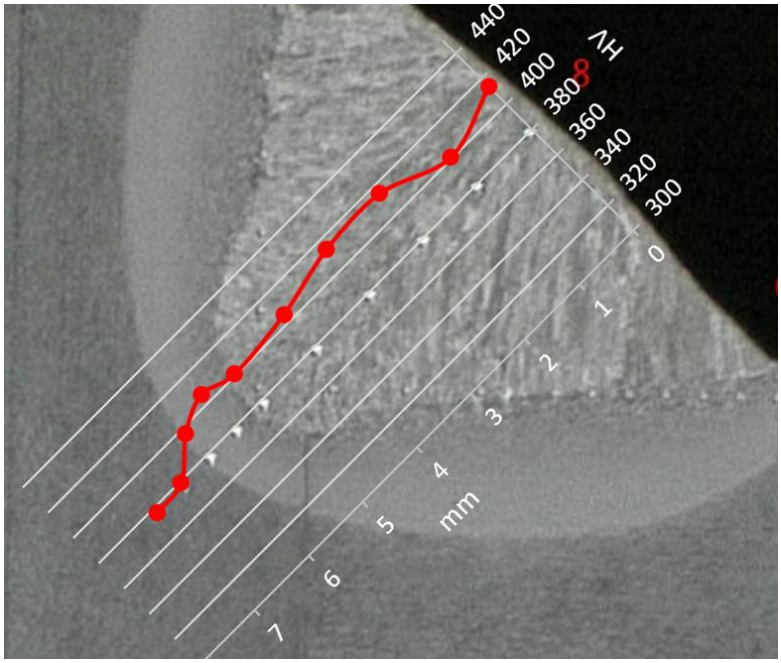

Figure V.12. Hardness diagram of LCX-specimen through the weld.

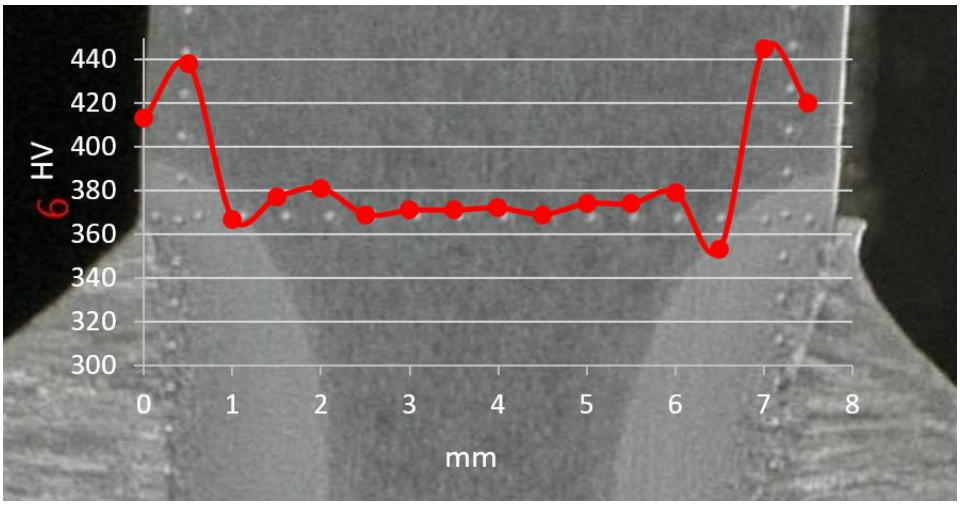

Figure V.13. Hardness diagram of LCX-specimen in thickness direction.

Hardness measurement

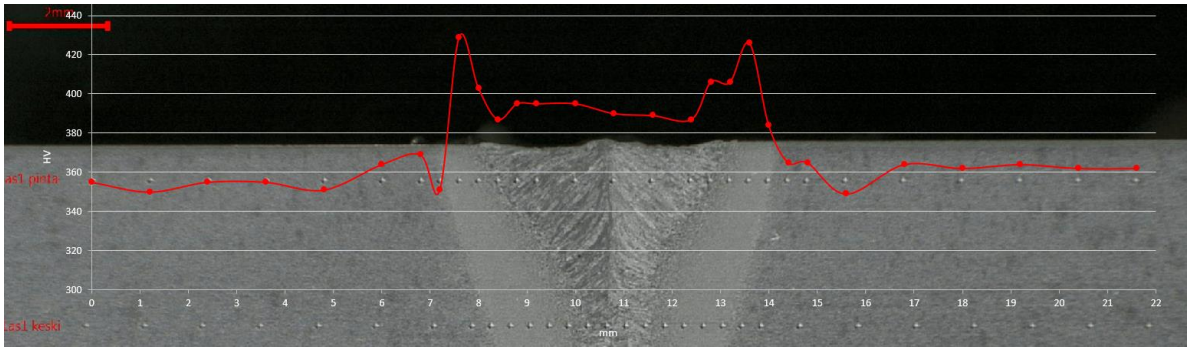

Figure V.14. Hardness diagram of LW-specimen in longitudinal direction.

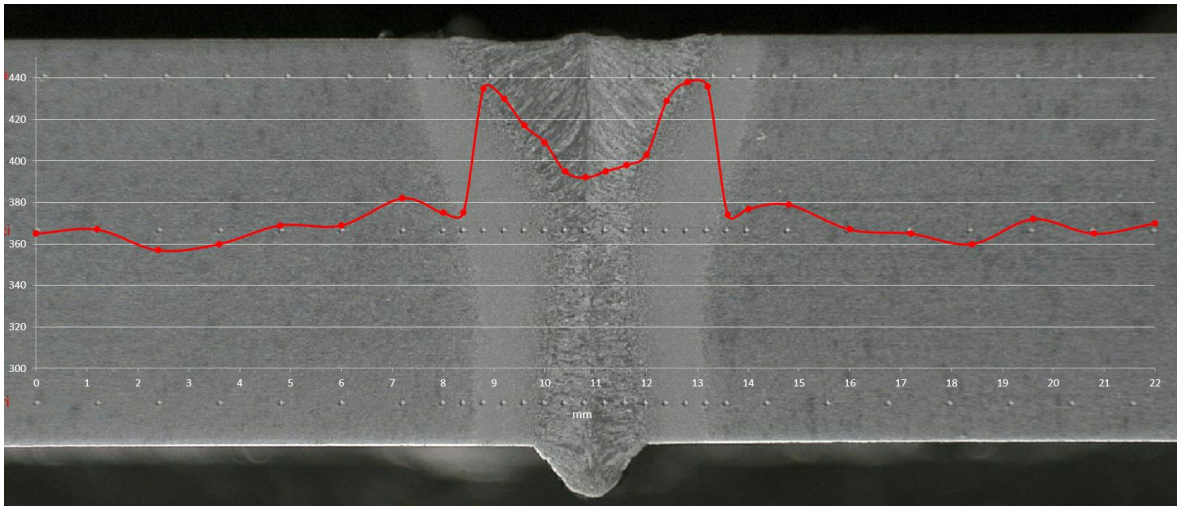

Figure V.15. Hardness diagram of LW-specimen in longitudinal direction.

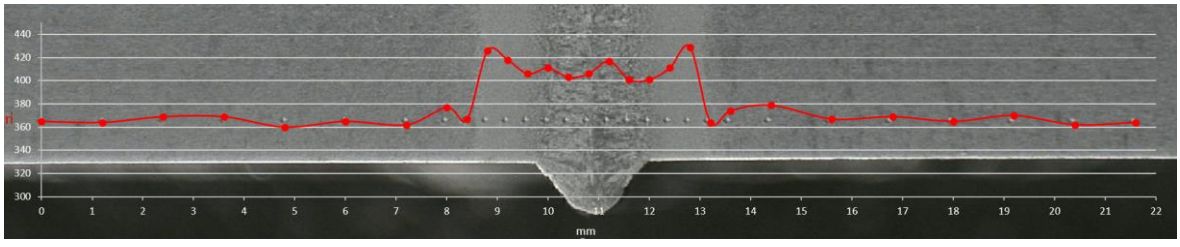

Figure V.16. Hardness diagram of LW-specimen in longitudinal direction.